

SPREADING DEPOLARIZATION IN THE EARLY POST-ISCHEMIC BRAIN

By

Dylan Andrew Petrin

A thesis submitted to the Graduate Program in The Centre for Neuroscience Studies in conformity with
the requirements for the Degree of Doctor of Philosophy

Queen's University

Kingston, Ontario, Canada

(September, 2017)

Copyright © Dylan Andrew Petrin

Abstract

Stroke is one of the leading causes of death and long-term disability throughout developed countries. A propagating wave of mass depolarization of neurons and glia, referred to as spreading depolarization (SD), occurs within minutes after insufficient blood supply expands brain territory with depleted ATP and tissue damage. By harvesting live brain slices from mice that underwent focal stroke via middle cerebral artery occlusion (MCAo), we were able to image the ignition site of post-ischemic SD, assess the precise spatiotemporal propagation of the accompanying wave and record brain tissue changes in response to further metabolic stress. Post-MCAo brain slices superfused with elevated $[K^+]_{ext}$, $[glu]_{ext}$ or oxygen-and-glucose deprivation (OGD) display a decreased propensity to generate SD and tissue swelling in response to these extracellular conditions evident following stroke in vivo. Although this observation is counterintuitive to the high incidence of spontaneous SD observed in vivo by others two hours following ischemia, it is concordant with an ensuing period of decreased SD incidence. Furthermore, carbetapentane or dibucaine pre-treatment significantly delay SD onset in post-ischemic cerebral slices, similar to their effects in non-stroke brain slices. The healthy tissue observed immediately post-MCAo in the future ischemic core rapidly deteriorates during the ensuing 12 hours of infarct maturation. Although dramatic evidence of infarction occurs 12 hours following ischemia, a small and diffuse subset of pyramidal neurons in neocortex survives within the core. How they are protected and if they continue to survive post-MCAo are two intriguing issues for future study.

Overall, this thesis specifically assesses the initiation, propagation and tissue changes in response to isolated mediators of swelling and SD in the post-ischemic brain. The observations of a delayed latency to SD onset and decreased susceptibility of swelling of the early post-

ischemic brain support previous hypotheses of an adaptive mechanism of the post-ischemic brain to prevent or limit further depolarizations. The post-ischemic resistance to SD was over-ridden by chemical blockade of the Na⁺/K⁺ pump (and SD induction) by 100 μM ouabain. This finding resonates with an initial hypothesis of SD resistance by Na⁺/K⁺ pump hyperactivation postulated by early investigators of SD.

Co-Authorship

DP was responsible for brain slice preparation, obtaining all light transmittance data as well as the preparation of this thesis. DP obtained all of the electrophysiological data with the exception of a few recordings from post-ischemic brain slices harvested 12 hours following ischemia, which were acquired with the help of Mr. Peter Gagolewicz. Ms. Nichole Peterson performed the middle cerebral artery occlusion procedure upon all mice and acquired light microscopy images from yellow-fluorescent protein expressing post-stroke mice in consultation with myself and Dr. Al Jin. DP harvested brains from post-MCAo mice and fixed them for the Golgi staining procedure and Jason Park prepared the microscope slides. Dr. David Andrew and Ms. Rasha Mehder acquired images from microscope slides fixed by the Golgi-Cox staining procedure. I wrote the first draft of this thesis, with all subsequent drafts written with feedback from Drs. Andrew and Jin.

Acknowledgements

I am very appreciative for the assistance of my colleagues Nichole Peterson, Peter Gagolewicz, Jason Park and Rasha Mehder who contributed to some of the data within this thesis. I am grateful for the guidance, mentorship and support provided by Dr. David Andrew and Dr. Al Jin throughout the acquisition, analysis and written communication of this thesis. I am especially thankful to Nichole Peterson who performed many, many stroke procedures while also being a very cheerful friend. I was also lucky to befriend Peter Gagolewicz, who helped train me to perform patch clamp electrophysiology. My gratitude extends to my fellow graduate students and staff members in the Centre for Neuroscience Studies and the School of Graduate Studies who exemplify dedication and personal sacrifice on the path of innovation and the improvement of the lives of others. I also owe a debt of gratitude to Queen's University athletics for the extraordinary experiences I enjoyed as a result of their passion towards uplifting people within the Queen's University and Kingston communities. I am especially grateful to my parents, Sheila and Gary Petrin, my brother, Neil Petrin, and my extended family for their unconditional love and support.

Table of Contents

Abstract	ii
Co-Authorship	iv
Acknowledgements	v
Table of Contents	vi
List of Tables	x
List of Figures	xi
Abbreviations	xiv
Chapter 1 General Introduction.....	1
1.1 Stroke and Spreading Depolarization	1
1.2 Temperature and CBF Variability Following Ischemia	5
1.3 Experimental Rationale	6
1.3.1 Light Transmittance Changes (Δ LT)	6
1.3.2 Δ LT and Electrophysiology During and After SD	7
1.3.3 Post-Ischemic Electrophysiology	8
1.4 In Vivo Ischemia and Brain Slice Models	9
1.4.1 Global Ischemia	9
1.4.2 Focal Cerebral Ischemia	9
1.4.3 Brain Slice Model	10
1.5 Overview of Manuscripts	11
1.5.1 Reduced propensity for spreading depolarization in the mouse neocortex immediately following focal cerebral ischemia.	11

1.5.2 Change in post-stroke electrophysiology and morphology after 12 hours of reperfusion.	13
1.5.3 Post-ischemic resistance to spreading depolarization.	15
1.6 Overall Objectives	17
Chapter 2 Reduced propensity for spreading depolarization in the mouse neocortex immediately following focal cerebral ischemia	18
2.1 Summary	18
2.2 Introduction	19
2.3 Materials and Methods	21
Middle Cerebral Artery Occlusion and Brain Slice Preparation	21
Imaging Changes in Light Transmittance (Δ LT) During OGD	21
Electrophysiology	22
Statistical Analysis	24
Golgi-Cox Staining	24
Neocortical Pyramidal Neurons Expressing Yellow Fluorescent Protein	25
2.4 Results	25
2.5 Discussion	37
Chapter 3 Spreading depolarization in the mouse neocortical brain slices immediately after 30 min MCAo compared to 12 hours later	42
3.1 Summary	42
3.2 Introduction	43
3.3 Materials and Methods	44
Middle Cerebral Artery Occlusion and Brain Slice Preparation	44

Imaging Changes in Light Transmittance (Δ LT) During OGD	45
Electrophysiology	46
Golgi-Cox Staining	48
Statistical Analysis	48
3.4 Results	48
Light Transmittance Imaging	48
Electrophysiology	54
Golgi-Cox Staining	55
3.5 Discussion	64
Post-ischemic SD and Leao's Initial Observations of SD	64
Elevated $[K^+]_{ext}$, Elevated $[glu]_{ext}$ and OGD Post-Ischemia	65
Post-Ischemic Microscopy and Electrophysiology	67
Conclusions	68
Chapter 4 Post-ischemic resistance to spreading depolarization	70
4.1 Summary	70
4.2 Introduction	71
4.3 Materials and Methods	73
Middle Cerebral Artery Occlusion and Brain Slice Preparation	73
Imaging Changes in Light Transmittance (Δ LT) During OGD	74
Electrophysiology	75
Statistical Analysis	77
4.4 Results	78
Region-Specific Light Transmittance Changes	78

Electrophysiology	81
Discrepancy of SD Onset Between Ischemic and Non-Ischemic Hemispheres Eliminated.....	81
4.5 Discussion	84
Post-Ischemic Resistance to SD	84
Adenosine	86
The Na ⁺ /K ⁺ pump	87
Conclusions	89
Chapter 5 General Discussion	91
5.1 Leao's Prescient Observations of SD	91
5.2 Post-Ischemic Electrophysiology.....	93
5.3 Elevated [K ⁺] _{ext} , [glu] _{ext} and Oxygen/Glucose Deprivation in the Post-Ischemic Brain ...	94
5.4 Delayed SD Onset and Decreased Incidence of Post-Ischemic SD	96
5.5 Conclusions	100
5.6 Strengths and Limitations of this Study	101
5.7 Future Directions	103
References	106

List of Tables

Table 1. Baseline electrophysiological properties of whole-cell patched pyramidal cells	41
Table 2. Baseline Electrophysiological Properties of Identified Pyramidal Neurons in the Ischemic and Non-Ischemic Hemispheres in Brain Slices Harvested 12 Hours After MCAo.....	69
Table 3. Baseline Electrophysiological Properties of Neurons Within ‘Core’ (Par _{lat}) and ‘Penumbra’ (Par _{med}) Post-Ischemic Neocortex and Corresponding Areas in the Non-Ischemic Hemisphere	90

List of Figures

Figure 1. Baseline electrophysiological properties of whole-cell patched pyramidal cells and neuronal morphology were similar in the ischemic and non-ischemic hemispheres	27
Figure 2. Evoked response in ischemic hemisphere after 50 mV stimulation was not significantly different between the ischemic and non-ischemic hemispheres	28
Figure 3. OGD-induced SD initiates with a similar incidence at various stereotaxic locations both within the ischemic and non-ischemic hemisphere of neocortical brain slices harvested immediately after 30 min MCAo	29
Figure 4. Latency to SD onset in the ischemic hemisphere was significantly delayed compared to the non-ischemic hemisphere	30
Figure 5. The SD wavefront speed in the ischemic hemisphere vs. the non-ischemic hemisphere was significantly slower	31
Figure 6. There is no difference between hemispheres in cell swelling during SD in regions where it is generated. There is significantly less light scatter in the ischemic hemisphere after OGD-induced SD	31
Figure 7. Carbetapentane (CP) and dibucaine (DB) significantly delay mean latency to SD onset in both the ischemic and non-ischemic hemispheres relative to control aCSF	33
Figure 8. Neuronal morphology in the early post-stroke brain	34
Figure 9. Neuronal morphology early post-stroke at intermediate magnification	35
Figure 10. Neuronal morphology early post-stroke at high magnification	36
Figure 11. Incidence of $[K^+]_{ext.}$ -induced SD in brain slices harvested immediately, and 12 hours after, 30 min MCAo	50

Figure 12. SD_K^+ initiated outside MCA territory when brain slices were harvested after 12 hours of reperfusion following MCAo	51
Figure 13. Significantly less incidence of glutamate-induced swelling in the ischemic hemisphere of brain slices harvested immediately, and 12 hours after, 30 min MCAo	52
Figure 14. SD development in the ischemic hemisphere is reduced by 12 hours, but not immediately, post-MCAo. Ischemic hemisphere after 12 hours of reperfusion displays a significantly lower incidence of OGD-SD	53
Figure 15. The evoked synaptic response incidence is significantly lower in the ischemic hemisphere of brain slices harvested 12 hours, but not immediately, after 30 min MCAo	54
Figure 16. Coronal sections through three brains of mice that each underwent 30 minute left hemisphere MCAo followed by a 12 hour recovery period	58
Figure 17. Ischemic hemisphere displays necrotic neurons clearly distinguishable from the intact non-ischemic hemisphere	59
Figure 18. Core area of the ischemic hemisphere displaying necrotic neurons A) at low magnification, B) in striatum, and C) in overlying neocortex	60
Figure 19. Isolated intact pyramidal neurons surrounded by necrotic and swollen neurons within the infarcted region	61
Figure 20. In the neocortical region of the ischemic core, neurons may be, A) swollen with dendrites that are beaded or B) necrotic with stunted and beaded dendrites. Also observed are rare intact pyramidal neurons (yellow arrows)	62
Figure 21. Baseline electrophysiological properties of whole-cell patched pyramidal cells were similar in the ischemic and non-ischemic hemispheres	63

Figure 22. Less light scatter after OGD-SD in MCAo future ‘core’ in comparison to the non-ischemic hemisphere and future ‘penumbra’ regions in ischemic hemisphere	79
Figure 23. Amplitude of synaptic responses evoked by an increasingly strong stimulus was not significantly different in the ischemic vs. the non-ischemic hemisphere	80
Figure 24. Na ⁺ /K ⁺ pump modulation, but not adenosine A1 receptor inhibition, eliminates the delayed SD onset observed in the post-ischemic hemisphere	83
Figure 25. OGD-induced SD wavefront is slower in the ischemic hemisphere, but not significantly different during SD induced by saline containing 100 μM ouabain	84

Abbreviations

aCSF, artificial cerebrospinal fluid

ATP, adenosine triphosphate

C57BL6, c 57 black 6

CBF, cerebral blood flow

CA1, cornu ammonis 1

CA3, cornu ammonis 3

CCD, charge-coupled device

COSBID, co-operative study on brain injury depolarizations

CP, carbetapentane

DB, dibucaine

DPCPX, dipropylpentylcyclohexanthine

ECoG, electrocorticogram

EEG, electroencephalogram

EPSP, evoked postsynaptic potential

fEPSP, field evoked postsynaptic potential

fAHP, fast afterhyperpolarization

[glu]_{ext}, extracellular glutamate concentration

Hyp, hypothalamus

Hipp, hippocampus

[K⁺]_{ext}, extracellular potassium concentration

ΔLT, light transmittance changes

MCAo, middle cerebral artery occlusion

Na⁺/K⁺ pump, sodium/potassium pump

Na⁺/K⁺ ATPase pump, sodium/potassium adenosine tri-phosphatase pump

NC, neocortex

NMDA, N-methyl-D-aspartate

OGD, oxygen-and-glucose deprivation

Par_{lat}, lateral parietal cortex

Par_{med}, medial parietal cortex

R_{in}, input resistance

SD, spreading depolarization

SD_{K⁺}, potassium-triggered spreading depolarization

S.E.M., standard error of the mean

Str, striatum

T_{cont}, control transmittance

T_{exp}, experimental transmittance

Thal, thalamus

YFP, yellow-fluorescent protein

Chapter 1

General Introduction

1.1 Stroke and Spreading Depolarization

Stroke is the second leading cause of disability worldwide. Stroke claims the lives of 7 million people each year and another 15 million suffer from long-term disability. In Canada, the numbers are also grim. An estimated 13 000 Canadians die each year and 49 000 patients require long-term assistance. The economic burden of stroke has been estimated to cost Canadians \$20.9 billion per year (Wilkins et al. 2012). Stroke prevalence in developing nations is also high with a trend of an increasing incidence over the last three decades (Feigin 2005).

Many experimental and clinical therapeutic interventions have been attempted to improve functional outcome following stroke. Over 1026 treatments for ischemic stroke have been tested without a successful demonstration of clinical benefit in human patients (O'Collins et al. 2006). Successful stroke treatments are difficult to achieve due to the inherent variability of cerebral blood flow, core body temperature, therapeutic time windows and temporospatial evolution of infarct maturation (Saver et al. 2009). In addition to compensating for these variables in clinical trials, it is important to perform experiments that investigate attenuation of stroke damage by minimizing inherent post-ischemic cerebral blood flow and temperature variability.

Stroke clinically manifests as an interruption of blood supply to the brain following arterial occlusion (~ 75% of patients) or rupture of blood vessels (~ 25% of patients). The most common form of focal cerebral ischemia is middle cerebral artery occlusion (MCAo). In rodent ischemic stroke models, MCAo precipitates a decline in cerebral blood flow (CBF) of < 20 % of pre-ischemic values in striatum and overlying somatosensory and temporal cortices (Belayev et al.

1997) and disrupted ionic homeostasis (Hossmann 1994). This region with low residual CBF is known as the ischemic 'core'. Brain areas with ~ 20-40 % residual CBF adjacent to the core are referred to as the ischemic 'penumbra'(Hossmann 1994; Belayev et al. 1997). At the edge of the core, partial ischemia precipitates a propagating wave of neuronal depolarization that expands the ischemic core outwards into the penumbra during the minutes, hours and days following stroke onset (Busch et al. 1996; Dohmen et al. 2008).

This propagating wave of neuronal depolarization following ischemia was proposed by Aristides Leao (Leao 1947) to resemble the 'spreading depression' of cortical activity (and mass depolarization of neurons) that he had observed following electrical stimulation of rabbit cortex (Leao 1944). In addition to the disruption of transmembrane gradients that causes neuronal depolarization, the spreading wavefront begins to induce neuronal swelling and beading of dendrites within several seconds. The propagating disruption of membrane potential gradients and neuronal morphology that occurs in response to various metabolic stressors are collectively referred to as spreading depolarization (SD) (Dreier 2011; Hartings et al. 2017). A similar propagating SD wave is also induced by $[K^+]_{ext}$ elevation, inhibitors of the mitochondrial transport chain, traumatic brain injury, aneurysmal hemorrhage, or chemical inhibition of the Na^+/K^+ pump (Anderson and Andrew 2002; Tanaka et al. 1997; Hartings et al. 2011; Dreier et al. 2009; Balestrino et al. 1995).

SD has been induced experimentally after ischemia by applying KCl to exposed neocortex. With each successive wave of potassium-triggered SD (SD_{K^+}) after the initial exposure to ischemia, there is a stepwise increase of brain areas with deficient energy production and compromised brain tissue (i.e. infarction) (Busch et al. 1996; Takano et al. 1996). Spontaneous post-ischemic SD is also correlated with infarct expansion and decreased ATP production (Mies

et al. 1994; Hartings et al. 2003). Localized ischemia using a light-sensitive dye (i.e. photothrombosis) partially mimics damage induced by arterial occlusion and results in dendritic beading, vasoconstriction and EEG suppression that can be imaged and recorded with high precision in vivo (Zhang et al. 2005; Brown et al. 2008). By using neocortical brain slices SD ignition sites are precisely identified, SD propagation is mapped with high spatial and temporal resolution, and acute tissue damage is easily examined following the wake of the SD wavefront (Obeidat and Andrew 1998).

Direct observation of recurring post-ischemic SD in patients has been carried out in six major hospital centres around the world by the COSBID research group (Cooperative Study on Brain Injury Depolarizations). It is not possible to demonstrate SD in patients using diagnostic imaging (Dreier et al. 2017). However, when electrocorticographic (ECoG) electrodes are placed on the brain surface in patients suffering from ischemic stroke, traumatic brain injury or aneurysmal subarachnoid hemorrhage, SD can be observed. It manifests as a propagating depression in ECoG activity as recorded with strip electrodes. They are placed radiating outwards from the damaged neocortical areas so that some electrodes are partially in contact with presumably viable brain tissue. An SD event can be observed propagating from one electrode pair to the next (Fabricius et al. 2006; Dohmen et al. 2008). Patients with poor outcome generally display a higher incidence of SD events, along with delayed recovery of synaptic communication in these ECoG recordings (Dohmen et al. 2008). Peri-infarct SD events after occlusive stroke also occur along with variable CBF hyperperfusion or hypoperfusion in human patients (Woitzik et al. 2013). Inherent CBF variability as well as limited access to exposed cortex with scalp electrodes in stroke patients create difficult conditions to observe post-ischemic SD.

Superfusing artificial cerebrospinal fluid (aCSF) devoid of oxygen and glucose on neocortical brain slices in a bath chamber experimentally simulates ‘core’ CBF loss during ischemia. Within minutes of oxygen-and-glucose deprivation (OGD), a propagating wave of neuronal and glial depolarization with swelling initiates at one or more foci (Anderson et al. 2005; Dietz et al. 2008). During ischemia a similar disruption of ion homeostasis occurs within 1-2 minutes after a drop in CBF to < 10 % of baseline (Astrup et al. 1977). In ischemic stroke patients this disruption evokes a propagating wave of SD (Nakamura et al. 2010; Dohmen et al. 2008), similar to ischemic rodents (Koroleva and Bures 1996; Back et al. 1996). A potassium-triggered propagating SD wave can also be elicited in neocortical brain slices with $[K^+]_{ext}$ elevation (Anderson and Andrew 2002). However, only dendritic depolarization occurs following SD_{K^+} (Dietz et al. 2008) and neurons quickly repolarize without evidence of neuronal injury in brain slices or the intact animal (Anderson and Andrew 2002; Nedergaard and Hansen 1988). In contrast, superfusing neocortical slices with OGD results in terminal depolarization of neurons, dendritic beading and neuronal death (Anderson et al. 2005; Andrew et al. 2007; Risher et al. 2009). OGD-induced SD in slices results in irreversible tissue damage (Jarvis et al. 2001; Anderson et al. 2005) similar to SD erupting near the ischemic core (Busch et al. 1996; Back et al. 1996). In contrast, neocortical slices quickly and completely recover from SD_{K^+} (Anderson and Andrew 2002) similar to SD propagating through non-ischemic brain areas following arterial occlusion (Koroleva and Bures 1996) or non-ischemic animals (Nedergaard and Hansen 1988).

Failure of the Na^+/K^+ pump evoked by metabolic stressors is the common precursor to SD. Approximately 50% of the brain’s energy is used by the Na^+/K^+ pump to maintain ion homeostasis (Tidow et al. 2010; Astrup et al. 1981b). Furthermore, inhibition of the Na^+/K^+ pump with 30-100 μ M ouabain results in SD with a similar profile of $[K^+]_{ext}$ elevation as

ischemia (Balestrino et al. 1995; Hansen and Zeuthen 1981; Tanaka et al. 1997). Ouabain bath application in neocortical slices at 100 μM induces a 2-5 mm/min propagating wave of swelling neurons and glia that results in irreversible neuronal depolarization and diminished synaptic communication, similar to OGD superfusion (Brisson and Andrew 2012; Anderson et al. 2005; Jarvis et al. 2001). A similar propagating SD wave occurs if the Na^+/K^+ pump is overwhelmed with elevated $[\text{K}^+]_{\text{ext}}$, or indirectly inhibited with disrupted ATP production using mitochondrial transport inhibitors or OGD (Anderson and Andrew 2002; Dietz et al. 2008; Tanaka et al. 1997; Anderson et al. 2005). Thus, overwhelming or inhibiting the Na^+/K^+ pump leads to SD.

1.2 Temperature and CBF Variability Following Ischemia

Core body temperature fluctuates and declines after ischemia (Connolly et al. 1996; Baker et al. 1992) which can affect the incidence and properties of SD. In mouse models of focal cerebral ischemia, hypothermia can also arise (Barber et al. 2004). Hypothermia is associated with a delayed latency to SD onset during in vivo KCl application (Takaoka et al. 1996) and during ischemia (Chen et al. 1993) as well as a decreased SD propagation speed during ischemia (Sasaki et al. 2009). Following hypothermia in neocortical brain slices, a decreased likelihood of SD is observed during OGD (Obeidat and Andrew 1998).

Although controlled temperature results in less variability of infarct volume following MCAo, CBF fluctuations and episodic hypoperfusion remain (Barber et al. 2004; Shin et al. 2006). With each SD event during and after ischemia, CBF declines abruptly and fails to recover to levels observed prior to SD (Shin et al. 2006; Bere et al. 2014; von Bornstädt et al. 2015). When hypoxia and hypoperfusion are induced in non-ischemic rats, the duration of SD increases (Sukhotinsky et al. 2010), similar to post-ischemic long-duration SD events observed in

neocortex under decreased CBF (Dijkhuizen et al. 1999). CBF decreases when hypoxia and hypoperfusion are applied to normal rats prior to SD (Sukhotinsky et al. 2008), similar to observations during ischemia (Shin et al. 2006). In contrast, a pronounced increase of CBF is observed when SD is induced by increasing $[K^+]_{ext}$ in normal rats without hypoxia and hypoperfusion (Farkas et al. 2008; Ayata et al. 2004). In summary, SD lasts longer and has a pronounced effect on CBF when oxygen and blood flow are experimentally lowered to simulate post-ischemic CBF levels. Thus SD causes CBF variability which in turn can alter the properties of SD. By harvesting brain slices after MCAo in this thesis I was able to investigate SD in the absence of confounding blood flow and temperature fluctuations.

1.3 Experimental Rationale

1.3.1 Light Transmittance Changes (ΔLT)

Some intrinsic responses of live tissue can be recorded by using only a light source and a detector (Aitken et al. 1999). For example, neocortical slices reversibly swell with hypo-osmolality and shrink with hyperosmolality within a pathophysiological range (Andrew and MacVicar 1994). Light passes more easily through swollen neocortical slices which increases in light transmittance (Aitken et al. 1999; Andrew and MacVicar 1994; Fayuk et al. 2002), primarily the result of glial swelling (Andrew et al. 2007). Conversely, when glia shrink in a hypertonic bath solution they scatter light (Andrew et al. 1999; Andrew et al. 2007). These light transmittance changes (ΔLT) can be recorded and mapped in real time, which provides an advantage over electrodes that register voltages from only a limited number of points (Obeidat and Andrew 1998).

1.3.2 Δ LT and Electrophysiology During and After SD

As SD initiates and propagates, a front of increased LT is observed, attributed to swelling of astrocytes and neurons (Andrew et al. 2007) as they depolarize (Brisson and Andrew 2012; White et al. 2012). After the SD front passes, decreased Δ LT develops over tens of seconds (Anderson et al. 2005; Jarvis et al. 2001). This decreased Δ LT was correlated with beading of dendrites (Andrew et al. 2007; Risher et al. 2009; Jarvis et al. 1999). Once decreased Δ LT and acute neuronal damage occur in the wake of SD, the associated lost synaptic communication and membrane depolarization are irreversible (Anderson et al. 2005; Brisson and Andrew 2012; White et al. 2012). Some recovery of synaptic communication along with attenuated light scattering is observed when OGD-induced SD is delayed by drug pre-treatment (Anderson et al. 2005). In SD-resistant neuronal subpopulations in the lower brain there is also attenuated light scatter and better recovery of membrane potential (Brisson and Andrew 2012). Brain tissue Δ LT is a good indicator of SD initiation and propagation, as well as neuronal injury indirectly measured as the light scattered by beading dendrites.

Certain dyes bind to cellular membranes and increase fluorescence electrical potential decreases, thereby identifying neuronal depolarization with high temporospatial resolution. These 'voltage-sensitive' dyes can be used to indicate localized changes in membrane potential over short time periods (Grinvald and Hildesheim 2004). The response of the dye mimics an intracellular recording (Grinvald et al. 1982). When direct intracellular recordings are observed in vivo, along with voltage-sensitive dye imaging, it is clearly evident that the dye signal displays changes in membrane potential (Petersen et al. 2003).

Voltage-sensitive dyes have verified that KCl and ischemia-induced SD occurs along with a propagating membrane depolarization along with a spreading DC shift across large cortical areas

with depression of cortical activity (Farkas et al. 2008). Similar membrane depolarization occurred during SD induced by ischemia, however the depression of cortical activity was more prolonged (Nedergaard and Hansen 1993). These studies demonstrated that membrane depolarization coincides with a propagating SD wavefront in successive clusters of neurons.

1.3.3 Post-Ischemic Electrophysiology

There are few investigations recording the single cell electrophysiology of post-ischemic neurons. Using the whole-cell patch-clamp technique, the membrane potential and the action potential threshold, duration and amplitude can be measured. When ‘step’ current pulses are applied to a neuron, additional parameters can be measured including the hyperpolarization observed shortly after multiple action potentials, called the ‘fast afterhyperpolarization (fAHP)’. Another parameter is the latency of the membrane potential to decay and approach the resting membrane potential following a hyperpolarizing pulse, measured as the ‘time constant’ (Gao et al. 1999, Hille 2001). Using brain slices harvested after MCAo, we measured the threshold, duration and width of action potentials, the fAHP following a train of action potentials and the time constant after a hyperpolarizing pulse in post-ischemic neocortical pyramidal neurons. We also determined the whole cell input resistance derived from the membrane voltage response to a family of hyperpolarizing and depolarizing current pulses. There have been many investigations of intrinsic neuronal properties and synaptic communication during and after SD but few studies in the post-ischemic brain.

1.4 In Vivo Ischemia and Brain Slice Models

1.4.1 Global Ischemia

Global ischemia most often results from CBF interruption during sudden cardiac arrest. To simulate the profile of CBF disruption that occurs during sudden cardiac arrest, the four major blood vessels supplying the brain are simultaneously occluded for 30 minutes or less (Pulsinelli and Buchan 1988; Lipton 1999). Infarction is mainly studied in the CA1 region of the hippocampus beyond 12 hours following ischemia (Lipton 1999). Four vessel occlusion provides a convenient model with reproducible lesion volume within the CA1 of the hippocampus (Lipton 1999) that enables reliable direct comparison between control and experimental groups. Among the few investigations that have examined electrophysiology in the post-ischemic brain, intact synaptic communication and single cell recordings were observed in the hippocampus 5 to 42 hours following ischemia using this model (Gao et al. 1998; Gao et al.1999).

1.4.2 Focal Cerebral Ischemia

Focal stroke most commonly results from middle cerebral artery occlusion (MCAo). Rodent models of MCAo attempt to mimic this focal ischemia that occurs in humans. This technique originally devised by Koziumi (1986) and adapted by Longa (1989) has variable infarct volume caused by interstrain differences in neurovascular architecture, animal to animal variation in collateral blood supply and discrepancies in core body temperature during/after ischemia (Maeda et al. 1999; McColl et al. 2004; Barber et al. 2004). Barber and colleagues (2004) refined the MCAo technique further by implementing non-invasive core body temperature regulation. They also used the C57BL6 mouse strain that has less collateral circulation and larger infarct volumes

than other strains (Maeda et al. 1999; Fujii et al. 1997) and more closely resembles human blood vessel distribution. Infarct volume is less variable in C57BL6 mice subjected to MCAo when temperature is controlled. However, CBF fluctuations remain after reperfusion (Barber et al. 2004).

1.4.3 Brain Slice Model

Neocortical brain slices allow for experimentation upon brain tissue in a stable and controlled ionic medium in the absence of CBF and respiratory fluctuations. Imaging light transmittance responses of the entire brain slice as well as recording single-cell electrophysiology and synaptic communication are possible using the brain slice preparation (Lipton 1999). By replacing oxygenated aCSF with saline lacking glucose and oxygen (i.e. OGD), physiological effects of lost CBF are simulated and SD is evoked (Anderson et al. 2005; Douglas et al. 2011; Obeidat and Andrew 1998). But with the brain slice technique, single cell electrophysiology, synaptic communication as well as tissue swelling and damage can be more easily observed in real time before, during and after metabolic challenge. An additional caveat to brain slices is that SD cannot be visualized in three dimensions. However, the latency to SD onset, propagation rate and initiation site can be quantified and localized as well as the expanding sequence of regions involved and resultant damage or recovery of areas affected by SD can be imaged and recorded (Obeidat and Andrew 1998). By harvesting brain slices after MCAo, we can observe electrophysiology and tissue changes of the post-ischemic brain in response to further metabolic stress. We can also assess the efficacy of drugs that delay SD onset and promote recovery of synaptic communication after OGD in the post-ischemic brain.

1.5 Overview of Manuscripts

1.5.1 Reduced propensity for spreading depolarization in the mouse neocortex immediately following focal cerebral ischemia.

Recurring SD spontaneously erupts in the first 1-2 hours following arterial occlusion. The duration of SD is prolonged near the ischemic core and is shorter in non-ischemic cortex (Dijkhuizen et al. 1999; Nedergaard and Hansen 1993). With repeated post-ischemic SD, brain areas with irreversible reductions in ATP and tissue damage expand (Busch et al. 1996; Takano et al. 1996). The territory of irreversibly compromised tissue expands in a stepwise fashion following each SD event (Busch et al. 1996; Takano et al. 1996). Although SD incidence is high in the initial 1-2 hours following ischemia, it declines thereafter (Back et al. 1994; Back et al. 1996; Koroleva and Bures 1996; Dijkhuizen et al. 1999; Hartings et al. 2003). Regardless of whether reperfusion or continued ischemia occurs, a quiescent phase of decreased SD incidence is evident 2-6 hours after ischemia (Hartings et al. 2003). Although many studies have investigated the post-ischemic brain in the initial 1-2 hours and beyond 24 hours after ischemia, few studies have examined the post-ischemic brain between 2-24 hours after ischemia.

In Part I of this thesis, I investigate the initiation and propagation of SD during the 1-5 hour post-ischemic epoch in coronal neocortical slices harvested immediately after 30 min MCAo. Observations of SD in the coronal plane in the post-ischemic brain were only possible previously using digitally-reconstructed images with low resolution (Busch et al. 1996). With our technique we can observe SD as it traverses through ischemic ‘core’ brain areas with residual CBF of < 20% of baseline (e.g. striatum, temporal and lateral parietal neocortex) as well as ‘penumbra’ neocortex with CBF declines between 20-40% of baseline CBF (e.g. medial parietal neocortex) (Belayev et al. 1997). By observing SD in neocortical brain slices, we can directly observe the

latency to SD onset and the propagating SD wavefront speed in the coronal plane. We also can observe and quantify the ΔLT caused by increased swelling as the SD wavefront propagates and the decreased ΔLT in the wake of SD induced by dendritic beading (Andrew et al. 2007; Anderson et al. 2005; Brisson and Andrew 2012).

SD incidence and damage can be decreased by drug treatment. Spontaneous and KCl-induced post-ischemic SD incidence are reduced along with decreased infarct volume by glutamate receptor antagonists. The glutamatergic NMDA receptor antagonist MK-801 decreases infarct volume and SD incidence (Iijima et al. 1992; Park et al. 1988; Hatfield et al. 1992). However MK-801 induces mild hypothermia (Corbett et al. 1990; Buchan and Pulsinelli 1990) and hypothermia by itself can decrease SD incidence and infarct volume (Zhang et al. 1993; Chen et al. 1993). When temperature is tightly controlled, MK-801 does not decrease infarct volume (Corbett et al. 1990; Buchan and Pulsinelli 1990). In addition, when neocortical brain slices are superfused with OGD saline in a temperature-controlled bath SD onset is not altered by NMDA antagonists and synaptic communication does not recover after SD (Jarvis et al. 2001; Anderson et al. 2005). The drugs carbetapentane (CP) and dibucaine (DB) delay the latency to SD onset and promote recovery of synaptic communication and membrane potential following OGD superfusion of neocortical brain slices (Anderson et al. 2005; Douglas et al. 2011; White et al. 2012). Dibucaine increases the action potential threshold and carbetapentane increases the magnitude and duration of the slow afterhyperpolarization resulting in decreased action potential frequency with both drugs (White et al. 2012). These subtle alterations of neuronal electrophysiology by CP and DB likely contribute to the delayed onset of SD and increased likelihood of recovery of synaptic communication thereafter. In experiments within Part I of the

thesis, we examine the effectiveness of CP and DB to delay the latency to OGD-induced SD onset in neocortical slices harvested immediately following 30 min MCAo.

There are few investigations examining synaptic communication and single cell electrophysiology in the post-ischemic brain. Most of the experimental models used to examine post-ischemic single-cell electrophysiology used global ischemia induced by 4-vessel occlusion which approximates clinical global ischemia following cardiac arrest. Gao and colleagues (1998 and 1999) applied global cerebral ischemia for 60 minutes and observed intact single cell electrophysiology and synaptic communication at 5 hours post-ischemia in regions known to be most adversely affected by the injury. These observations following global ischemia warrant further investigation within a MCAo model that produces focal cerebral ischemia (Barber et al. 2004), which models the most prevalent form of human embolic stroke in the clinic. In Part I of this thesis, we examine single cell electrophysiology and synaptic communication in post-ischemic neocortical slices.

1.5.2 Spreading depolarization in the mouse neocortical brain slices immediately after middle cerebral artery occlusion compared to 12 hours later.

External potassium ($[K^+]_{ext}$) rises within minutes after ischemia onset (Nedergaard and Hansen 1993). Just prior to SD initiation $[K^+]_{ext}$ slowly approaches ~ 10 mM (Heinemann and Lux 1977) then abruptly spikes to > 60 mM during SD (Nedergaard and Hansen 1993). After ischemia, SD has a slower profile of $[K^+]_{ext}$ elevation in comparison to non-ischemic neocortex (Nedergaard and Hansen 1993). When SD is triggered in the post-ischemic brain by KCl, expansion of lesion volume occurs (Busch et al. 1996; Takano et al. 1996; Back et al. 1996). In contrast, when KCl is topically applied to non-ischemic neocortex SD is abrupt and non-damaging (Nedergaard and Hansen 1988). SD initiates when 9.7 mM $[K^+]_{ext}$ saline is superfused

upon neocortical brain slices (Tanaka et al. 1997). Direct comparison of SD_{K^+} in non-ischemic and ischemic neocortex is enabled by superfusing post-ischemic brain slices with 9.7mM $[K^+]_{ext}$.

During ischemia, extracellular glutamate elevates ~4-7-fold above baseline (Morimoto et al. 1996; Sciotti et al. 1992; Globus et al. 1988; Hagberg et al. 1985). An increase of $[glu]_{ext}$ during anoxia and ischemia-induced SD has also been observed (Satoh et al. 1999; Iijima et al. 1998) which is not surprising given the degree of neuronal depolarization. Furthermore, during OGD in neocortical brain slices, application of 10 mM $[K^+]_{ext}$ or 3 mM $[glu]_{ext}$ accelerates SD onset (Tanaka et al. 1997). Although glutamate release occurs along with the propagating SD wavefront (Zhou et al. 2013), directly applying glutamate in normal brain slices only produces slow general swelling of brain tissue (Polischuk and Andrew 1996; Obeidat and Andrew 1998). This swelling is not the characteristic SD wave of tissue swelling propagating 2-5 mm/min SD wave of tissue swelling that traverses through the entire cortex induced by ischemia, OGD, $[K^+]_{ext}$ or ouabain (Tanaka et al. 1997; Anderson and Andrew 2002; Dietz et al. 2008; Anderson et al. 2005; Dohmen et al. 2008). It is generally accepted that glutamate release promotes normoxic SD but is not required for acute damage to develop following ischemic SD both in vivo (Murphy et al. 2008) or in brain slices (Anderson et al. 2005). The effect of elevated $[glu]_{ext}$ upon the post-ischemic brain can be examined by superfusing brain slices harvested after MCAo with experimental saline.

OGD causes irreversible damage in normal neocortical brain slices (Obeidat and Andrew 1998; Anderson and Andrew 2002; Anderson et al. 2005). Persistent, terminal depolarization as well as morphological damage is evident in neocortical brain slices after OGD-induced SD (Anderson et al. 2005; Andrew et al. 2007; White et al. 2012) which imitates the prolonged depolarization after ischemia-induced SD (Dijkhuizen et al. 1999). Superfusion of post-ischemic

neocortical brain slices with OGD saline simulates the pronounced hypoperfusion within the ischemic core.

The post-ischemic brain undergoes periods of spontaneous SD eruption interspersed among epochs of quiescence. Immediately following ischemia, frequent spontaneous SD events occur for 1-2 hours. After this initial phase of recurrent SD, a period of diminished SD activity is observed (Dijkhuizen et al. 1999; Koroleva and Bures 1996; Back et al. 1996). Following 4-6 hours of few, if any SD events, a late secondary phase of spontaneous SD events ensues regardless of reperfusion (Hartings et al. 2003).

The frequency of SD events in the late secondary phase of SD eruption is correlated with infarct expansion (Hartings et al. 2003). Infarct maturation and SD initiation vary after ischemia. Therefore, we examined the morphology, synaptic communication and single cell electrophysiology of layer II/III neocortical pyramidal neurons both immediately and 12 hours following MCAo. We also superfused elevated $[K^+]_{ext}$, elevated $[glu]_{ext}$ and OGD saline solutions upon brain slices harvested immediately, and 12 hours after, 30 min MCAo. With this technique the baseline electrophysiology, morphology and response of the post-ischemic brain to further metabolic stress can be observed as infarct maturation ensues without confounding CBF fluctuations.

1.5.3 Post-ischemic resistance to spreading depolarization.

For 1-2 hours following ischemia, SD recurs but declines in frequency shortly thereafter for 3-6 hours (Back et al. 1996; Dijkhuizen et al. 1999; Nallet et al. 1999; Koroleva and Bures 1996). Then there is another phase of increased SD incidence 12-18 hours after ischemia with or

without reperfusion (Hartings et al. 2003), indicating suppressed excitability during this period (Nallet et al. 1999).

Our experiments specifically address the suppression of post-ischemic excitability. During global ischemia post-ischemic suppression of synaptic communication was observed to reverse by adenosine A1 receptor antagonism using dipropylcyclopentylxanthine (DPCPX) (Ilie et al. 2006). The involvement of adenosine in suppression of excitability following ischemia seems plausible considering that adenosine concentration increases relative to other metabolites (Phillis et al. 1991). Longer duration SD has been correlated with a) greater adenosine release following ischemia (Lindquist and Shuttleworth 2014); and b) closer proximity to ischemic territory with reduced CBF (Dijkhuizen et al. 1999; Mies 1997). Thus changes in post-ischemic SD mediated by adenosine might be reversed with adenosine A1 receptor antagonism. In part III of this thesis, we examine the effects of DPCPX upon post-ischemic OGD-SD.

Post-ischemic synaptic failure is more sensitive to reduced CBF than is disruption of ion homeostasis (Hossmann 1994) leading to SD. Considering that the Na^+/K^+ pump is involved with resting membrane potential equilibrium and SD (Dreier et al. 2013), any post-ischemic modification of the pump could affect SD. At low concentrations (0.1-1.0 μM), ouabain increases Na^+/K^+ pump activity (Gao et al. 2002) and decreases damage of cultured neurons deprived of oxygen and glucose (Oselkin et al. 2010). In contrast, high (30-100 μM) doses of ouabain induce a large inward depolarizing current (Gao et al. 2002) and SD (Anderson et al. 2005; Tanaka et al. 1997). The effect of ouabain at high and low doses upon SD in post-ischemic brain slices was examined in part III of this thesis.

1.6 Overall Objectives

I) Demonstrate that the post-ischemic neocortex has an altered swelling response to further metabolic stress that varies considerably 12 hours following a 30 minute MCAo, as compared to shortly after MCAo.

II) Show that the post-ischemic MCAo core displays essentially intact neuronal morphology and electrophysiology immediately following reperfusion, whereas 12 hours later the core is devastated. Despite this we search for and find some pyramidal neurons that appear only minimally injured.

III) Demonstrate that some aspects of ischemic stress to the post-ischemic mouse neocortex can be reversed.

Chapter 2

Reduced propensity for spreading depolarization in the mouse neocortex immediately following focal cerebral ischemia

2.1 Summary

A spreading depolarization (SD) wave of ionic disruption occurs after ischemia and evokes swelling of neurons and glia that can lead to neuronal death. SD also elicits beading of dendrites, loss of synaptic function and, if recurrent, expands the brain territory compromised by ischemia. By harvesting neocortical slices immediately after a 30 minute middle cerebral artery occlusion (MCAo), we were able to quantify and compare differences in latency to SD onset, the speed of the propagating SD wavefront. We also measured tissue light transmittance changes (ΔLT) during and after SD in non-ischemic and ischemic neocortex. The brain slice technique provides an isolated experimental environment to test the effect of drugs (such as dibucaine and carbetapentane) upon SD in the post-stroke brain in the absence of inherent cerebral blood flow and temperature fluctuations. It also allowed examination of synaptically-evoked excitability of the neurons in layers II-III of the cerebral cortex as well as the intrinsic neurophysiology of single neocortical pyramidal cells in the immediate post-stroke brain. In this investigation we found delayed SD onset and a slower SD propagation rate induced by OGD in the ischemic hemisphere compared to the non-ischemic hemisphere. The ischemic hemisphere also displayed viable synaptic communication together with intact pyramidal cell electrophysiology and morphology. Carbetapentane and dibucaine effectively delay SD onset in the immediately post-ischemic brain, similar to neuroprotection demonstrated during OGD superfusion of non-ischemic rat neocortical brain slices. These results demonstrate not only evidence of viability of

the post-ischemic brain, but a possible resistance to damaging events such as SD that can be augmented by carbetapentane and dibucaine.

2.2 Introduction

Stroke is the second leading cause of disability in the world. According to the World Health Organization, 15 million people worldwide suffer a stroke every year and nearly six million die. For the five million people that are left permanently disabled, the quality of life after the disease is severely impaired. Unfortunately attempts to salvage brain areas compromised by stroke have resulted in many failed clinical trials (O'Collins et al. 2006). One mechanism of stroke injury that was overlooked in these trials was the onset of a spreading wave of depressed neural activity that includes swelling of brain tissue and ensuing neuronal damage called 'spreading depolarization' (SD) (Dreier 2011; Pietrobon and Moskowitz 2014). Recurring SD following ischemia is associated with increased metabolic compromise and brain tissue damage (i.e. infarction) over the hours following ischemia onset (Busch et al. 1996; Hartings et al. 2003; Takano et al. 1996; Dijkhuizen et al. 1999; Mies et al. 1994).

Infarct expansion in vivo is correlated with increased spontaneous SD incidence (Hartings et al. 2003; Mies et al. 1994; Takano et al. 1996; Dijkhuizen et al. 1999) along with a stepwise decrease in CBF (Shin et al. 2006). Recurring post-ischemic SD waves induced with KCl or electrical stimulation travel across ischemic neocortex and expand the territory of metabolic compromise and infarction in neocortex and striatum (Busch et al. 1996; Takano et al. 1996; Back et al. 1996). Post-ischemic SD incidence tends to erupt in phases interspersed with quiescence (Dijkhuizen et al. 1999; Hartings et al. 2003), further adding to the inherent variability of SD in the post-stroke brain. Post-ischemic SD also induces a sequential stepwise

decrease of residual CBF (Shin et al. 2006; Bere et al. 2014). Furthermore, the properties of SD are altered when CBF perfusion pressure is manipulated in control animals (Sukhotinsky et al. 2010). Thus, SD incidence is variable and confounded by CBF fluctuations during in vivo ischemia.

During SD induced by oxygen-and-glucose deprivation (OGD) in neocortical slices, increased light transmittance (LT) (Douglas et al. 2011; Jarvis, Anderson and Andrew 2001) correlates with glial and neuronal swelling (Andrew et al. 2007), whereas reduced LT following the initial spread of swelling/depolarization represents dendritic beading which scatters light. In neocortical slices dibucaine (DB) and carbetapentane (CP) delay the latency to OGD-induced SD onset, reduce light scatter by dendritic beading and promote recovery of synaptic communication after reperfusion with normoxic aCSF (Douglas et al. 2011; Anderson et al. 2005). In this investigation, we examine the effect of CP and DB upon SD in the post-ischemic brain independent of CBF fluctuations.

Few studies have characterized the properties of ischemic neocortex immediately following ischemia. Here we remove the brain immediately after a 30 minute middle cerebral artery occlusion (MCAo) (Longa et al. 1989; Barber et al. 2005). We then incubated the coronal brain slices in aCSF. We examine synaptically-evoked excitability of neocortical layers II-III, the intrinsic neurophysiology of single pyramidal cells and their morphology of neurons in the immediate post-ischemic brain. We also quantify and compare differences in latency to SD onset, the speed of the propagating SD wavefront and light transmittance changes (Δ LT) during and after SD between non-ischemic and ischemic neocortex.

2.3 Materials and Methods

Middle Cerebral Artery Occlusion and Brain Slice Preparation

Male C57/BL6 mice (20-25g) were anaesthetized using isoflurane (3% initial, 1% to 1.5% maintenance) in O₂ and air (80%:20%). The animal remained under general anesthesia for the duration of the surgical procedure, with time under anesthesia approximately 80-90 minutes. Focal cerebral ischemia was then induced by intraluminal occlusion of the left middle cerebral artery (MCAo). After 30 min MCAo, the anaesthetized mice were decapitated with a guillotine. Following craniotomy, the brain was quickly removed and immersed in ice-cold and oxygenated (95 % O₂, 5 % CO₂) artificial cerebral spinal fluid (aCSF) composed of (in mM) 240 sucrose, 3.3 KCl, 26 NaHCO₃, 1.3 MgSO₄·7H₂O, 1.23 NaH₂PO₄, 11 D-glucose and 1.8 CaCl₂. The aCSF osmolality was adjusted to 310 mOsm using mannitol and pH was 7.4. Using a Leica 1200-T vibratome, 350 μm coronal brain slices were cut in the sucrose aCSF through the coronal plane between Bregma levels 1.2 to -1.34 and then incubated in regular aCSF (equimolar NaCl replacing sucrose above) at 34°C for at least 1 hour and up to 5 hours prior to experimentation. Slices were then transferred to a recording/imaging chamber where they were submerged in flowing aCSF (3.5 ml/min.) at 34°C ± 0.5°C.

Imaging Changes in Light Transmittance (ΔLT) During OGD

Slices were transferred to a recording/imaging chamber on an inverted microscope (Axoscope 2FS, Zeiss) with a 10x objective lens and an additional zoom lens that can adjust magnification by 0.5-1.6 X to fit the coronal section to entirely fit within the field of view. The brain slices were submerged in flowing aCSF (3.5 ml/min.) at 34°C ± 0.5°C. Video frames were acquired using a cooled charge-coupled device (CCD) that was set at maximum gain and medium black

level (Hamamatsu C4742) controlled by Imaging Workbench 6 software (Indec Biosystems Inc.). The CCD gamma level was set to 1.0 so that the CCD output was linear with respect to changes in light intensity. Frames acquired at 30 Hz were averaged and digitized using a frame grabber (DT 3155, Data Translation). The first image of the series was the control transmittance (T_{cont}) which was subtracted from each of the subsequent images (T_{exp}) in the series. The difference signal was normalized by dividing by T_{cont} , which varies across the slice depending on the zone sampled. For example, T_{cont} was lower in white matter than gray matter. This value was then presented as a percentage of the digital intensity of the control image of that series. That is, $\Delta LT = [(T_{exp} - T_{cont}) / T_{cont}] \times 100 = [\Delta T / T] \%$. The change in LT was displayed using a pseudocolour intensity scale. The slice image in bright field was displayed using a gray intensity scale. OGD solution was superfused onto the brain slices in the bath chamber. The OGD aCSF was of similar composition to control aCSF, except for substituting of 95 % O₂/5 % CO₂ bubbling of aCSF with 95 % N₂/5 % CO₂. In addition, 11 mM glucose was reduced to 1 mM glucose with osmotic adjustment using NaCl. Peak ΔLT during OGD has previously been associated with maximal tissue swelling, while the ensuing nadir indicates dendritic beading (neuronal damage) causing light scattering in the wake of SD. This beading is generally not reversible in acute brain slices. ΔLT was imaged and quantified in the ipsi- and contralateral hemispheres in post-ischemic brain slices pre-incubated with oxygenated aCSF for at least one hour or with 20 min pre-incubation of 10 μ M dibucaine (DB) or 30 μ M carbetapentane (CP).

Electrophysiology

Whole Cell Patch Clamp: Visually guided whole-cell patch recordings were obtained using micropipettes pulled from borosilicate glass (outside diameter 1.2 mm, inside diameter 0.68 mm;

World Precision Instruments) to a resistance of 4-6 M Ω . The internal pipette solution contained (in mM) 125 K- gluconate, 10 KCl, 2 MgCl₂, 5.5 EGTA, 10 HEPES, 2 Na-ATP and 0.1 CaCl₂ (pH was adjusted to 7.3 with KOH). Neurons were visualized using near-infrared illumination and Dodt gradient contrast optics (Luigs and Neumann, Ratingen, Germany) through an upright microscope (Axoscope 2FS, Zeiss) with a 10x immersion objective lens. All recordings were acquired in whole cell current clamp mode of an Axoclamp 2A amplifier and a Digidata 1322 A/D converter. Clampex 10.2 software was used for data acquisition with subsequent analysis using Clampfit 10.2 software. Resting membrane potential was measured by patch clamping neocortical pyramidal neurons with whole cell configuration in neocortical LII/III in the ischemic and non-ischemic hemispheres. Action potential width, amplitude and threshold were measured from the second action potential elicited during current pulses increased stepwise by 0.1 nA (200 ms, -0.4 to 0.4 nA). The action potential threshold was measured as the beginning of the upstroke of the action potential. Action potential width was measured (in milliseconds) as the time between the beginning of the action potential upstroke and the point at which the ‘downstroke’ reached the same membrane potential as the initial action potential threshold. Action potential amplitude was measured from the beginning of the upstroke to the corresponding peak membrane depolarization. The whole cell time constant of ischemic and non-ischemic neocortical pyramidal neurons were derived from a ‘curve-of-best-fit’ of exponential decay of the membrane potential following a hyperpolarizing pulse of the stepped current pulses (200 ms, -0.1 nA) using data analysis program Clampfit 10.2 (Molecular Devices, Inc.). Fast afterhyperpolarizations (fAHP) were measured as the deviation from the beginning of the upstroke of an action potential within 5 ms after the peak of a single spike that follows individual action potentials in neocortical pyramidal neurons. Input resistance (R_{in}) was derived

from the linear portion of the current-voltage plot 170 ms from the beginning of constant current pulses increased stepwise by 0.1 nA from -0.4 to ~ 0.1 nA.

Evoked Synaptic Responses: To record field potentials of evoked EPSPs, a micropipette (2–4 M Ω) was pulled from thin-walled capillary glass, filled with 200 mM NaCl, and mounted on a three dimensional (3-D) micromanipulator. It was connected by a chloride-coated silver wire to an amplifier probe, and output was monitored on an on-line oscilloscope. The tip was placed in layers II/III of the neocortex and a concentric bipolar electrode (Rhodes Electronics) placed in layer VI to stimulate the immediate overlying layers. A current pulse (0.1-ms duration; 0.1 Hz) was applied at 50mV to produce an evoked response. The amplified signals were digitized, displayed, and plotted using pCLAMP software.

Statistical Analysis

A multiple comparisons ANOVA was used to assess the effect of drug treatment upon the latency to SD onset. Field EPSPs, baseline electrophysiological properties, latency to SD onset, speed of SD propagation and Δ LT during and after SD were compared in the ischemic vs. non-ischemic hemispheres of post-stroke brain slices using Student's t-tests. These parameters were expressed as mean \pm S.E.M.

Golgi-Cox Staining

Following 30 min MCAo, the mouse brains were extracted and immersed in freshly prepared impregnation solution. Brains were processed according to the protocol provided by *FD Neurosciences* using the FD Rapid GolgiStain kit (FD NeuroTechnologies 2012). Coronal brain sections cut at 50 microns thick were processed. The ischemic and non-ischemic hemispheres

were imaged with a 10 X objective to observe gross tissue morphology and with a 60 X objective higher magnification to observe individual neuronal morphology.

Neocortical Pyramidal Neurons Expressing Yellow Fluorescent Protein

The MCAo procedure was also applied to 30+ day-old C57 black mice of the B6.Cg-Tg (Thy1-YFP) 16Jrs/J strain. These mice have a proportion of pyramidal neurons that express yellow fluorescent protein (YFP) (Feng et al. 2000). The mouse was decapitated immediately after the 30 min MCAo while under anaesthetic and perfused with 30 mL of 0.9% saline followed by 30 mL of 4% paraformaldehyde in phosphate buffer solution. The head was then left under immersion fixation for 3 days. The brain was isolated and cut on a Leica VT1000S vibratome in the ice cold sucrose saline composed of (in mM) 240 sucrose, 3.3 KCl, 26 NaHCO₃, 1.3 MgSO₄·7H₂O, 1.23 NaH₂PO₄, 11 D-glucose and 1.8 CaCl₂. Sections were cut at 100 μm and mounted on superfrost slides, air dried and stored at 4 degrees. All slices were cut in coronal section and mounted on slides using glycerol/PBS or Fluoro-Gel with TES buffer. They were dried overnight in the dark. Images were taken with a Zeiss fluorescent microscope (Imager A1) with AxioVision software using excitation and emission filters appropriate for YFP.

2.4 Results

The viability of synaptic communication in the non-ischemic vs. ischemic hemispheres of brain slices harvested after MCAo was assessed. Stimulation of neocortical layer VI resulted in field EPSPs evoked in cortical layers II/III in the ischemic (0.4 ± 0.1 mV, n=11) and non-ischemic hemispheres (0.7 ± 0.1 mV, n=6) that were not significantly different ($p = 0.07$) as

shown in Figures 1C and 2. This provided support for intact synaptic communication in the ischemic hemisphere of brain slices harvested after 30 minute MCAo.

We then patch clamped pyramidal neurons of neocortical layer II/III pyramidal neurons in the ischemic or non-ischemic hemispheres. As seen at 40X magnification there were abundant pyramidal neurons in the ischemic hemisphere with normal morphology under contrast optics. Action potential width, amplitude and threshold were compared in ischemic and non-ischemic neocortical pyramidal neurons. As well, the fast afterhyperpolarization (fAHP) which followed a depolarizing pulse evoking a spike train was measured. None of these properties were significantly different between the two hemispheres as shown in Table 1 and representative electrophysiological traces (Figs. 1A, B). Resting membrane potential, whole cell input resistance and the time constant of membrane potential decay following a hyperpolarizing pulse were not significantly different between neurons in the ischemic hemisphere (n=21) and neocortical neurons in the non-ischemic hemisphere (n=16) as shown in Table 1 and Figure 1A.

Intact neocortical pyramidal neurons were evident in the ischemic hemisphere of YFP-expressing mouse brains harvested immediately post-MCAo. Pyramidal neurons expressing yellow-fluorescent protein (YFP) in neocortex within brain areas in the ischemic hemisphere known to be supplied by the occluded middle cerebral artery appeared similar to neurons within same areas in the non-ischemic hemisphere (Figure 1D).

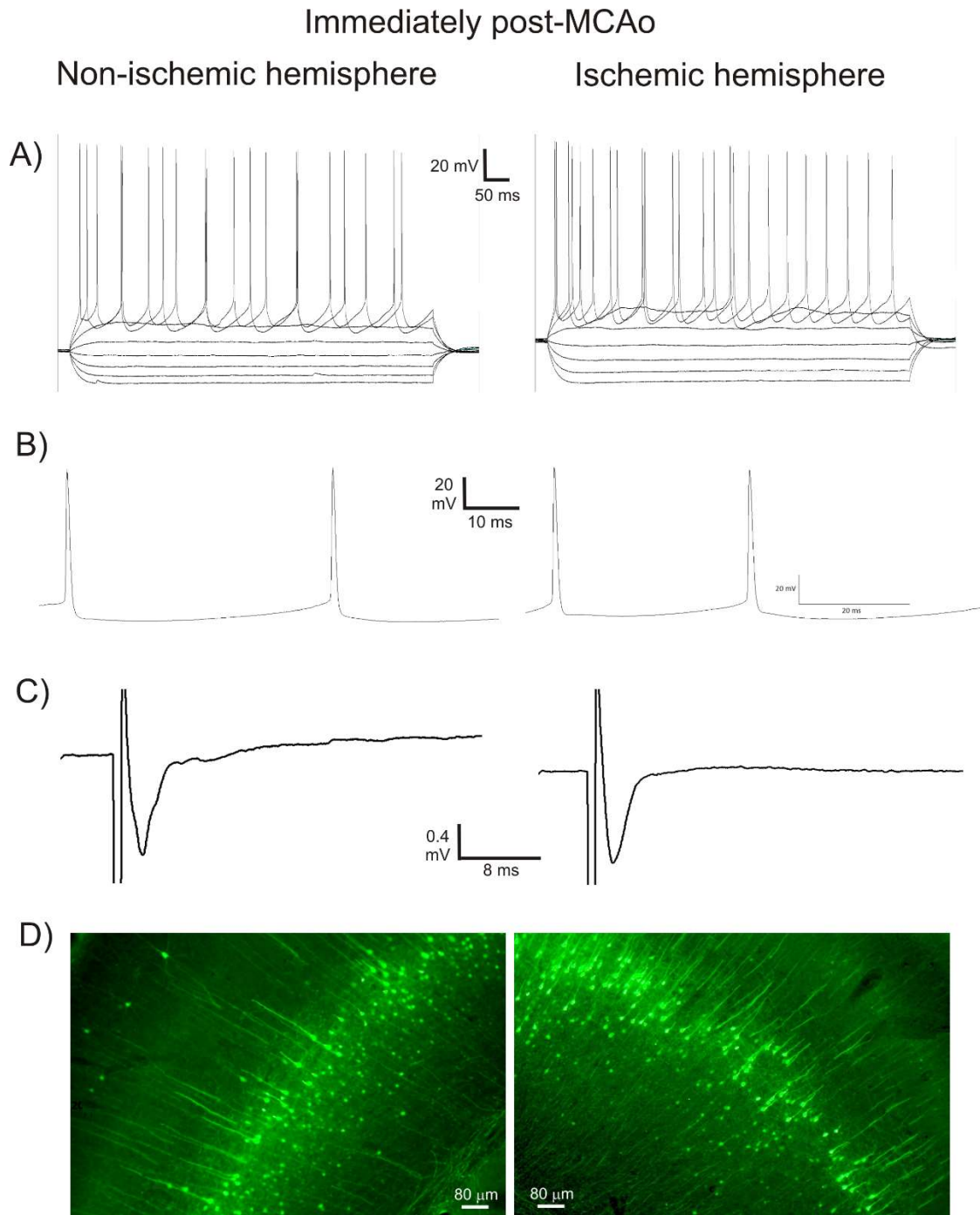


Figure 1. Baseline electrophysiological properties of whole-cell patched pyramidal cells and neuronal morphology were similar in the ischemic and non-ischemic hemispheres. (A) The input resistance (R_{in}), fast afterhyperpolarization (fAHP) and time constant (τ) obtained from a series of hyperpolarizing and depolarizing current steps were similar in the ischemic and non-ischemic hemispheres (see Table 1). (B) The action potential threshold, amplitude and width were similar in the ischemic and non-ischemic hemisphere. (C) The evoked synaptic responses were also similar in the two hemispheres. (D) Neuronal morphology was similar in both hemispheres in YFP expressing pyramidal neurons of the neocortex.

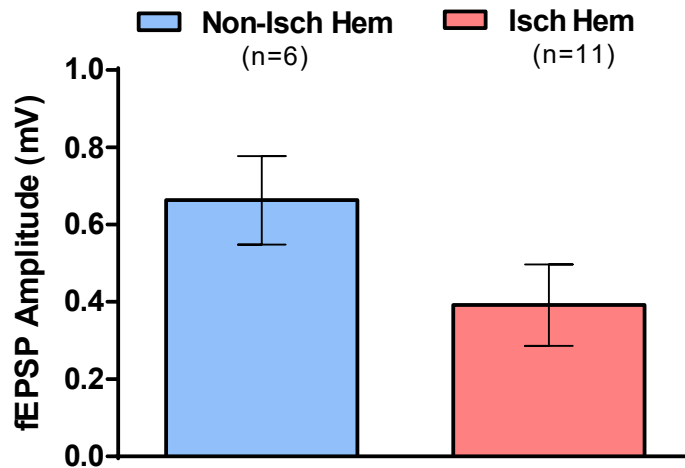


Figure 2. Evoked response in ischemic hemisphere after 50 mV stimulation was not significantly different between the ischemic and non-ischemic hemispheres. Field EPSPs evoked by 50 mV stimulation in the non-ischemic hemisphere (0.7 ± 0.1 mV, $n = 11$) and ischemic hemisphere (0.4 ± 0.1 mV, $n = 6$) of brain slices harvested immediately after 30 min MCAo were not significantly different ($p = 0.10$).

OGD resulted in SD initiation and propagation within both the ischemic and non-ischemic hemispheres of brain slices harvested immediately after 30 min MCAo. At SD onset, a focal increase in ΔLT appeared in neocortical gray and propagated outward from each focus. SD appeared to initiate at random stereotaxic locations within the neocortex of the previously ischemic hemisphere, similar to the non-ischemic hemisphere (Figure 3). SD waves initiated both peripherally or within neocortex associated with core CBF declines during MCAo. SD onset was significantly delayed in the ischemic hemisphere, occurring after 417 ± 19 seconds following OGD bath application compared to 297 ± 13 seconds in the non-ischemic hemisphere ($p < 0.001$, $n=31$) as shown in Figure 4.

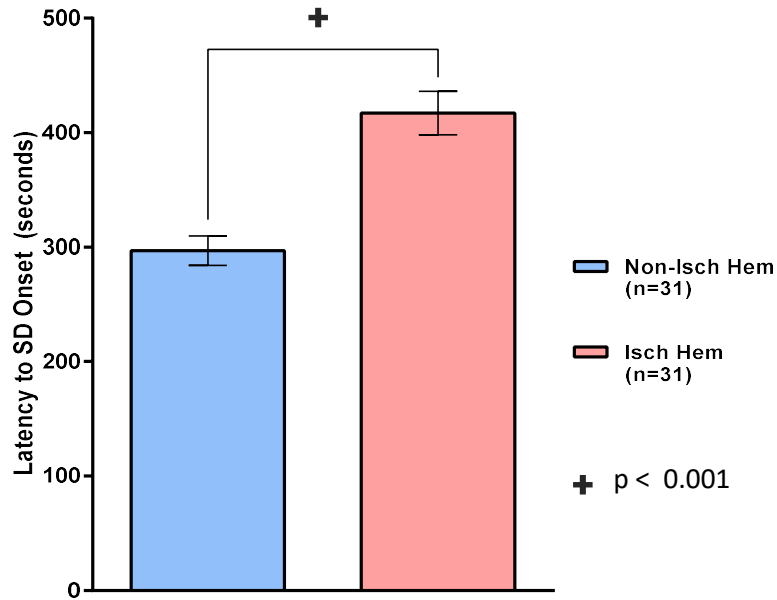


Figure 4. Latency to SD onset in the ischemic hemisphere (417 ± 19 sec) was significantly delayed compared to the non-ischemic hemisphere (297 ± 13 sec) ($p < 0.001$, $n=31$ slices each).

The SD wavefront propagated at an average of 2.6 ± 0.6 mm/min in the non-ischemic hemisphere but was significantly slower at 1.7 ± 0.5 mm/min in the ischemic hemisphere ($p < 0.01$, $n=5$) as shown in Figure 5. There was no significant difference between the mean peak Δ LT increase in neocortical layers II/III of the ischemic hemisphere and non-ischemic hemisphere ($4.2 \pm 0.7\%$ vs $5.3 \pm 0.7\%$ respectively, $p = \text{n.s.}$, $n=31$). However, the nadir in Δ LT (decreased LT associated with light scattering) in layers II/III of the ischemic hemisphere was significantly less than within the non-ischemic hemisphere ($-7 \pm 0.7\%$ vs $-10 \pm 0.8\%$ respectively, $p < 0.05$, $n=31$) as shown in Figure 6.

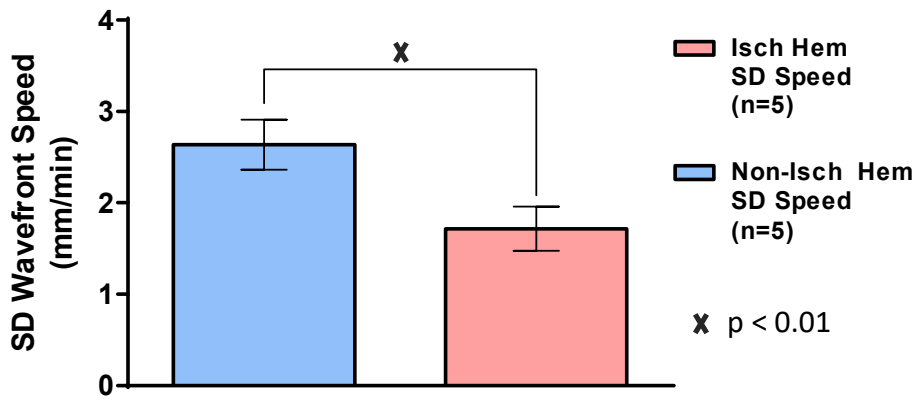


Figure 5. The SD wavefront speed in the ischemic hemisphere vs. the non-ischemic hemisphere was significantly slower (1.7 ± 0.5 mm/min vs. 2.6 ± 0.6 mm/min, $p < 0.01$, $n=5$).

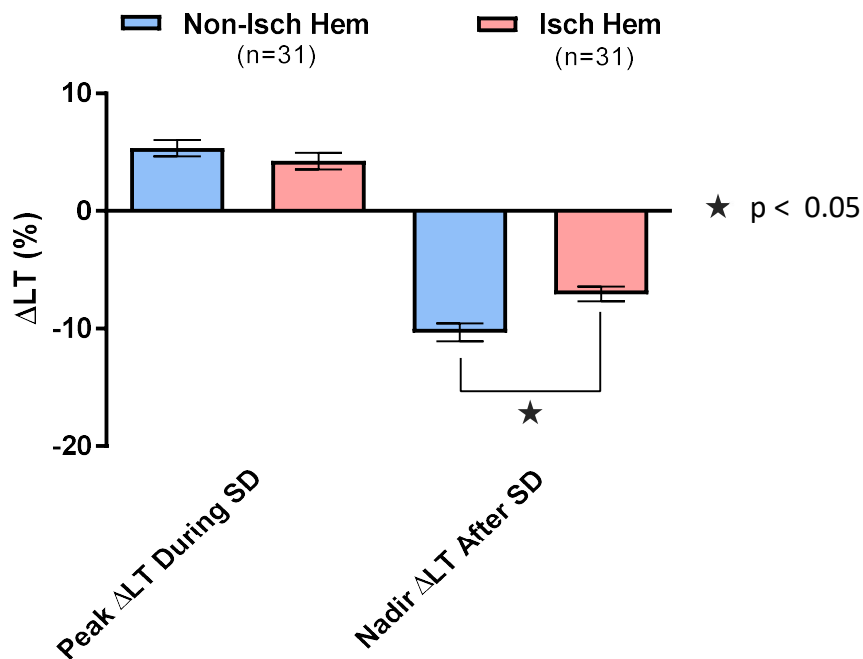


Figure 6. There is no difference between hemispheres in cell swelling during SD in regions where it is generated. There is significantly less light scatter in the ischemic hemisphere after OGD-induced SD. Percentage change of light scatter relative to baseline in two regions-of-interest in the ischemic hemisphere (-7 ± 0.8 %), vs. the non-ischemic hemisphere (-10 ± 0.8 %) were significantly less ($p < 0.05$, $n = 31$).

A multiple comparisons ANOVA was performed to test differences in SD onset as a function of hemisphere (within-subject factor) and drug (between-subject factor). The analysis revealed a significant main effect for drug pre-treatment upon latency to SD onset ($F = 15.03$, $p < 0.001$, partial $\eta^2 = .39$). *Post-hoc* one-way analysis of variances indicated that CP or DB significantly delayed the latency to SD onset in both hemispheres. Latency to SD onset in slices of the ischemic hemisphere pre-incubated with CP or DB prior to bath superfusion of OGD solution was 511 ± 32 and 527 ± 25 seconds, respectively ($n=9$ for each) as shown in Figure 7. A Student's *t* test revealed latency to SD onset was significantly delayed in comparison to the 417 ± 19 seconds latency to OGD-induced SD onset with post-MCAo brain slices incubated in aCSF alone ($p < 0.05$ and $p < 0.01$, respectively). The latency to SD onset in the non-ischemic hemisphere of post-ischemic brain was as follows: 410 ± 12 sec with CP pretreatment ($n = 9$); 405 ± 23 sec with DB pretreatment ($n = 9$); and 297 ± 13 sec with control aCSF pretreatment ($n=31$). Both CP and DB pretreatment induced significant delay relative to aCSF control ($p < 0.001$ and $p < 0.01$, respectively).

To search for morphological evidence of neuronal deterioration immediately following MCAo, three brains were sectioned following Golgi-Cox treatment. A qualitative comparison of both neocortical and striatal regions between hemispheres showed no obvious swelling, dendritic beading or necrosis of stained neurons throughout the ischemic hemisphere (Figures 8-10).

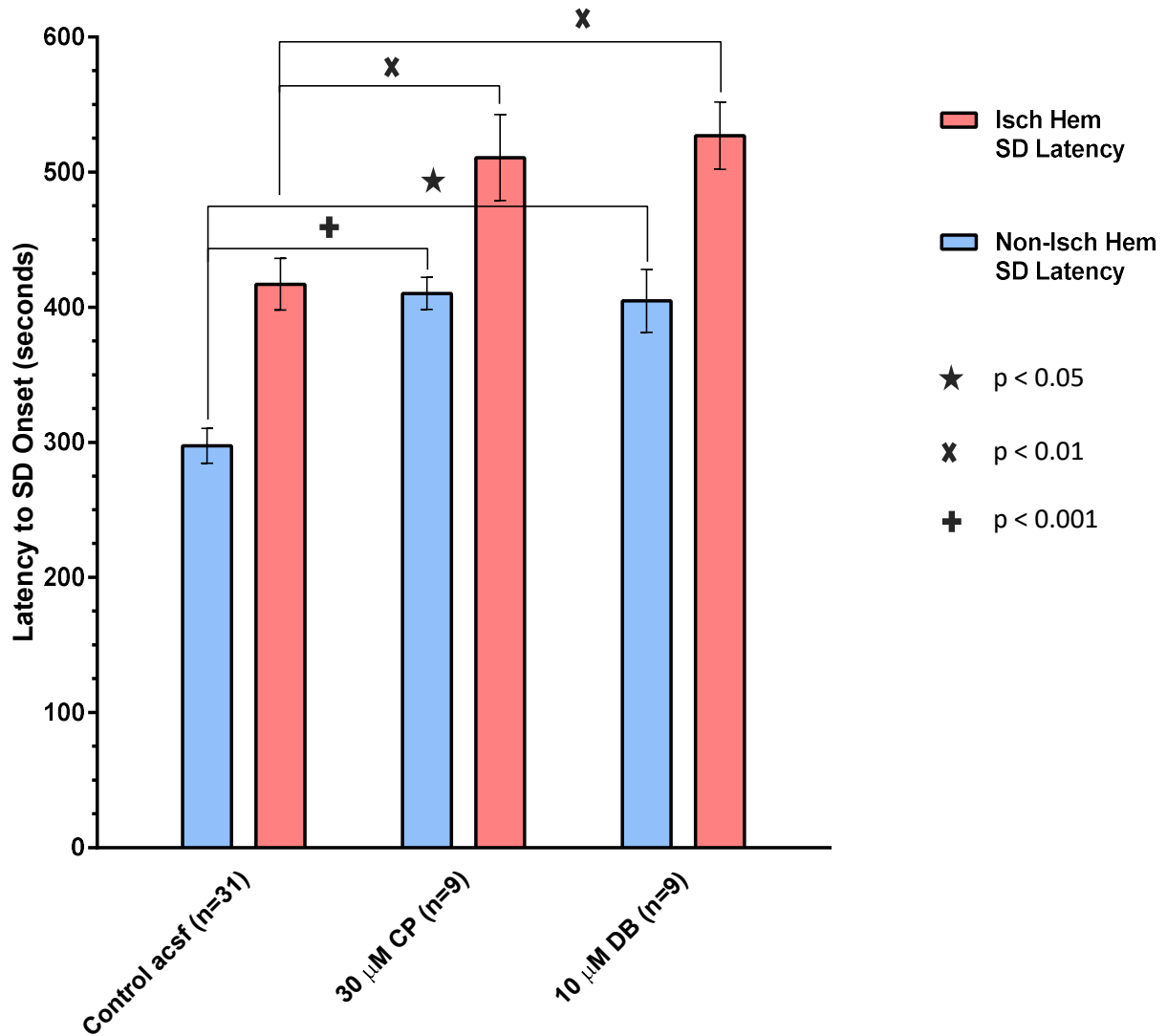


Figure 7. Carbetapentane (CP) and dibucaine (DB) significantly delay mean latency to SD onset in both the ischemic and non-ischemic hemispheres relative to control aCSF.

Latency to SD onset in the ischemic hemisphere of post-ischemic brain slices pre-incubated with CP (511 ± 32 sec, $n = 9$) and DB (527 ± 25 sec, $n = 9$) were significantly delayed ($p < 0.05$ and $p < 0.01$, respectively) relative to the ischemic hemisphere of control acsf incubated post-ischemic brain slices (417 ± 19 sec, $n = 31$). Similarly, SD onset in the non-ischemic hemisphere of post-ischemic brain slices pre-incubated with CP (410 ± 12 sec, $n = 9$) and DB (405 ± 23 sec, $n = 9$) were significantly delayed ($p < 0.001$ and $p < 0.01$, respectively) relative to SD onset in the non-ischemic hemisphere of control acsf incubated post-ischemic brain slices (297 ± 13 sec, $n = 31$).

Immediate post-MCAo Brain 2

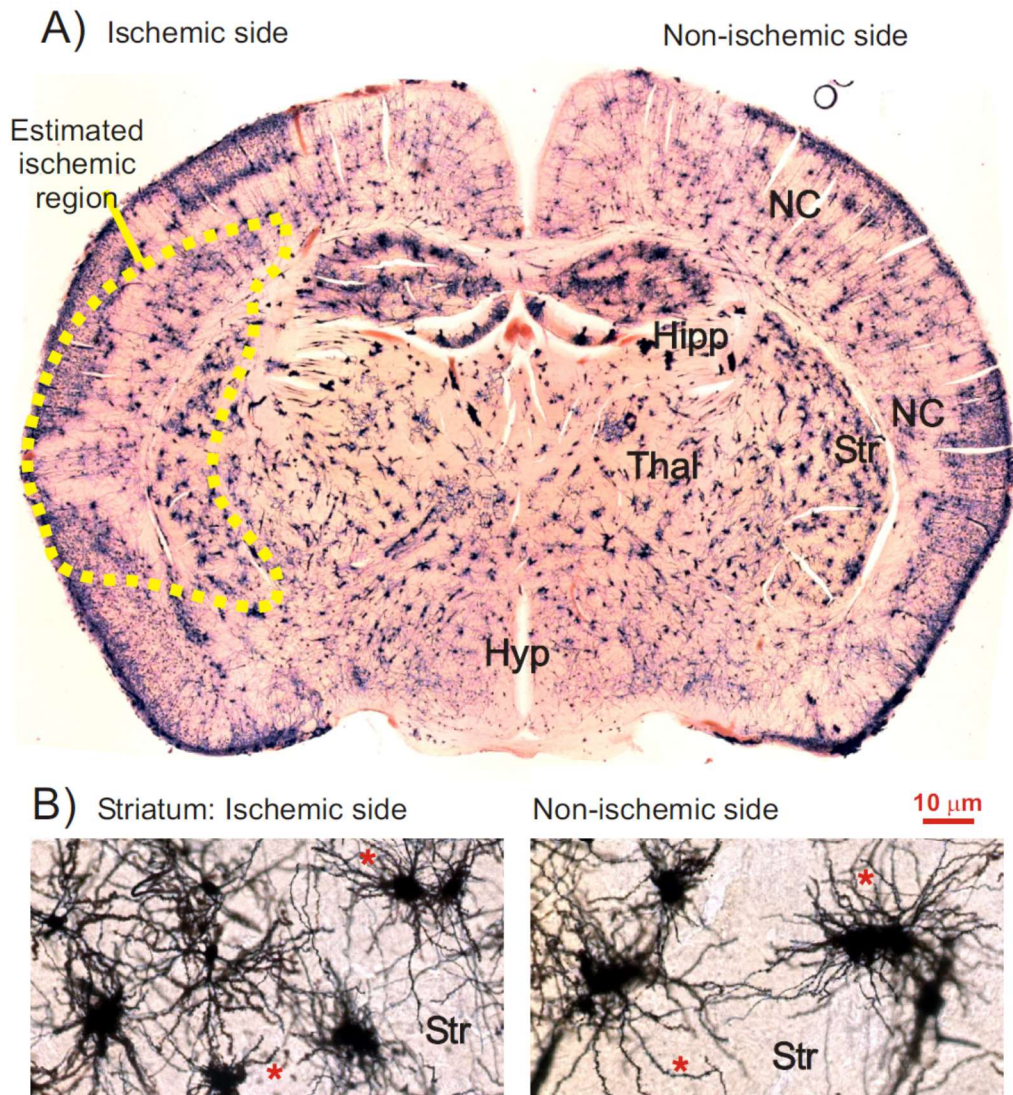
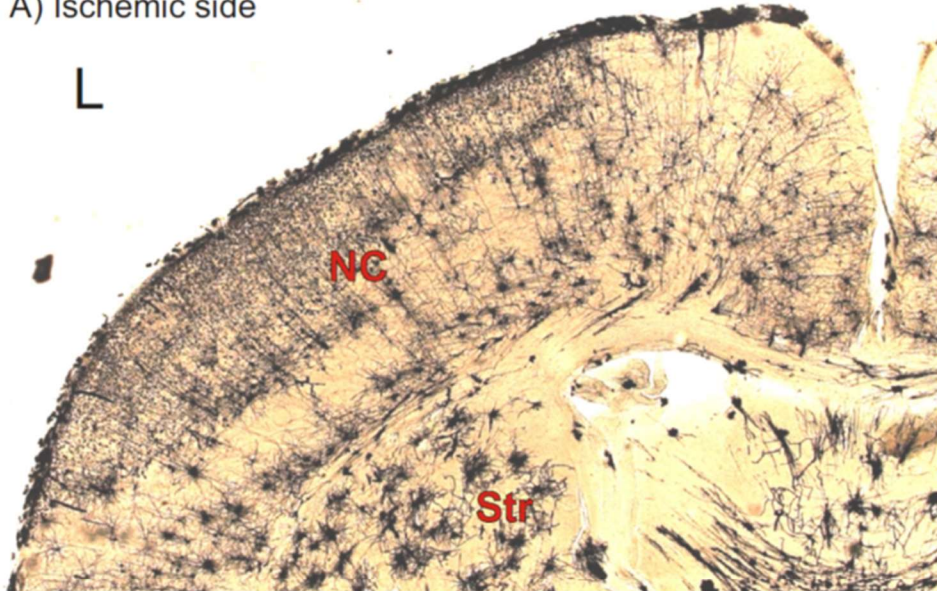


Figure 8. Neuronal morphology in the early post-stroke brain. A) Golgi-Cox stained coronal section of a brain that underwent a 30 minute left MCAo immediately followed by sacrifice and fixation. Staining reveals no apparent irregularities to neuronal structure as examined in the predicted MCAo lesion outlined by the dotted line. The future lesion involves the left striatum (Str) and variable parts of the overlying neocortex (NC), but not hippocampus (Hipp), thalamus (Thal) or hypothalamus (Hyp). B) Higher magnification view of medium spiny neurons in the ischemic (left) and non-ischemic striatum (Str). These neurons appear qualitatively similar and bear no signs of structural damage.

Immediate post-MCAo Brain 1

A) Ischemic side



B) Non-ischemic side

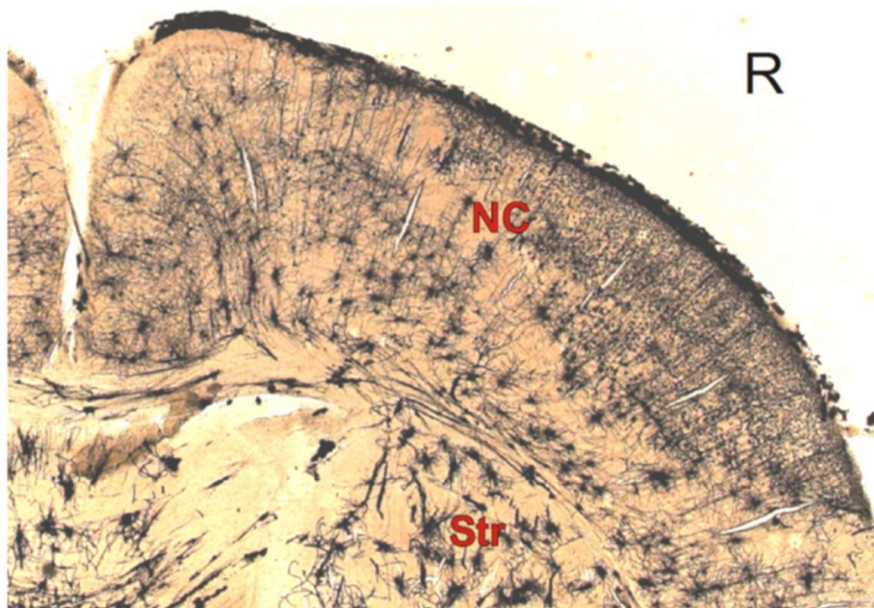


Figure 9. Neuronal morphology early post-stroke at intermediate magnification. A comparison of neuronal staining at intermediate magnification shows no obvious morphological differences between A) the ischemic neocortex (NC) and striatum (Str) and B) the non-ischemic contralateral regions.

Immediate post-MCAo Brain2

Pyramidal neurons on ischemic side in future core.

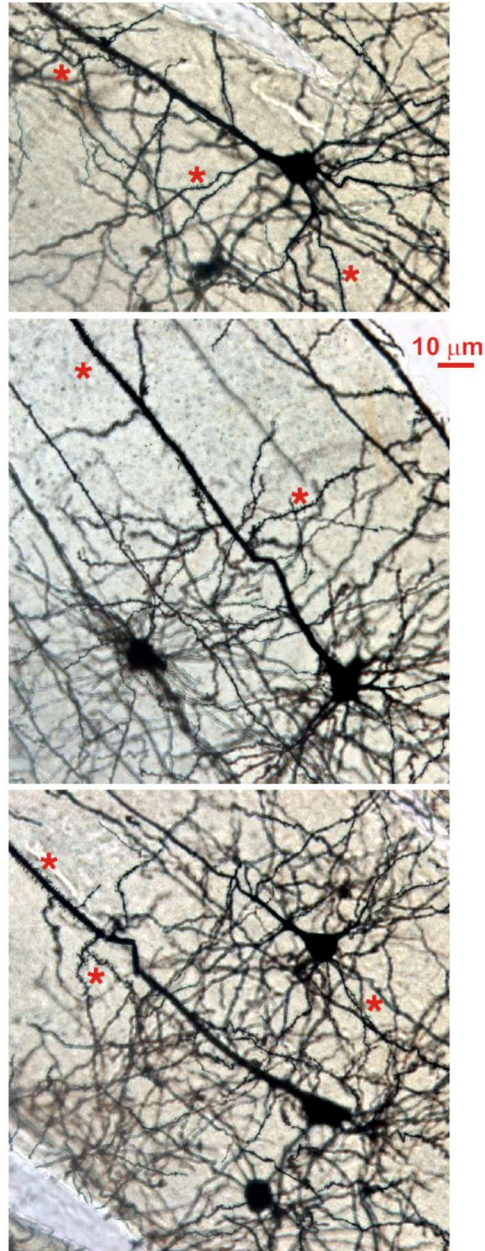


Figure 10. Neuronal morphology early post-stroke at high magnification. The neocortex of the ischemic (left) hemisphere within the prospective MCAo core (see Figure 8) contains normal-appearing pyramidal neurons and interneurons that are qualitatively indistinguishable from cells in the neocortex of the non-ischemic (right) side. None of the neuronal somata are swollen or dysmorphic nor are their dendrites beaded which would indicate injury. Instead, the pyramidal neurons have an extensive number of dendritic spines (*) and are intact.

2.5 Discussion

SD is commonly evoked in brain slices by OGD and in vivo by focal cerebral ischemia. The current study is the first to characterize SD in the early post-ischemic brain without the confounding influence of CBF fluctuations. SD propagation speed and latency to SD onset were measured in brain slices taken from mice that had undergone acute MCAo, extending previous work examining SD in slices taken from non-stroked rats. This distinction is important because of the altered biochemical and physiological milieu of post-stroke brain tissue which includes: increased extracellular glutamate and other metabolites (Morimoto et al. 1996; Hillered et al. 1989), the initiation of necrotic and apoptotic processes (Katsman et al. 2003), the initiation of neuroinflammatory processes (Tóth et al. 2016), and a gradient of tissue damage extending from the infarct core, to the ischemic penumbra to non-ischemic tissue (Maeda et al. 1999). Previous in vivo studies of SD during ischemia show SD originating in tissue regions already compromised by altered CBF and so it has not been clear how the tissue's propensity to SD is altered by the initial onset of cerebral ischemia. Contrary to our expectations, we found that neocortical gray matter immediately post-stroke is more resistant to SD onset and propagation than normal brain tissue, despite our findings of functioning synaptic communication, normal neuronal morphology, normal resting membrane potential, and normal action potential threshold. Furthermore, we found that the latency to SD onset is delayed in post-ischemic brain slices pre-incubated with CP and DB, as observed previously in normal brain slices (Anderson et al. 2005; Douglas et al. 2011).

Variability in CBF occurs during reperfusion following ischemia (Dreier 2011). By mimicking the hypoxia and hypotension after ischemia, hypoperfusion is observed (Sukhotinsky et al. 2008), similar to the post-SD hypoperfusion measured during ischemia (Shin et al. 2006;

von Bornstädt et al. 2015). In addition to episodic hypoperfusion following SD, perfusion incrementally decreases stepwise after each post-ischemic SD event (Shin et al. 2006; von Bornstädt et al. 2015). Increased SD duration is observed in close proximity to the infarct core (Koroleva and Bures 1996), is associated with infarct expansion (Back et al. 1996; Dijkhuizen et al. 1999) and also occurs during hypoperfusion (Sukhotinsky et al. 2010). In contrast, vasodilation and increased CBF occurs in non-ischemic neocortex after SD (Shibata et al. 1990; Piper et al. 1991; Sukhotinsky et al. 2008). By using brain slices harvested 30 min post-MCAo in our experiments, we were able to observe the effects of MCAo on neocortical brain tissue as well as ensuing SD initiation and propagation without confounding blood flow fluctuations.

We performed intracellular recordings on pyramidal neurons from within and around neocortical regions supplied by the occluded middle cerebral artery. This region was identified based on dramatic neuronal necrosis in mice undergoing the identical MCAo but fixed 12 hours post-stroke (not shown). Our measurements of resting membrane potential, whole-cell input resistance, whole-cell time constant, action potential width, amplitude and threshold as well as the fast afterhyperpolarization were not significantly different between the ischemic and non-ischemic hemisphere. Similarly, Gao and colleagues (1999) found that these same electrophysiological measurements were unchanged from pre-ischemic controls in hippocampal CA1 pyramidal neurons as observed 5 hours after global cerebral ischemia. In another study, afferent stimulation of the CA1 hippocampal field after global ischemia during 5 hours of reperfusion evoked responses that were intact following ischemia (Gao et al. 1998). The threshold, amplitude, and width of action potentials as well as the time constant decay following a spike train in post-ischemic brain slices were also similar to regular-spiking neocortical pyramidal neurons in control animals from other studies (McCormick et al. 1985; Silva et al.

1991). Global ischemia models in rodents mimic brain ischemia that occurs after cardiac arrest (Lipton 1999), whereas cerebral ischemia induced by MCAo mimics embolic focal stroke (Carmichael 2005). We likewise observed evoked responses that were not significantly different throughout the MCA territory in the ischemic hemisphere and contralateral areas in the non-ischemic hemisphere in brain slices harvested immediately after MCAo. The intact synaptic communication and single cell electrophysiology observed by others at 5 hours following global cerebral ischemia are also evident for the 1-5 hours that we record in brain slices harvested immediately following MCAo.

When we applied OGD for 10 minutes to post-ischemic brain slices, the latency to SD onset in the ischemic hemisphere was significantly delayed compared to the non-ischemic hemisphere. This decreased propensity for SD differs from previous observations of neocortex in the immediate 1-2 hours following in vivo ischemia. SD in vivo was more readily induced in the border of the penumbra (Busch et al. 1996) with more spontaneous SD events (Takano et al. 1996) correlated with infarct volume expansion (Mies et al. 1993) within 1-2 hours following ischemia. The post-ischemic reduced susceptibility to SD in our experiments was more like the quiescent episode 2-8 hours post-MCAo where very few SD events occur (Hartings et al. 2003). Our findings of a delayed latency to SD onset and slower SD propagation that we observed in post-ischemic neocortex support observations of a slower and delayed increase of $[K^+]_{ext}$ in the penumbra in comparison to non-ischemic cortex (Nedergaard and Hansen 1993), and a more slowly propagating SD wavefront during infarct maturation (Hartings et al. 2003) and in clinical ischemic stroke (Dohmen et al. 2008).

In neocortical brain slices a propagating SD wavefront evoked by OGD resulted in ΔLT increases. Swelling induced by hypo-osmotic challenge also results in ΔLT increases (Andrew

and MacVicar 1994; Andrew et al. 1997). But unlike hypo-osmotic swelling which is primarily glial, OGD swells neurons and astrocytes (Andrew et al. 2007; Risher et al. 2009; Steffensen et al. 2015). After SD propagates through neocortex, Δ LT decreases (Anderson et al. 2005; Douglas et al. 2011) as a result of dendritic beading and other cellular disruption (Andrew et al. 2007; Obeidat et al. 2000; Douglas et al. 2011). CP or DB pre-treatment were shown to increase recovery of evoked synaptic activity after OGD-induced SD and decrease the amount of light scatter after reperfusion with oxygenated aCSF (Anderson et al. 2005; Douglas et al. 2011). The current study also observed less light scatter after OGD-induced SD in the ischemic hemisphere of brain slices harvested after MCAo, possibly indicating a potential for increased survivability under ischemic stress.

The delayed OGD-induced SD evoked by pre-treatment with DB (Douglas et al. 2011; Yamada et al. 2004) or CP (Anderson et al. 2005) in neocortical brain slices was also observed in both the ischemic and non-ischemic hemispheres in our experiments. In normal rat brain slices, action potential frequencies were reduced by a CP-induced increased fast afterhyperpolarization and a DB-induced elevated action potential threshold, respectively (White et al. 2012). CP and DB effectively delay the latency to SD onset in the post-ischemic brain, as in control neocortical slices.

In this investigation we found delayed SD onset and a slower SD propagation rate induced by OGD in the ischemic hemisphere of brain slices harvested after 30min MCAo compared to SD in the non-ischemic hemisphere. This was unexpected because these ischemia-exposed regions displayed intact synaptic communication, electrophysiology and morphology. We also showed that carbetapentane and dibucaine effectively delay SD onset in the post-ischemic brain, similar to neuroprotection demonstrated during OGD superfusion of non-ischemic rat neocortical brain

slices (Anderson et al. 2005). Among the many investigations performed upon the post-ischemic brain, very few studies have examined neuronal injury within the first several hours after ischemia. Further investigation is warranted into the viability of the post-ischemic brain as well as possible attenuation of SD by drugs such as carbetapentane and dibucaine in the absence of confounding CBF and temperature fluctuations.

Table 1. Baseline electrophysiological properties of whole-cell patched pyramidal cells. Neurons in the ischemic and non-ischemic hemispheres of brain slices harvested immediately after 30 min MCAo.

	RMP (mV)	Action Potential Threshold (mV)	Action Potential Amplitude (mV)	Width of Action Potential (msec)	fAHP (mv)	R _{in} (MΩ)	Tau
Non-Ischemic Hemisphere (n=16)	-72 ± 5	-37 ± 3	83 ± 6	0.7 ± 0.1	9 ± 3	122 ± 38	16 ± 4
Ischemic Hemisphere (n=21)	-71 ± 7	-34 ± 6	79 ± 14	0.7 ± 0.2	10 ± 5	113 ± 31	16 ± 6
p values	0.60	0.11	0.16	0.64	0.54	0.43	0.73

Chapter 3

Spreading depolarization in the mouse neocortical brain slices immediately after middle cerebral artery occlusion compared to 12 hours later.

3.1 Summary

While many studies have examined the properties of the neocortex either in the first 2 hours or several days following ischemia, there is little information regarding the initial 12 hours post-stroke. Here we examine mouse neocortex immediately and 12 hours after 30 minutes of middle cerebral artery occlusion (MCAo), comparing non-ischemic and ischemic hemispheres with regard to propensity to tissue swelling and spreading depolarization (SD) as well as evoked synaptic responses and single pyramidal neuron electrophysiological properties. We found that neocortical gray matter is surprisingly intact in brain slices harvested immediately post-stroke but by 12 hours the fields of pyramidal and striatal neurons that comprise the infarcted core are morphologically devastated. Surprisingly, there are a subset of diffusely distributed “healthy” neurons that are still present in the core at 12 hours post-MCAo, based on their relatively intact electrophysiology and morphology.

3.2 Introduction

During ischemia, cerebral blood flow (CBF) declines precipitously in brain areas supplied by an occluded artery. Within 1-2 minutes, Na^+/K^+ pump failure leads to gray matter depolarization that spreads across the neocortex (Dijkhuizen et al. 1999; Takano et al. 1996; Busch et al. 1996; Hossmann 1994). This ‘spreading depolarization’ (SD) manifests as neurons (and glia) precipitously lose their membrane potential, which drives a large negative extracellular current that propagates at 2-5 mm/min across gray matter (Somjen 2001; Dreier 2011). Within minutes ischemic neurons can lose their dendritic spines as they swell and form beaded processes, as observed following photothrombosis in vivo (Murphy et al. 2008) and in acute brain slices after oxygen-and-glucose deprivation (OGD) (Andrew et al. 2007; Jarvis et al. 2001).

Increased SD incidence has been correlated with infarct expansion (Mies et al. 1994; Back et al. 1996). Furthermore, KCl-triggered SD (SD_{K^+}) waves traverse into partially ischemic gray matter and increase infarct volume (Takano et al. 1996; Busch et al. 1996; Dijkhuizen et al. 1999). SD incidence is common up to 2 hours after middle cerebral artery occlusion (MCAo)-induced ischemia and is then followed by a 6 hour period of few, if any, SD events (Dijkhuizen et al. 1999; Koroleva and Bures 1996; Back et al. 1996). A later secondary phase of spontaneous SD follows 10-16 hours after 30 minutes of MCAo (Hartings et al. 2003).

There have been many investigations of post-ischemic SD, but few with observations during the first 24 hours after a focal stroke. In this study, we harvested brain slices both immediately following a 30 min MCAo and 12 hours later. We then compared the effects of elevated extracellular potassium ($[\text{K}^+]_{\text{ext}}$), elevated extracellular glutamate ($[\text{glu}]_{\text{ext}}$), as well as 10 minutes of oxygen- glucose deprivation (OGD) in these post-ischemic brain slices. This enabled us to examine gray matter responsivity in the absence of inherent CBF fluctuations that follow stroke

in vivo (Shin et al. 2006; von Bornstädt et al. 2015) and that can confound SD properties (Sukhotinsky et al. 2010).

Superfusion of neocortical slices with elevated $[K^+]_{ext}$, elevated $[glu]_{ext}$ and OGD simulate the extracellular milieu of the post-ischemic brain. A $[K^+]_{ext}$ of ~ 10 mM arises prior to SD during ischemia (Heineman and Lux 1977; Hansen and Zeuthen 1981; Nedergaard and Hansen 1993) and induces SD in hippocampal slices (Tanaka et al. 1997). After MCAo, $[glu]_{ext}$ becomes elevated (Sciotti et al. 1992; Morimoto et al. 1996) and glutamate release during SD contributes to the propagation of SD_{K^+} (Zhou et al. 2013). OGD also initiates SD in cortical slices by mimicking the decrease in glucose and oxygen coincident with CBF decline. By applying elevated $[K^+]_{ext}$, elevated glutamate or OGD in slices harvested after MCAo, we observe their individual effects upon the post-ischemic brain in the absence of changes in CBF.

3.3 Materials and Methods

Middle Cerebral Artery Occlusion and Brain Slice Preparation

Male C57/BL6 mice (20-25g) were anaesthetized using isoflurane (3% initial, 1% to 1.5% maintenance) in O_2 and air (80%:20%). The animal remained under general anesthesia for the duration of the surgical procedure. The time under anesthesia was 80-90 minutes. While isoflurane can inhibit SD initiation in the intact animal (Piper 1996), SD onset in our harvested brain slices on the non-stroked side was similar to that in non-anaesthetized mice in previous studies (Joshi and Andrew 2001). Focal cerebral ischemia was then induced by intraluminal occlusion of the left middle cerebral artery for 30 minutes. Brains were harvested either immediately following 30 min MCAo or following 12 hours of in vivo reperfusion. The

anaesthetized mouse was then decapitated with a guillotine. Following craniotomy, the brain was quickly removed and immersed in ice-cold and oxygenated (95 % O₂, 5 % CO₂) artificial cerebral spinal fluid (aCSF) composed of (in mM) 240 sucrose, 3.3 KCl, 26 NaHCO₃, 1.3 MgSO₄·7H₂O, 1.23 NaH₂PO₄, 11 D-glucose and 1.8 CaCl₂. Using a Leica 1200-T vibratome, 350 µm slices were cut in the sucrose aCSF through the coronal plane between Bregma levels 1.2 to -1.34 and then incubated in regular aCSF (equimolar NaCl replacing sucrose above) at 35°C for at least 1 hour prior to experimentation. The aCSF osmolality was increased to 310 mOsm using mannitol and pH was 7.4. Brain slices were recorded during the following 4 hours.

Imaging Changes in Light Transmittance (Δ LT) During OGD

Brain slices were transferred to a recording/imaging chamber mounted on an inverted microscope (Axoscope 2FS, Zeiss) with a 10x objective lens and zoom lens that can adjust magnification by 0.5-1.6 X to fit the coronal section to entirely fit within the field of view. Slices were submerged in flowing aCSF (3.5 ml/min.) at 34°C ± 0.5°C. Video images were captured with a cooled charged coupled device (Hamamatsu C4742) using Imaging Workbench 6 software (Indec Biosystems Inc.). Each image of a video series consisted of 16 averaged frames acquired at 10 Hz. The first image of the series was the control transmittance (T_{cont}) which was subtracted from each of the subsequent images (T_{exp}) in the series. The difference signal was normalized by dividing by T_{cont} , which varies across the slice depending on the zone sampled. For example, T_{cont} was lower in white matter than gray matter. This value was then presented as a percentage of the digital intensity of the control image of that series. That is, Δ LT = $[(T_{exp} - T_{cont}) / T_{cont}] \times 100 = [\Delta T / T] \%$. The change in LT was displayed using a pseudocolour intensity scale. The slice image in bright field was displayed using a gray intensity scale. Δ LT

was recorded in the hemisphere ipsi- and contralateral to the lesion during bath application of OGD, 500 μ M glutamate or 9.7 mM $[K^+]_{ext}$ acsf solutions. The OGD aCSF was of similar composition to control aCSF, except for substituting of carbon dioxide and oxygen (95% O₂, 5% CO₂) bubbling of aCSF with nitrogen and oxygen (95% N₂, 5% CO₂). In addition, 11 mM glucose was reduced to 1 mM glucose with osmotic adjustment using NaCl.

Electrophysiology

Whole Cell Patch Clamp: Visually guided whole-cell patch recordings were obtained using micropipettes pulled from borosilicate glass (outside diameter 1.2 mm, inside diameter 0.68 mm; World Precision Instruments) to a resistance of 4-6 M Ω . Pyramidal neurons were identified in neocortical gray using Dodt optics based on their size and shape. The internal pipette solution contained (in mM) 125 K- gluconate, 10 KCl, 2 MgCl₂, 5.5 EGTA, 10 HEPES, 2 Na-ATP and 0.1 CaCl₂ (pH was adjusted to 7.3 with KOH). All recordings were acquired in current clamp mode of an Axoclamp 2A 23 amplifier and a Digidata 1322 A/D converter. Clampex 10.2 software was used for data acquisition with subsequent analysis using Clampfit 10.2 software. Resting membrane potential was measured by patch clamping neocortical pyramidal neurons with whole cell configuration in neocortical LII/III in the ischemic and non-ischemic hemispheres. Action potential width, amplitude and threshold were measured from the second action potential elicited during current pulses increased stepwise by 0.1 nA (200 ms, -0.3 to 0.5 nA). The action potential threshold was measured as the beginning of the upstroke of the action potential. Action potential width was measured (in milliseconds) as the time between the beginning of the action potential upstroke and the point at which the 'downstroke' reached the same membrane potential as the initial action potential threshold. Action potential amplitude was

measured from the beginning of the upstroke to the corresponding peak membrane depolarization. The whole cell time constant of ischemic and non-ischemic neocortical pyramidal neurons were derived from a 'curve-of-best-fit' of exponential decay of the membrane potential following a hyperpolarizing pulse of the stepped current pulses (200 ms, -0.1 nA) using data analysis program Clampfit 10.2 (Molecular Devices, Inc.). Fast afterhyperpolarizations (fAHP) were measured as the deviation from the beginning of the upstroke of an action potential within 5 ms after the peak of a single spike that follows individual action potentials in neocortical pyramidal neurons. Input resistance (R_{in}) was derived from the linear portion of the current-voltage plot 170 ms from the beginning of constant current pulses increased stepwise by 0.1 nA from -0.3 to ~ 0.1 nA. Pyramidal neurons were recorded in neocortical layers II/III from either the ischemic or non-ischemic hemisphere in brain slices harvested immediately and 12 hours following MCAo.

Evoked Synaptic Responses: To record evoked field potentials, a micropipette (2–4 M Ω) was pulled from thin-walled capillary glass, filled with 200 mM NaCl, and mounted on a three dimensional (3-D) micromanipulator. It was connected by a chloride-coated silver wire to an amplifier probe, and output was monitored on an on-line oscilloscope. The tip was placed in layers II/III of the neocortex and a concentric bipolar electrode (Rhodes Electronics) placed in layer VI to stimulate the immediately overlying layers. A current pulse (0.1-ms duration; 0.1 Hz) was applied at 50mV to produce an evoked response. The amplified signals were digitized, displayed, and plotted using pCLAMP 10 software (Axon Instruments).

Golgi-Cox Staining

Following 30 min MCAo, mouse brains were extracted and immersed in freshly prepared impregnation solution. Brains were processed according to the protocol provided by *FD Neurosciences* using the FD Rapid GolgiStain Kit™. Coronal brain sections cut at 50 microns thick were processed (FD NeuroTechnologies 2012). The ischemic and non-ischemic hemispheres were imaged with a 10 X objective to observe gross tissue morphology and with a 60 X objective higher magnification to observe individual neuronal morphology. More detailed analysis of neuronal structural changes were carried out by Ms. Rasha Mehder but are not included as part of this thesis.

Statistical Analysis

Field EPSPs, baseline electrophysiological properties, latency to SD onset, speed of SD propagation and LT changes during and after SD were compared in the ischemic vs. non-ischemic hemispheres of post-stroke brain slices using a Student t-test. Incidence of SD and evoked synaptic responses as well as Δ LT swelling in the ischemic vs. non-ischemic hemispheres were compared using Mann Whitney U non-parametric analyses. Electrophysiological parameters were described using mean \pm S.E.M.

3.4 Results

Light Transmittance Imaging

During ischemia, oxygen and glucose levels decrease significantly in brain areas where CBF declines. Extracellular K⁺ and glutamate also become elevated. Independent of blood flow and

its fluctuations, we individually bath-applied elevated $[K^+]_{ext}$, elevated $[glu]_{ext}$ or OGD saline to post-ischemic brain slices harvested immediately or 12 hours after MCAo.

In brain slices harvested immediately after 30 min MCAo, spontaneous SD events at baseline 3.2mM $[K^+]_{ext}$ were observed in 7% (n = 1 of 14) of slices in the non-ischemic hemisphere and 25% (n = 5 of 20) of brain slices in the ischemic hemisphere. At 9.6 mM $[K^+]_{ext}$, the SD incidence in the non-ischemic hemisphere was 80% (n = 11 of 14) vs. 35% (n = 7 of 20) of slices in the ischemic hemisphere. When 9.6 mM $[K^+]_{ext}$ was bath applied to brain slices harvested 12 hours after MCAo, the SD incidence in the non-ischemic hemisphere was 89% (n = 8 of 9 slices) vs. 33% (n = 3 of 9 slices) in the ischemic hemisphere. A significantly decreased incidence of SD_{K^+} in the ischemic hemisphere vs. the non-ischemic hemisphere was observed 12 hours after MCAo (Mann Whitney U, $p < 0.05$) as shown in Figure 11. SD_{K^+} initiated and propagated both within and outside neocortex supplied by the middle cerebral artery in brain slices harvested immediately after MCAo. However, only three SD_{K^+} events occurred within MCA territory of the ischemic hemisphere in slices 12 hours post-MCAo. On several instances, SD propagated from the non-ischemic hemisphere across the interhemispheric fissure and into areas of the ischemic hemisphere supplied by circulation from the unaffected anterior cerebral artery (Figure 12).

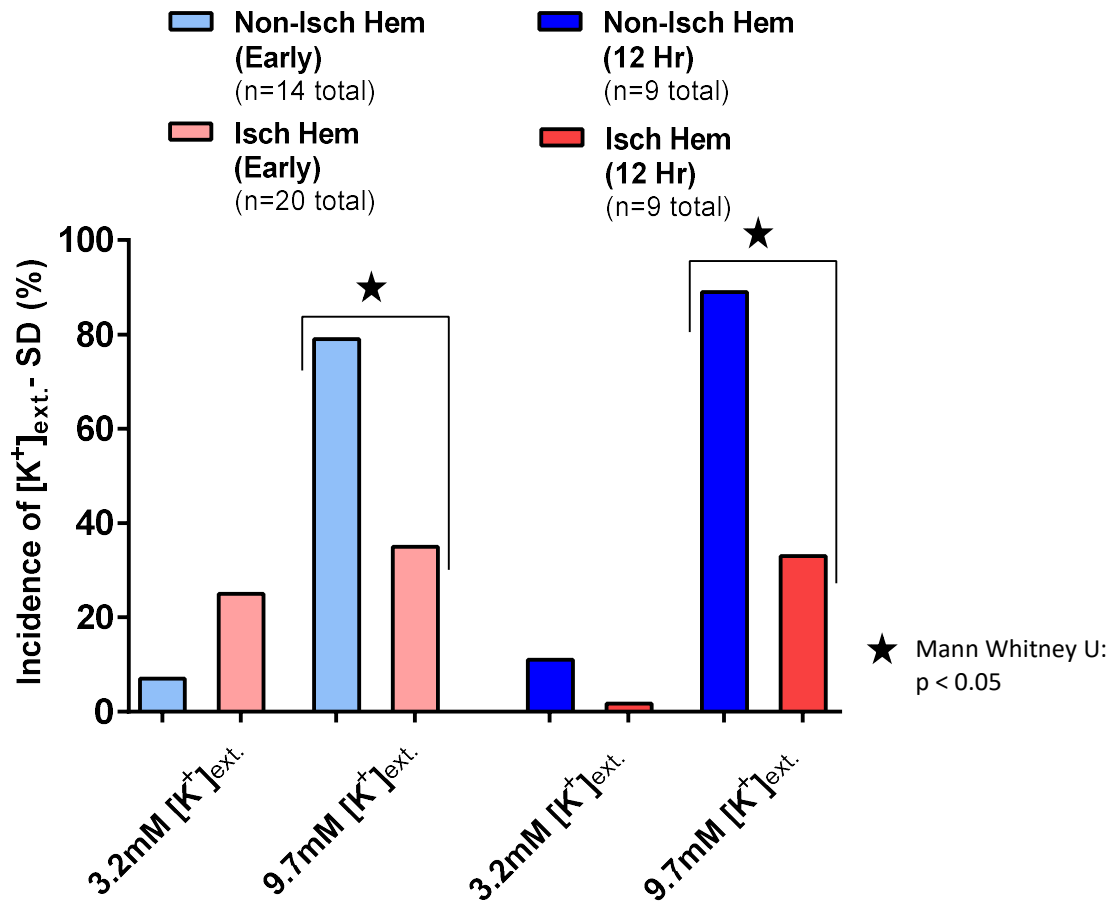


Figure 11. Incidence of $[K^+]_{ext.}$ -induced SD in brain slices harvested immediately, and 12 hours after, 30 min MCAo. Slices taken immediately and 12 hours following MCAo rarely display SD spontaneously within the ischemic hemisphere when superfused with 3.2 mM K^+ saline.

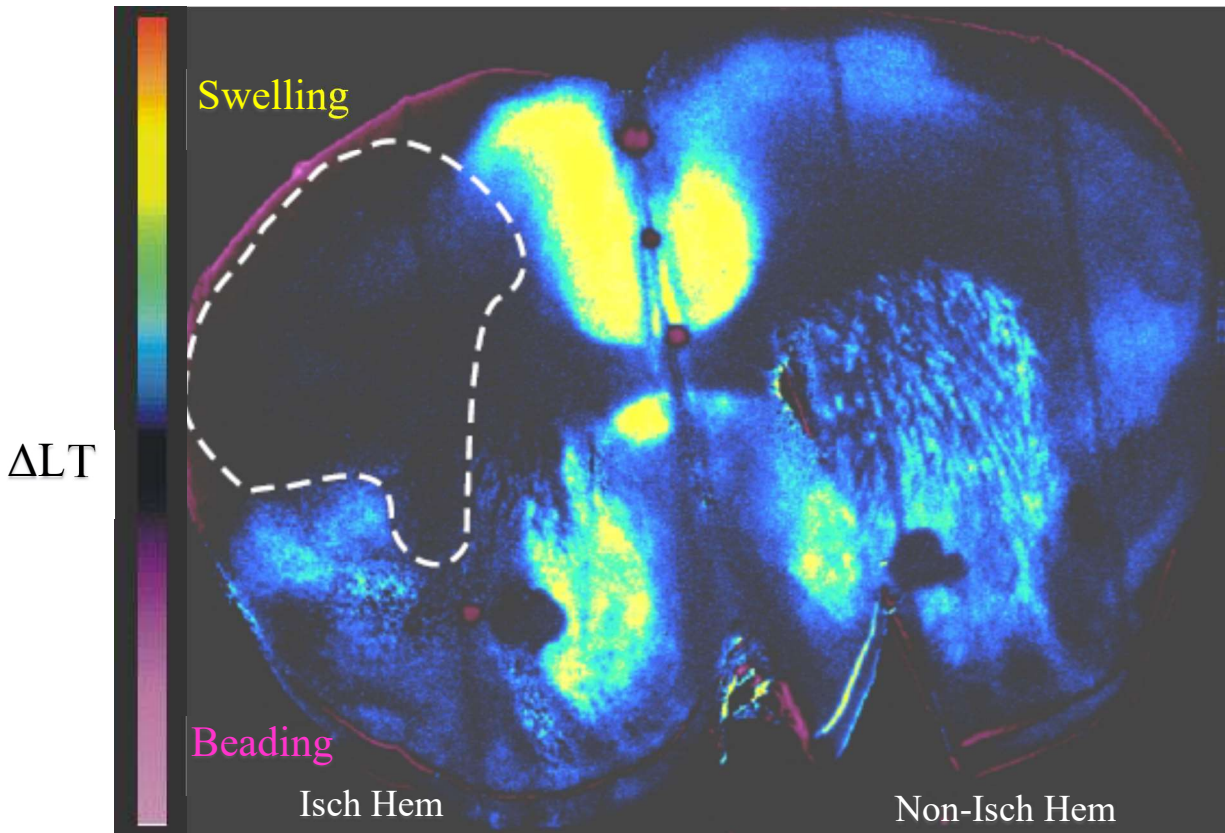


Figure 12. SD_{K^+} initiated outside MCA territory when brain slices were harvested after 12 hours of reperfusion following MCAo. Change in light transmittance (ΔLT) was imaged during superfusion of brain slices with 9.6 mM $[K^+]_{ext}$. In this pseudocoloured image, green/yellow depicts increased ΔLT and cell swelling and purple indicates decreased ΔLT and dendritic beading. It is apparent in this image that SD initiates and propagates throughout the entire right (non-ischemic hemisphere), but only involves a small portion of the left (ischemic) hemisphere.

In vivo, extracellular glutamate levels become significantly elevated after ischemia. When we bath-applied glutamate at 500 μM onto brain slices harvested immediately after MCAo, ΔLT was elevated by greater than a 5% threshold (that occurs during superfusion of slices with only hypo-osmotic solution [Andrew and Macvicar 1994]) in 64% of slices ($n = 7$ of 11) in the non-ischemic hemisphere and in 65% ($n = 11$ of 19) of slices in the non-ischemic hemisphere after 12 hours of reperfusion. Swelling exceeding the 5% ΔLT threshold above baseline was never observed in neocortex in the ischemic hemisphere known to be affected by MCAo (i.e. lateral

parietal cortex). It also did not arise in neocortex near the central sulcus outside of MCA territory which is less affected by MCAo (i.e. medial motor and cingulate neocortex) at both time points. Using a Mann Whitney U statistical analysis, the incidence of swelling evoked by 500 μ M glutamate was significantly lower in the ischemic than the non-ischemic hemisphere both immediately ($p < 0.01$, $n=11$ slices) and 12 hours after MCAo ($p < 0.01$, $n=19$ slices) as shown in Figure 13.

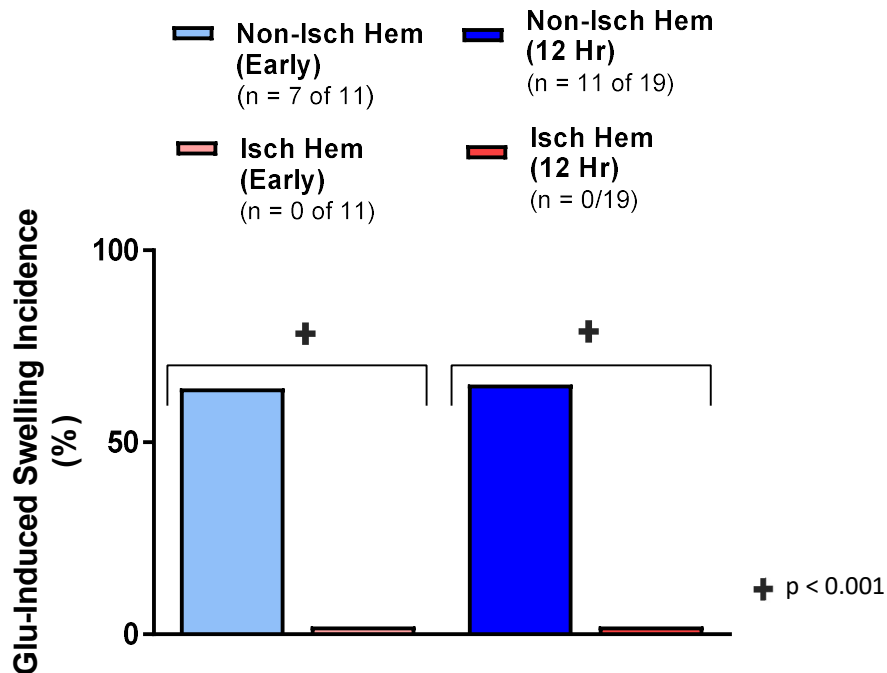


Figure 13. Significantly less incidence of glutamate-induced swelling in the ischemic hemisphere of brain slices harvested immediately, and 12 hours after, 30 min MCAo. Slices taken immediately and 12 hours following MCAo did not display swelling within the ischemic hemisphere when superfused with 500 μ M glutamate aSCF. The ischemic hemisphere displays a significantly lower incidence of glutamate-induced tissue swelling, exceeding a 5% threshold Δ LT both immediately and 12 hours following MCAo (Mann Whitney U: $p < 0.001$).

When OGD aCSF was bath-applied to post-ischemic brain slices, the ischemic hemisphere displayed a significantly decreased incidence of OGD-induced SD (42%, n = 5 of 12 slices) compared to the non-ischemic hemisphere (100%, n = 12 of 12 slices) 12 hours after MCAo (Mann Whitney U; $p < 0.01$). However, SD occurred in every neocortical brain slice harvested *immediately* after MCAo in both the ischemic (100%, n = 31 of 31 slices) and non-ischemic hemisphere (100%, n = 31 of 31 slices) during OGD superfusion as shown in Figure 14. OGD-induced SD initiated within neocortex supplied by the middle cerebral artery (i.e. lateral parietal neocortex) and anterior cerebral artery (i.e. medial motor and cingulate neocortex) in the ischemic hemisphere of brain slices harvested immediately after MCAo. In contrast, SD occurred mostly outside of MCA territory (i.e. medial motor and cingulate neocortex) when brain slices were harvested after 12 hours of reperfusion following 30 min MCAo.

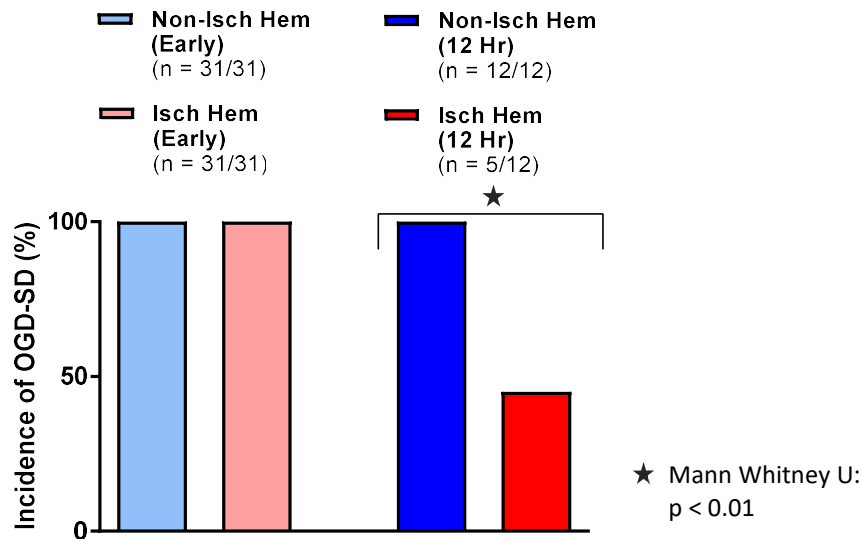


Figure 14. SD development in the ischemic hemisphere is reduced by 12 hours, but not immediately, post-MCAo. Ischemic hemisphere after 12 hours of reperfusion displays a significantly lower incidence of OGD-SD. Ischemic hemisphere of brain slices harvested 12 hours, but not immediately, after MCAo supports a significantly decreased incidence of OGD-induced SD (42%) than the non-ischemic hemisphere (100%) (Mann Whitney U; $p < 0.05$).

Electrophysiology

To test in slices whether the reduction of SD in the ischemic hemisphere at the early and late timepoints could involve a reduction in synaptic function, we assessed evoked field EPSPs at multiple recording sites in cortical layers II/III nearby and within neocortical regions supplied by the MCA in ischemic and non-ischemic hemispheres. The ischemic hemisphere 12 hours after MCAo had a significantly decreased incidence of evoked responses (22%, n = 2 of 9 recordings) than the non-ischemic hemisphere (100%, n = 9 of 9 recordings) as shown in Figure 15 (Mann Whitney U; $p < 0.05$). This contrasts with brain slices harvested immediately post-MCAo, which displayed intact evoked synaptic responses at every stimulation site.

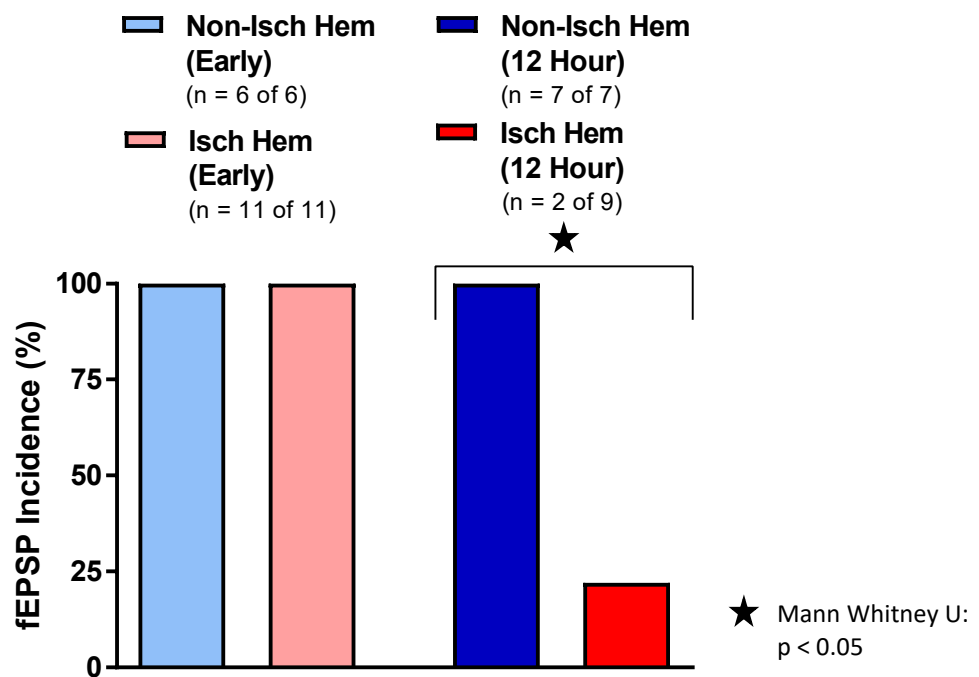


Figure 15. The evoked synaptic response incidence is significantly lower in the ischemic hemisphere of brain slices harvested 12 hours, but not immediately, after 30 min MCAo. Ischemic hemisphere of brain slices harvested 12 hours, but not immediately, after 30 min MCAo has a significantly decreased incidence of evoked synaptic responses (22%) than the non-ischemic hemisphere (100%) (Mann Whitney U; $p < 0.05$).

We then searched through the ischemic cortex of live brain slices harvested 12 hours after MCAo to find viable neurons for electrophysiological recordings in whole cell configuration under current clamp. Compared to non-ischemic neocortex in either hemisphere, very few normal-appearing neurons could be visualized with contrast optics within the suspected infarct region. Surprisingly, we were able to locate a few isolated but apparently intact pyramidal neurons. We were able to patch on and assess the electrophysiological properties of five identified pyramidal neurons, all of which seemed fairly normal in their single cell properties. We found a slight but significant depolarization in the average resting membrane potential of pyramidal neurons in the ischemic hemisphere (n=5) in comparison to the non-ischemic hemisphere (n=6) in 12 hour post-MCAo brain slices (-65 ± 8 vs -72 ± 3 ; $p = 0.05$). Otherwise the mean values for the post-train fast afterhyperpolarization, whole cell input resistance and whole cell time constant as well as action potential threshold, amplitude and width were not significantly different between the ischemic and non-ischemic hemispheres (Table 2).

Golgi-Cox Staining

We wanted to visualize these surviving neurons to determine if their morphology was also spared using Golgi-Cox staining. The technique randomly stains perhaps 1% of the neurons present, but all parts of each single neuron are revealed. Three mice underwent left MCAo and then recovered for 12 hours prior to fixation and Golgi-Cox processing. Coronal sections of each brain in Figure 16 are shown with their ischemic core/penumbra delineated. In the non-ischemic hemisphere stained pyramidal neurons in neocortex display classic characteristics of long apical dendrites with secondary and tertiary branches possessing dendritic spines that receive axonal input (Fig. 17A). Various non-pyramidal neurons also stain, in particular a spherical cell type

with varicose dendrites (not shown). The underlying striatum also appears normal, being comprised of medium spiny neurons (Fig. 17A) which represent 95% of the neuronal population. As described in the previous chapter, the region of the future infarct immediately after 30 minutes of MCAo was indistinguishable from surrounding gray matter based on Golgi staining.

In contrast 12 hours post-MCAo, most neurons in the visibly damaged core area (dashed lines in Figure 16) lack highly branched neurons as seen at intermediate magnification in Figures 17 and 18A. Every one of the striatum's principle cells have shrunken and retracted their dendrites. The neocortical response is more variable, displaying regions of uniformly swollen cell bodies (Figs. 19A; 11A) that generally retain their pyramidal cell shape. The dendrites have lost their spines and taken on a beaded appearance, typical of ischemic neurons in the early phase of deterioration. More commonly the remaining neocortical neurons appear shrunken and necrotic with retracted and limited dendrites that lack spines (Figs. 18C; 11B). This contrasts with gray matter immediately outside the MCAo infarct region which appears normal. It is difficult to distinguish an intermediate area of injury that could represent the ischemic penumbra. No doubt a penumbral area exists, but its narrow size and regional variability make it difficult to identify 12 hours following stroke.

As predicted from the `normal` electrophysiological properties recorded in five pyramidal cells (Table 2) and the representative electrophysiological traces (Fig. 21), it was possible to identify some neurons that had survived 12 hours post-MCAo with intact axon, dendrites and pyramidal cell body shape. They were observed in the MCAo core containing swollen pyramidal neurons (Fig. 9A) or necrotic pyramidal neurons (Fig. 20B). These sparsely distributed neurons displayed an extensive dendritic tree with branches where spines, rather than beads,

predominated. Nonetheless, even these neurons displayed some minor dendritic beading with loss of spines (not shown). This was not the case with pyramidal neurons in the non-ischemic hemisphere which appeared normal as expected as shown in Chapter 2, Figures 8-10.

Post-MCAo 12 hr

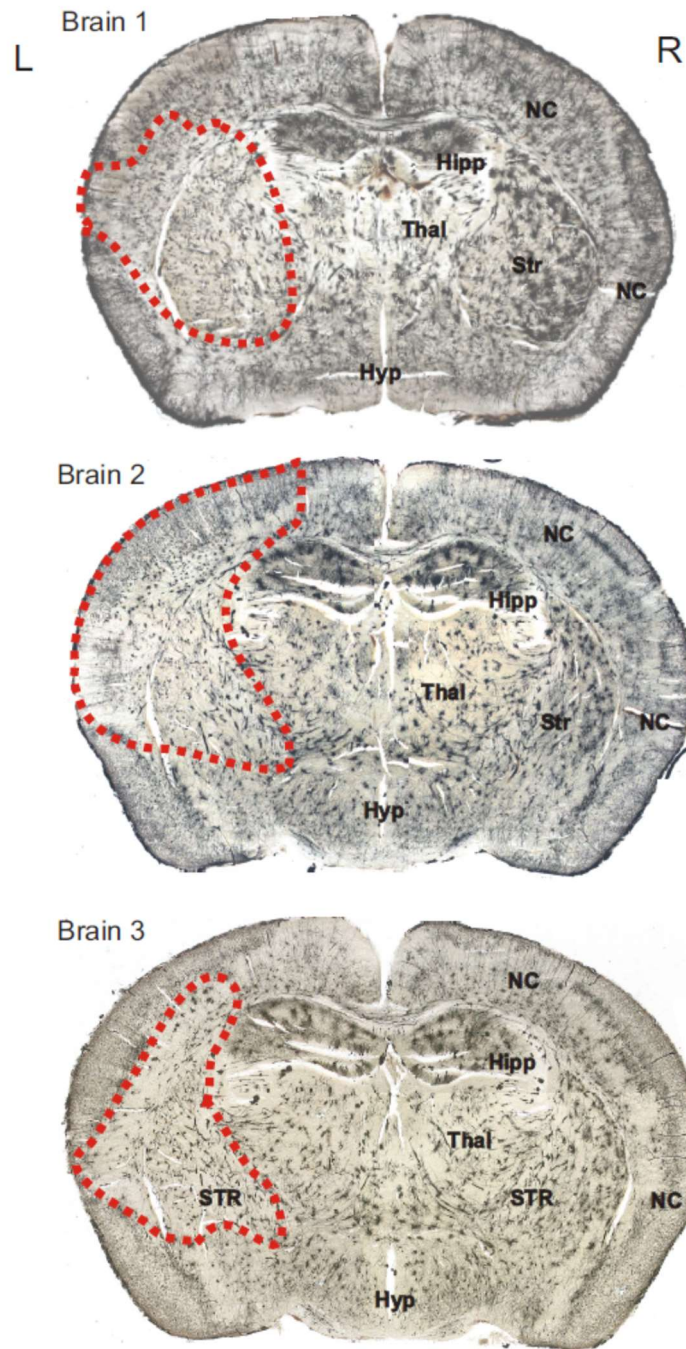
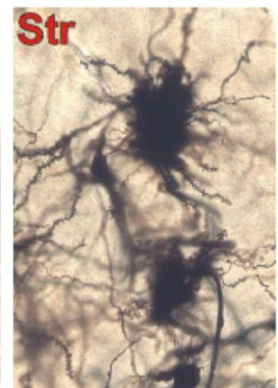


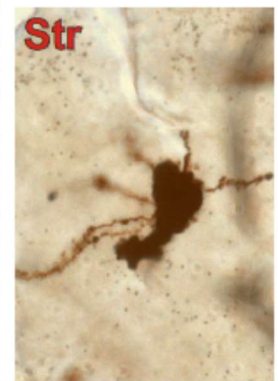
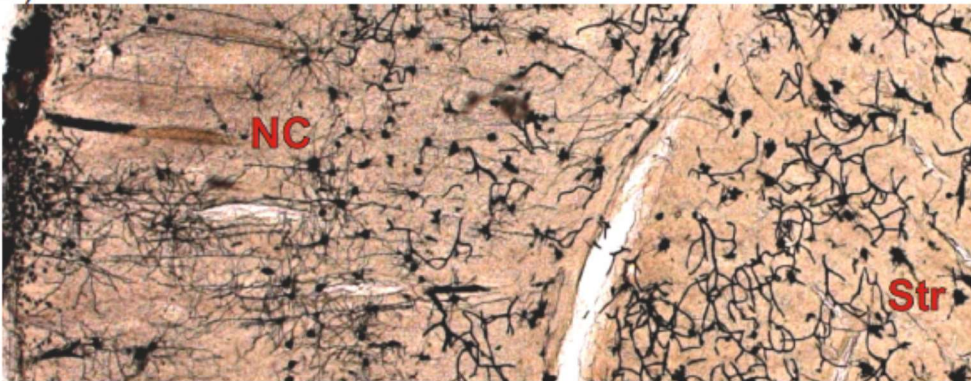
Figure 16. Coronal sections through three brains of mice that each underwent 30 minute left hemisphere MCAo followed by a 12 hour recovery period. Golgi –Cox staining reveals irregularities to neuronal structure that can be roughly outlined as the MCAo lesion (dashed lines). The lesion involves the left striatum (STR) and variable parts of the overlying neocortex (NC), but not hippocampus (Hipp), thalamus (Thal) or hypothalamus (Hyp).

Post-MCAo 12 hr Brain 2

A) Non-ischemic side



B) Ischemic side



10 μ m

Figure 17. Ischemic hemisphere displays necrotic neurons clearly distinguishable from the intact non-ischemic hemisphere. A) The striatum (Str) in the non-ischemic (right) hemisphere displays normal spider-like medium spiny neurons with short but numerous dendrites (inset right). The overlying neocortex (NC) contains normal-appearing pyramidal neurons and interneurons. B) In contrast, the striatum in the ischemic hemisphere is devoid of healthy-appearing cells, containing only shrunken and necrotic cell bodies with beaded and stunted dendrites as shown in the inset right.

Post-MCAo 12 hr Brain 2

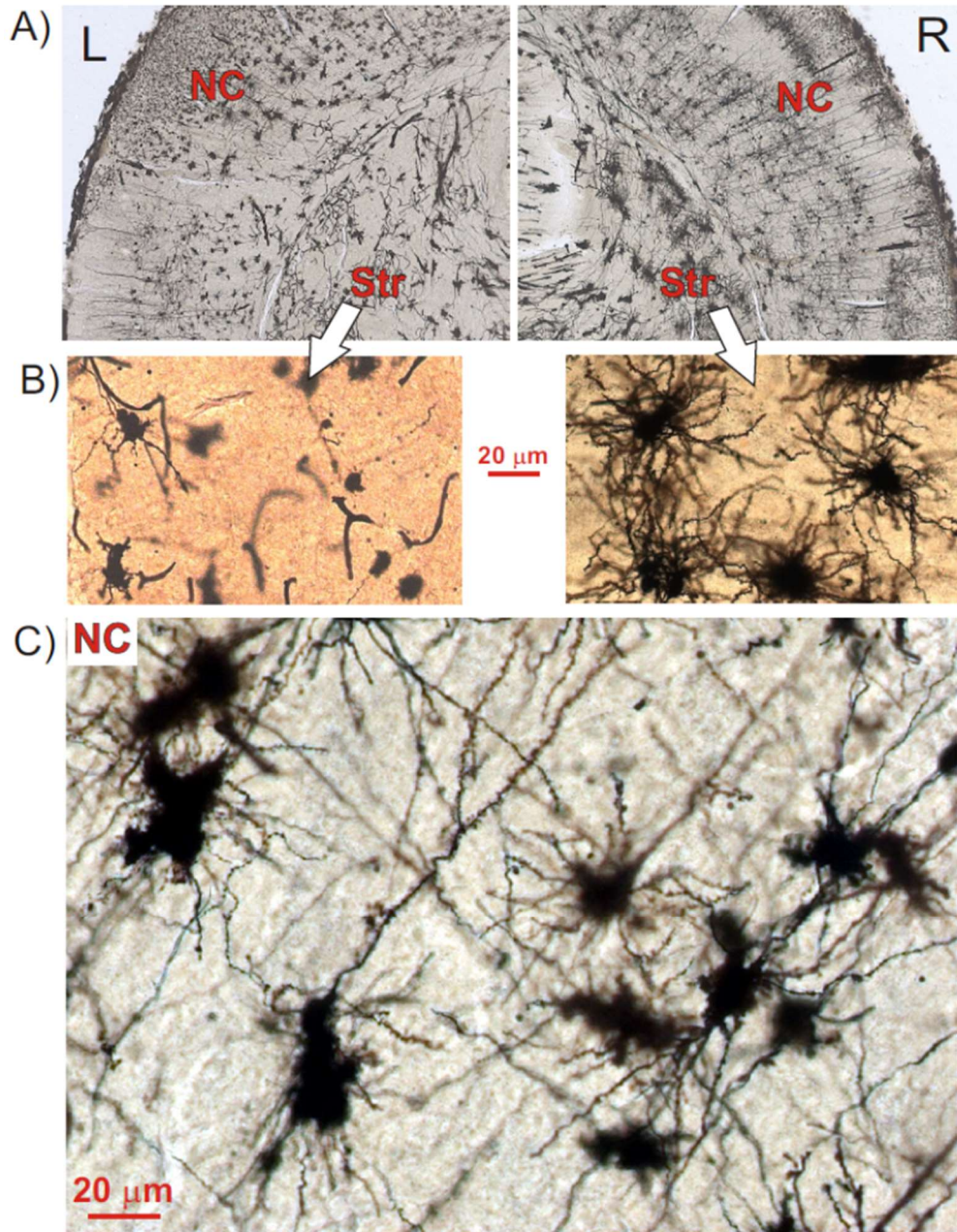
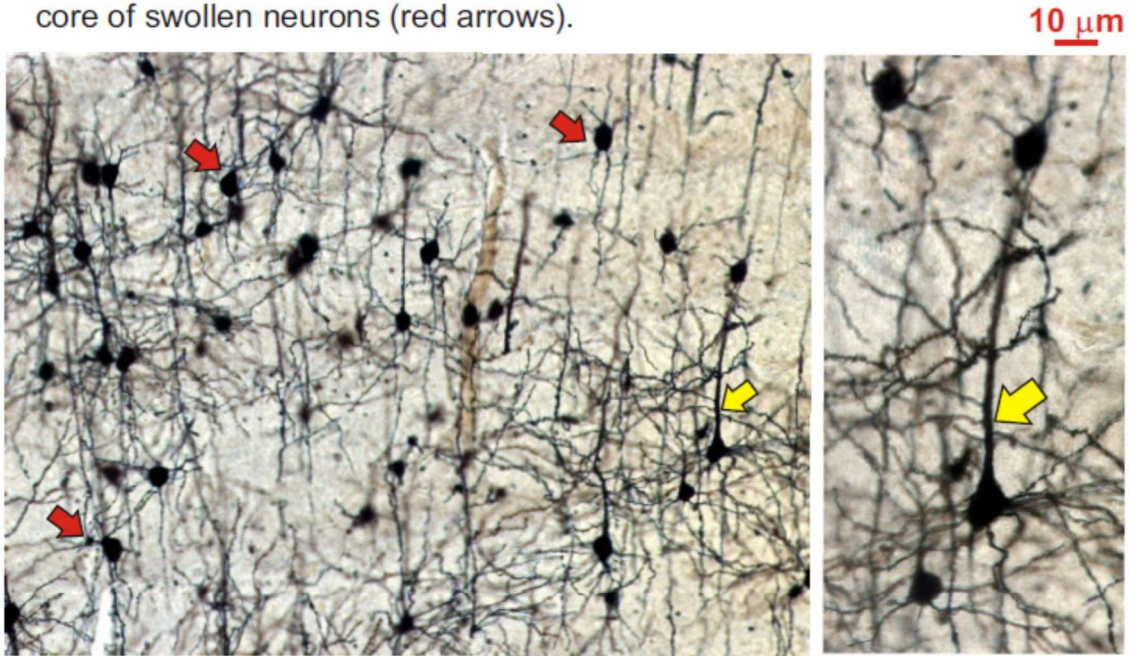


Figure 18. Core area of the ischemic hemisphere displaying necrotic neurons A) at low magnification, B) in striatum, and C) in overlying neocortex. Both striatal medium spiny neurons and neocortical pyramidal somata become dysmorphic. Their dendrites are stunted and beaded and most dendrites have lost their spines. Loss of the shorter striatal dendrites is more obvious as seen in 18B, left.

Post-MCAo 12 hr Brain 1

A) Isolated but intact pyramidal neuron (yellow arrow) within stroke core of swollen neurons (red arrows).



B) Other rare but normal-appearing pyramidal neurons within the core.

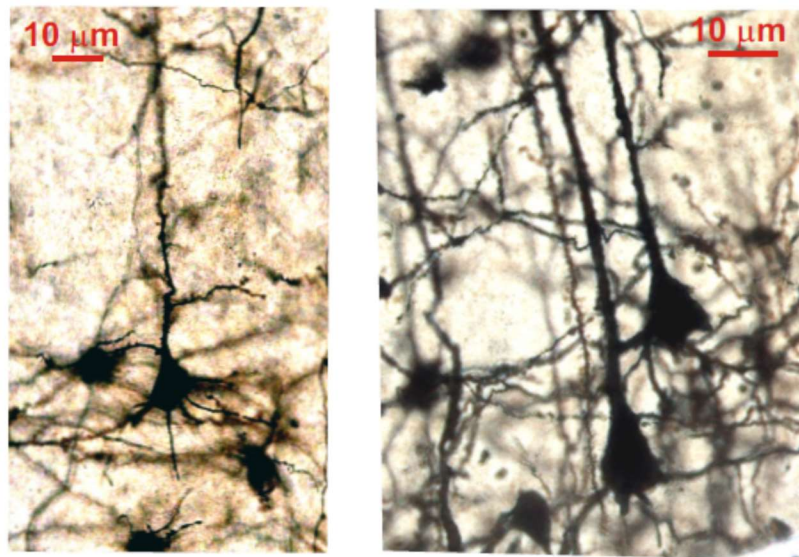
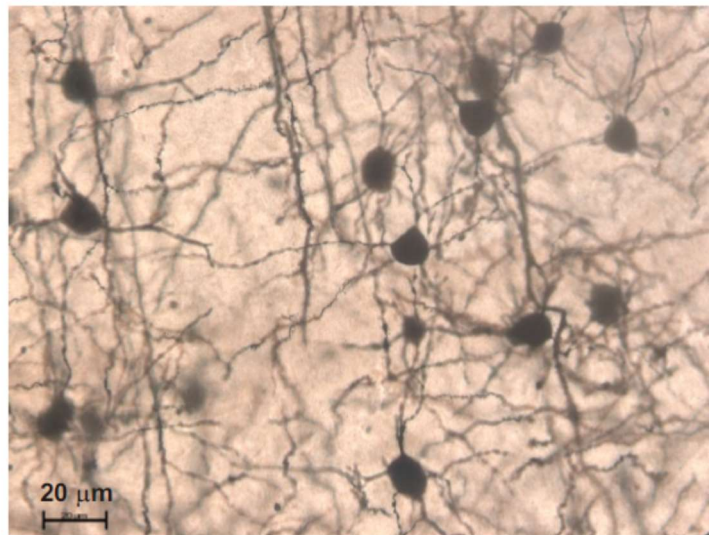


Figure 19. Isolated intact pyramidal neurons surrounded by necrotic and swollen neurons within the infarcted region. Golgi-Cox staining reveals primarily swollen pyramidal neurons (red arrows) within the ischemic core, as opposed to the brain in Figure 18 which displays primarily necrotic neurons. In either case, interspersed among these damaged cells are comparatively normal-appearing pyramidal neurons (yellow arrows) with extensive dendritic arbors and numerous dendritic spines

Post-MCAo 12 hr

A) Swollen neurons with beaded dendrites



B) Necrotic neurons surround two intact pyramidal cells

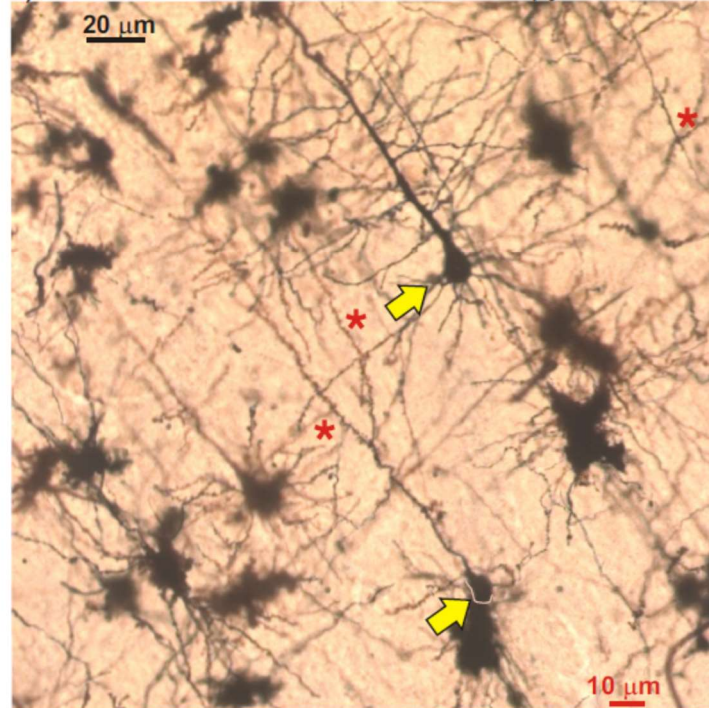


Figure 20. In the neocortical region of the ischemic core, neurons may be, A) swollen with dendrites that are beaded or B) necrotic with stunted and beaded dendrites. Also observed are rare intact pyramidal neurons (yellow arrows). These neurons display numerous dendritic spines, unlike their necrotic neighbors where dendrites appear retracted and cell bodies are dysmorphic.

12 hour post-MCAo

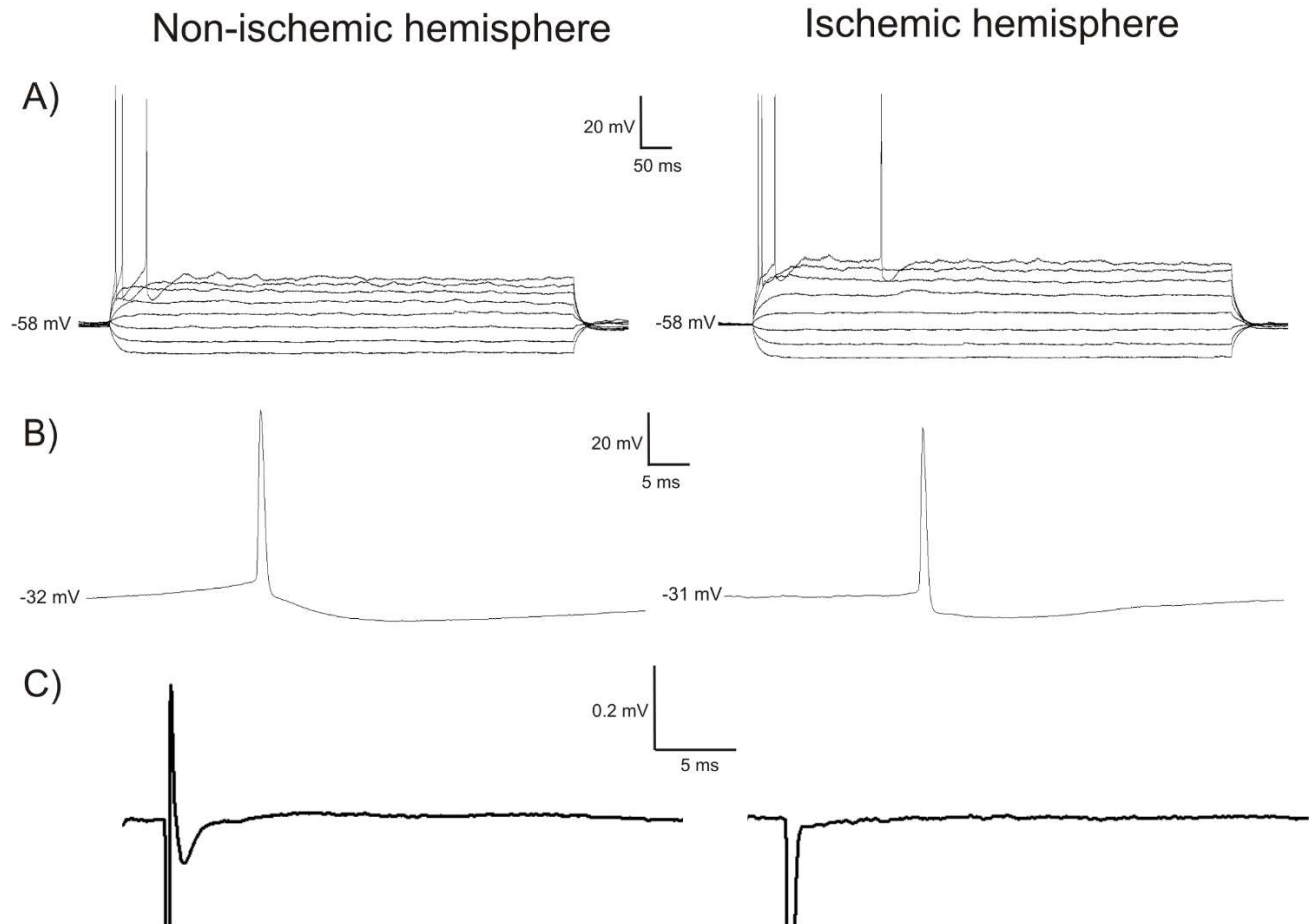


Figure 21. Baseline electrophysiological properties of whole-cell patched pyramidal cells were similar in the ischemic and non-ischemic hemispheres. (A) The fast afterhyperpolarization (fAHP) and time constant (τ) obtained from a series of hyperpolarizing and depolarizing current steps were similar in the ischemic and non-ischemic hemispheres (see Table 2). Although a wider range in input resistance (R_{in}) was evident in current-voltage plots derived from stepped current pulses, the R_{in} recorded from layer II/III pyramidal neocortical neurons were not significantly different between the ischemic and non-ischemic hemispheres. (B) The action potential threshold, amplitude and width were similar in the ischemic and non-ischemic hemisphere. (C) The evoked synaptic response was attenuated but present in the non-ischemic hemisphere, but was absent in infarcted regions within the ischemic hemisphere.

3.5 Discussion

Post-ischemic SD and Leao's Initial Observations of SD

Aristides Leao initially observed a slowly propagating wave of depressed EEG activity following electrical stimulation of rabbit and cat neocortex (Leao 1944). This so-called cortical spreading depression (CSD) was later determined to be reversible, repeatable and could be evoked by focally elevating K^+ or with brief hypoxia (Somjen 2001). Leao then interrupted the cerebral circulation of rabbits and noted the similarity of electrically-induced 'cortical spreading depression' to a 'change of the same nature as one resulting from prolonged interruption of the circulation occurs in the cerebral cortex' (Leao 1947). The depolarizing wave was subsequently determined to also be induced by oxygen-and-glucose deprivation or by inhibition of the Na^+/K^+ pump or mitochondrial transport chain (Somjen 2001). These events are now collectively referred to as 'spreading depolarization' (SD) (Dreier 2011; Hartings et al. 2017).

Other metabolites such as ATP, lactate and creatine phosphate vary along with CBF levels after ischemia (Obrenovitch et al. 1988) and with SD_{K^+} in intact rats (Lauritzen et al. 1990). Post-ischemic SD events also induce a stepwise decrease in CBF (Shin et al. 2006; von Bornstädt et al. 2015). CBF fluctuations are also influenced by $[K^+]_{ext}$, nitric oxide (Windmuller et al. 2005; Dreier et al. 1998), hypoxia and hypotension (Sukhotinsky et al. 2008) and alter properties of SD (Sukhotinsky et al. 2010). In our experiments we observed SD induced by elevated $[K^+]_{ext}$, or OGD and swelling in response to elevated $[glu]_{ext}$ in post-ischemic brain slices in the absence of post-ischemic CBF fluctuations (Shin et al. 2006; von Bornstädt et al. 2015). Brain slices harvested after MCAo were incubated with oxygenated aCSF, thereby reducing variability of extracellular metabolites as well as CBF, oxygen and glucose inherent after ischemia.

Elevated $[K^+]_{ext}$, Elevated $[glu]_{ext}$ and OGD Post-Ischemia

A $[K^+]_{ext}$ threshold of ~10-12 mM is measured prior to SD initiation during ischemia (Heineman and Lux 1977; Hansen and Zeuthen 1981; Nedergaard and Hansen 1993) and in brain slices (Tanaka et al. 1997). When we applied 9.6 mM $[K^+]_{ext}$ to brain slices harvested immediately after 30 min MCAo, SD was more difficult to induce in the ischemic hemisphere. This contrasted with KCl application in ischemic cortex in vivo which increases ATP depletion and diffusion-imaged lesion volume (Dijkhuizen et al. 1999; Busch et al. 1996) as well as the SD incidence (Takano et al. 1996; Dijkhuizen et al. 1999; Busch et al. 1996; Mies et al. 1993). However, the 25% incidence of spontaneous SD events in post-ischemic brain slices harvested immediately after MCAo was similar to observations during in vivo ischemia (Takano et al. 1996). Although SD incidence is high initially after ischemia, spontaneous and KCl-induced SD incidence peaks in the initial 20 min after MCAo and subsequently declines sharply (Back et al. 1996; Dijkhuizen et al. 1999; Koroleva and Bures 1996). A quiescent phase of minimal spontaneous SD ensues 4-6 hours following reperfusion after ischemia (Hartings et al. 2003). This decreased post-ischemic SD incidence is congruent with our findings of reduced SD incidence induced by elevated $[K^+]_{ext}$ in the ischemic hemisphere of brain slices immediately following 30 min MCAo.

The ischemic hemisphere of brain slices 12 hours post-MCAo also displayed a decreased incidence of tissue swelling during 9.6 mM $[K^+]_{ext}$ saline superfusion. There was obvious damage in the ischemic hemisphere in Golgi-stained brain sections at 12 hours following ischemia and reperfusion compared to undamaged immediate fixation. Thus, the failure of the ischemic hemisphere to elicit SD_{K^+} at the later timepoint resulted from neuronal death in the infarcted brain. However, SD was evident in brain regions peripheral to the infarcted neocortex

supplied by the unoccluded anterior cerebral artery. These SD events originated within the contralateral non-ischemic hemisphere and propagated across the longitudinal fissure and into the ischemic hemisphere, which does not occur in the intact brain during ischemia in vivo (Nedergaard and Hansen 1993). However it was apparent that an infarcted ischemic ‘core’ with a decreased propensity to tissue swelling and SD events was juxtaposed next to a medial ‘penumbra’ that could sustain SD_{K^+} 12 hours following 30 MCAo.

In addition to elevated $[K^+]_{ext}$, during ischemia (Branston et al. 1977; Strong et al. 1983; Nedergaard and Hansen 1993), extracellular glutamate ($[glu]_{ext}$) also increases for 1-2 hours (Sciotti et al. 1992; Benveniste et al. 1984; Phillis et al. 1991; Hillered et al. 1989). Extracellular glutamate increases from a baseline concentration of $\sim 20 \mu M$ to $\sim 200 \mu M$ during anoxia-induced SD and $\sim 80 \mu M$ during ischemia-induced SD (Sato et al. 1999; Iijima et al. 1998). Elevated $[glu]_{ext}$ is also associated with the propagating SD wavefront (Zhou et al. 2013). However directly applying glutamate to normal brain slices produces only a graded general swelling of gray matter (Polischuk and Andrew 1996; Obeidat and Andrew 1998). This swelling does not resemble the characteristic propagating SD front of cell swelling that traverses gray matter upon exposure to ischemia, OGD, elevated $[K^+]_{ext}$ or ouabain (Tanaka et al. 1997; Anderson and Andrew 2002; Dietz et al. 2008; Anderson et al. 2005; Dohmen et al. 2008). When we bath-applied $500 \mu M [glu]_{ext}$ to brain slices harvested immediately, and 12 hours after MCAo, we observed an LT increase $> 5\%$ only in the non-ischemic hemisphere. This $5\% \Delta LT$ response is comparable to superfusion with hypo-osmotic (-30 mOsm) aCSF (Andrew and MacVicar 1994). It takes a 5 mM concentration of glutamate to elicit a similar regional increased ΔLT response and tissue swelling as only $100 \mu M$ of NMDA (Andrew et al. 1996; Obeidat and Andrew 1998), a specific agonist at ionotropic glutamate receptors. This is because uptake

mechanisms constantly remove the extracellular glutamate (Obeidat and Andrew 1998). This glutamate uptake may be enhanced in brains harvested immediately after a 30 min MCAo similar to in vivo observations of increased glutamate transporter expression and decreased neuronal death after ischemic post-conditioning (Zhang et al. 2010). In contrast, brain slices harvested after 12 hours post-MCAo display minimal glutamate-evoked swelling because neuronal death and pre-existing swollen neurons (both evident in Golgi-stained tissue) preclude further depolarization and swelling.

Unlike elevated $[\text{glu}]_{\text{ext.}}$ and $[\text{K}^+]_{\text{ext.}}$ which cause reversible swelling of gray matter, OGD causes irreversible damage in the gray matter of higher brain (Obeidat and Andrew 1998; Anderson and Andrew 2002; Anderson et al. 2005; Brisson et al. 2014). The decreased likelihood of OGD-induced SD in the ischemic hemisphere of brain slices harvested 12 hours after MCAo is probably the result of the sparse number of remaining intact neurons (evident with Golgi-Cox staining) that are able to drive SD.

Post-Ischemic Microscopy and Electrophysiology

In brain sections harvested immediately after MCAo, there was no detectable evidence of infarction in Golgi-stained tissue. These findings support our electrophysiological recordings indicating that single neocortical pyramidal neurons were not significantly altered in their intrinsic or synaptic properties immediately post-MCAo (Chapter 2). Evoked responses and baseline electrophysiological properties of pyramidal neurons were not significantly different between the two hemispheres. Supporting these results, the electrophysiological properties and synaptic communication in pyramidal CA1 neurons were not significantly different from pre-ischemic controls up to 5 hours after reperfusion following 19 minutes of global ischemia (Gao

et al. 1999; Gao et al. 1998). The threshold, amplitude, and width of action potentials as well as the decay of the time constant following an action potential train in post-ischemic brain slices were also similar to regular-spiking neocortical pyramidal neurons in control animals from other studies (McCormick et al. 1985; Silva et al. 1991).

In brain slices harvested 12 hours after MCAo, evoked synaptic responses were lost within and near the core. The ischemic hemisphere in those brain slices displayed a decreased incidence of OGD-induced and K^+ -induced SD as well as decreased glutamate-evoked swelling compared to the non-ischemic hemisphere. The ischemic hemisphere 12 hours post-MCAO also showed dramatic neuronal swelling or necrosis in Golgi-stained sections of the MCAo core. The few remaining 'healthy'-appearing pyramidal neurons found in the core could not be expected to override these greatly diminished responses caused by extensive neuronal injury.

Conclusions

While many studies have examined the properties of the neocortex several days following stroke, there is little information regarding the state of the neurons in the ischemic core at 12 hours post-stroke. Here we examined mouse neocortex immediately and 12 hours after 30 minutes of MCAo, comparing non-ischemic and ischemic hemispheres with regard to propensity to cell swelling and spreading depolarization, as well as evoked synaptic responses and single pyramidal neuron properties. We found that neocortical gray matter is surprisingly intact in brain slices harvested immediately post-stroke even as the propensity to induce cell swelling or SD is dramatically reduced. By 12 hours, synaptic responses are disrupted and most of pyramidal and striatal neurons are devastated morphologically. However, a few electrophysiologically and morphologically normal-appearing pyramidal neurons are still present in the neocortical region

of the core 12 hours after MCAo. How long these neurons continue to survive and the mechanism supporting their neuroprotection are issues that our laboratory will pursue.

Table 2. Baseline Electrophysiological Properties of Identified Pyramidal Neurons in the Ischemic and Non-Ischemic Hemispheres in Brain Slices Harvested 12 Hours After MCAo. Only recordings from five normal-appearing neurons from the ischemic side could be maintained.

	<i>RMP</i> (mV)	<i>AP</i> Threshold (mV)	<i>AP</i> Amplitude (mV)	<i>Width of</i> <i>Action</i> <i>Potential</i> (msec)	<i>fAHP</i> (mv)	<i>R_{in}</i> (MΩ)	<i>Tau</i>
Non-Ischemic Hem (n=6)	-72 ± 3	-34 ± 5	77 ± 4	0.7 ± 0.2	14 ± 5	108 ± 13	16 ± 3
Ischemic Hem (n=5)	-65 ± 8	-34 ± 6	69 ± 11	0.6 ± 0.2	11 ± 5	109 ± 41	27 ± 15
p value	0.05	0.44	0.16	0.62	0.11	0.95	0.18

Chapter 4

Post-ischemic resistance to spreading depolarization.

4.1 Summary

Cerebral blood flow (CBF) declines following ischemic stroke in a gradient outward from the blocked artery. Depending upon the degree of remaining blood flow, synaptic communication or ionic homeostasis can be disrupted in brain areas most adversely affected by the blocked artery. After this initial insult, recurrent waves of mass depolarization along with swelling of neurons and glia ensue, regardless of whether the cerebral artery blockage is removed. These recurrent waves further expand the territory of disrupted synaptic communication and ionic homeostasis in the post-stroke brain. This spreading depolarization (SD) occurs when the Na^+/K^+ pump is metabolically overwhelmed or simply fails. Considering that synaptic communication or ionic homeostasis are disrupted following ischemia and SD, the post-ischemic brain might undergo alterations to preserve these functions. Suppressed synaptic communication in the post-ischemic brain has been previously shown to be reversed by adenosinergic inhibition. In this investigation we attempt to eliminate a delayed onset and slower propagation of in the ischemic hemisphere propensity of immediately post-middle cerebral artery occlusion (MCAo) cerebral slices. We attempted to reverse the non-ischemic vs. post-ischemic discrepancy in SD onset and speed using an adenosine receptor antagonist or by inhibiting the Na^+/K^+ pump (and inducing SD) with a high-dose (100 μM) of ouabain. By harvesting brain slices immediately following MCAo, we were able to image and record single-cell electrophysiology and tissue changes following SD with precise region-specific localization in the coronal plane. We observed a decreased propensity of regions supplied with blood by the middle cerebral artery to undergo tissue change after SD, with normal electrophysiological properties in these same regions. Adenosinergic

inhibition did not alter the delayed latency to SD onset observed in the ischemic hemisphere, whereas ouabain eliminated the discrepancy in SD onset between the non-ischemic and ischemic hemispheres, likely by modulating activity of the Na^+/K^+ pump. Considering that the delayed latency to SD onset observed in the ischemic hemisphere occurred along with intact single cell electrophysiology and neuronal morphology, our findings suggest that the discrepancy in post-ischemic SD between the non-ischemic and ischemic hemispheres is a reversible phenomenon affected by ouabain. The possibility of a reversible suppression of SD that may involve the Na^+/K^+ pump is apparent, but requires further investigation.

4.2 Introduction

Decreased blood flow and the subsequent reduction in energy production during acute ischemic stroke induces failure of the Na^+/K^+ pump. This in turn causes an initially slow, but then sudden, depolarization of neurons and astrocytes. This spreading ‘ischemic’ or ‘anoxic’ depolarization (SD) kills neurons in the future infarct core within minutes if ischemia is prolonged beyond a few minutes. Where there is some residual cerebral blood flow (CBF), SD may recover and then recur in the adjacent regions (the future ischemic penumbra) (Hossmann 1994; Hartings et al. 2017). Many drugs have been tested to decrease infarct damage and thereby improve functional outcome after ischemia but to date all have failed (O’Collins et al. 2006). Few drugs have been tested within the first 4-6 hours after ischemia (Ginsberg 2008).

Regarding therapeutic intervention after ischemia, one clinical approach that has not been tested is to decrease the incidence of recurring SD. The SD wavefront of neuronal depolarization and swelling propagates between 2-5 mm/min, regardless of whether SD is initiated by mitochondrial inhibitors, elevated $[\text{K}^+]_{\text{ext.}}$, oxygen-and-glucose deprivation (OGD), ouabain

exposure or ischemia (Tanaka et al. 1997; Anderson and Andrew 2002; Dietz et al. 2008; Anderson et al. 2005; Dohmen et al. 2008). All of these disrupt or overload the Na^+/K^+ pump. As Dohmen and colleagues (2008) demonstrated, recurrent waves of SD are associated with infarct expansion in human patients in the hours and days following acute ischemic stroke.

Studying stroke treatments which may attenuate SD are subject to experimental sources of variability which include: spontaneous SD incidence that changes over time (Hartings et al. 2003); a stepwise and decreased CBF that accompanies each SD event (Shin et al. 2006); variability in post-ischemic perfusion pressure (von Bornstädt et al. 2015) and variability in brain temperature (Busto et al. 1987). Temperature and perfusion pressure affect SD initiation, propagation and duration (Sukhotinsky et al. 2010; Chen et al. 1993). By investigating post-ischemic SD generation in brain slices harvested immediately after middle cerebral artery occlusion (MCAo) we can eliminate confounding CBF and temperature fluctuations confounding SD initiation and propagation.

Reduced electrocortical activity follows transient global ischemia (Ilie et al. 2006). SD suppresses synaptic communication and cortical activity which results in post-ischemic energy conservation (Hossman 1990; Nagashima 1994). Reduced synaptic communication follows SD in neocortical slices (Lindquist and Shuttleworth 2012). Suppression of electrocortical activity and synaptic communication after ischemia and KCl-induced SD, respectively, were abolished by the adenosine A_1 receptor antagonist DPCPX (Lindquist and Shuttleworth 2012; Ilie et al. 2006). These experiments demonstrated that suppressed synaptic communication following ischemia and SD can be reversed, implying that an energy conservation strategy could be beneficial.

The Na⁺/K⁺ pump is another target for mediating post-ischemic energy conservation. This pump uses ~ 40% of the brain's energy to maintain and restore the membrane potential following action potential discharge (Attwell and Laughlin 2001). However, the energy required to restore ionic homeostasis following complete loss of the membrane potential during ischemic SD arising from pump failure is considerable (Dreier et al. 2013). Any induced alteration of its expression or function could improve neuronal viability during metabolic stress. Increased activity of the Na⁺/K⁺ ATPase is observed after hypoxia (Guo et al. 2011) and altered expression of the pump at the cell surface is also observed following anoxia and glucose deprivation (Belliard et al. 2013). Pre-treatment of neuronal tissue cultures with low-dose ouabain increases Na⁺/K⁺ pump activity (Gao et al. 2002) and attenuates cellular damage after anoxia and glucose deprivation (Oselkin et al. 2010), suggesting that neuroprotection can be derived from pump upregulation.

In this investigation we evaluated post-ischemic SD in the absence of confounding blood flow and temperature fluctuations. Was the ischemic hemisphere more prone to SD evoked by OGD? Were the electrophysiological properties changed immediately following MCAo? We hypothesized that if SD was attenuated in post-ischemic neocortex of brain slices harvested immediately after a 30 min MCAo it could be reversed by Na⁺/K⁺ pump and/or adenosinergic inhibition.

4.3 Materials and Methods

Middle Cerebral Artery Occlusion and Brain Slice Preparation

Male C57/BL6 mice (20-25g) were anaesthetized using isoflurane (3% initial, 1% to 1.5% maintenance) in O₂ and air (80%:20%). The animal remained under general anesthesia for the

duration of the surgical procedure, which was 80-90 minutes. Focal cerebral ischemia was then induced by intraluminal occlusion of the left middle cerebral artery (MCAo). After 30 min MCAo, the anaesthetized mouse was decapitated with a guillotine. The brain was quickly removed and immersed in ice-cold and oxygenated (95 % O₂, 5 % CO₂) artificial cerebral spinal fluid (aCSF) composed (in mM) of 240 sucrose, 3.3 KCl, 26 NaHCO₃, 1.3 MgSO₄·7H₂O, 1.23 NaH₂PO₄, 11 D-glucose and 1.8 CaCl₂. Using a Leica 1200-T vibratome, 350 µm slices were cut in the sucrose aCSF through the coronal plane between Bregma levels 1.2 to -1.34 and then incubated in regular aCSF (equimolar NaCl replacing sucrose above) at 35°C for at least 1 hour prior to experimentation. Slices were then transferred to a recording/imaging chamber where they were submerged in flowing aCSF (3.5 ml/min.) at 34°C ± 0.5°C. The aCSF osmolality was adjusted to 310 mOsm using mannitol and pH was 7.4.

Imaging Changes in Light Transmittance (Δ LT) During OGD

Brain slices were transferred to a recording/imaging chamber of an inverted microscope (Axoscope 2FS, Zeiss) submerged in flowing aCSF (3.5 ml/min.) at 34°C ± 0.5°C with a 10x objective lens and an additional zoom lens that can adjust magnification by 0.5-1.6 X to fit the coronal section to entirely fit within the field of view. Video images were captured with a cooled charged coupled device (Hamamatsu C4742) using Imaging Workbench 6 software (Indec Biosystems Inc). The first image of the series was the control transmittance (T_{cont}) which was subtracted from each of the subsequent images (T_{exp}) in the series. The difference signal was normalized by dividing by T_{cont} , which varies across the slice depending on the zone sampled. For example, T_{cont} was lower in white matter than gray matter. This value was then presented as a percentage of the digital intensity of the control image of that series. That is, Δ LT = [(T_{exp} -

$T_{cont}/ T_{cont}] \times 100 = [\Delta T/T] \%$. The change in LT was displayed using a pseudocolour intensity scale. The slice image in bright field was displayed using a gray intensity scale. OGD solution was superfused onto the brain slices in the bath chamber. The OGD aCSF was of similar composition to control aCSF, except for substitution of oxygen and carbon dioxide bubbling of aCSF (95% O₂, 5% CO₂) with nitrogen and carbon dioxide (95% N₂, 5% CO₂). In addition, 11 mM glucose was reduced 1 mM glucose with osmotic adjustment using mannitol. Peak Δ LT has previously been associated with maximal tissue swelling, while the ensuing nadir Δ LT indicates maximal dendritic beading (neuronal damage) after SD onset. Δ LT was measured in regions-of-interest placed in the ipsi- and contralateral hemispheres in post-ischemic brain slices pre-incubated with oxygenated aCSF. These regions of interest were identified as 'core' (< 15% of baseline CBF reduction) in lateral parietal neocortex (Par_{lat}) and 'penumbra' (20-40% of baseline CBF) in medial parietal neocortex (Par_{med}) within the ischemic hemisphere (Belayev et al. 1997). Δ LT was measured in the same regions-of-interest in the non-ischemic hemisphere. Δ LT was also measured in post-ischemic brain slices pre-incubated with 1 μ M DPCPX or 1 μ M ouabain for 20 min prior to bath application of OGD. Also, 100 μ M ouabain was used to induce SD in separate experiments.

Electrophysiology

Whole Cell Patch Clamp: Visually guided whole-cell patch recordings were obtained using micropipettes pulled from borosilicate glass (outside diameter 1.2 mm, inside diameter 0.68 mm; World Precision Instruments) to a resistance of 4-6 M Ω . The internal pipette solution contained (in mM) 125 K- gluconate, 10 KCl, 2 MgCl₂, 5.5 EGTA, 10 HEPES, 2 Na-ATP and 0.1 CaCl₂ (pH was adjusted to 7.3 with KOH). All recordings were acquired in whole cell current clamp mode using an Axoclamp 2A amplifier and a Digidata 1322 A/D converter. Clampex 10.2

software was used for data acquisition and subsequent analysis with Clampfit 10.2 software. Resting membrane potential was measured by patch clamping neocortical pyramidal neurons with whole cell configuration in neocortical LII/III in the ischemic and non-ischemic hemispheres. Action potential width, amplitude and threshold were measured from the second action potential elicited during current pulses increased stepwise by 0.1 nA (200 ms, -0.4 to 0.4 nA). The action potential threshold was measured as the beginning of the upstroke of the action potential. Action potential width was measured (in milliseconds) as the time between the beginning of the action potential upstroke and the point at which the 'downstroke' reached the same membrane potential as the initial action potential threshold. Action potential amplitude was measured from the beginning of the upstroke to the corresponding peak membrane depolarization. The whole cell time constant of ischemic and non-ischemic neocortical pyramidal neurons were derived from a 'curve-of-best-fit' of exponential decay of the membrane potential following a hyperpolarizing pulse of the stepped current pulses (200 ms, -0.1 nA) using data analysis program Clampfit 10.2 (Molecular Devices, Inc.). Fast afterhyperpolarizations (fAHP) were measured as the deviation from the beginning of the upstroke of an action potential within 5 ms after the peak of a single spike that follows individual action potentials in neocortical pyramidal neurons. Input resistance (R_{in}) was derived from the linear portion of the current-voltage plot 170 ms from the beginning of constant current pulses increased stepwise by 0.1 nA from -0.4 to ~ 0.1 nA. The electrophysiological recordings were obtained from pyramidal neurons in either the lateral parietal cortex (Par_{lat}) 'core' or medial parietal neocortex (Par_{med}) 'penumbra' within the ischemic hemisphere and compared to each other and the same regions within the non-ischemic hemisphere.

Evoked Responses: To record electrically-evoked field potentials, a micropipette (2–4 M Ω) was pulled from thin-walled capillary glass, filled with 200 mM NaCl, and mounted on a Scientifica Patch Star three dimensional (3-D) micromanipulator. It was connected by a chloride coated silver wire to an amplifier probe, and output was monitored on an on-line oscilloscope. The tip was placed in layers II/III of the neocortex and a concentric bipolar electrode (Rhodes Electronics) placed in layer VI to stimulate the immediately overlying layers. A current pulse (0.1-ms duration; 0.1 Hz) was applied at 50mV, 70mV, 100mV and 130 mV to produce an evoked response at each recording site. The amplified signals were digitized, displayed and plotted using Clampfit 10 software. The stereotaxic co-ordinates of the recording site in both the ischemic and non-ischemic hemispheres were identified using Paxinos and Watson Mouse Brain Atlas (Franklin and Paxinos 2007).

Statistical Analysis

A multiple comparisons ANOVA was used to assess the effect of drug treatment upon the latency to SD onset. An ANOVA with 2 between-subject levels (hemisphere and intensity of stimulation) was performed on evoked synaptic responses pooled in the non-ischemic and ischemic hemispheres at 50, 70, 100 and 130 mV stimulus intensity. Field EPSPs, baseline electrophysiological properties, latency to SD onset, speed of SD propagation and Δ LT during and after SD were also compared in the ischemic vs. non-ischemic hemispheres of post-stroke brain slices using a student's t-tests. These parameters were expressed as mean \pm S.E.M.

4.4 Results

Region-Specific Light Transmittance Changes

Based on a previous investigation (Belayev et al. 1997), we assessed Δ LT in cortical regions identified as ‘core’ (< 15% of baseline CBF) and compared it to the ‘penumbra’ (20-40% of baseline CBF). In the latter study, ‘core’ CBF reduction occurred in lateral parietal neocortex (Par_{lat}) and ‘penumbra’ CBF reduction was evident in medial parietal neocortex (Par_{med}) (Belayev et al. 1997). When we observed Δ LT following OGD-induced SD in brain slices harvested immediately after MCAo, there was significantly less light scatter in the “core” Par_{lat} cortical regions in the ischemic hemisphere relative to the corresponding Par_{lat} area in the non-ischemic hemisphere ($-6 \pm 0.7\%$ vs. $-10 \pm 0.9\%$; $p < 0.01$). There was also significantly less light scatter in the “core” Par_{lat} region in the ischemic hemisphere in comparison to “penumbral” Par_{med} in the ischemic ($-6 \pm 0.7\%$ vs. $-8 \pm 0.8\%$; $p < 0.05$) and non-ischemic hemispheres ($-6 \pm 0.7\%$ vs. $-11 \pm 0.8\%$; $p < 0.01$). Penumbral Par_{med} cortical regions in the ischemic hemisphere had significantly less light scatter than core Par_{lat} areas in the non-ischemic hemisphere ($-8 \pm 0.8\%$ vs. $-10 \pm 0.9\%$; $p < 0.05$) (Figure 22).

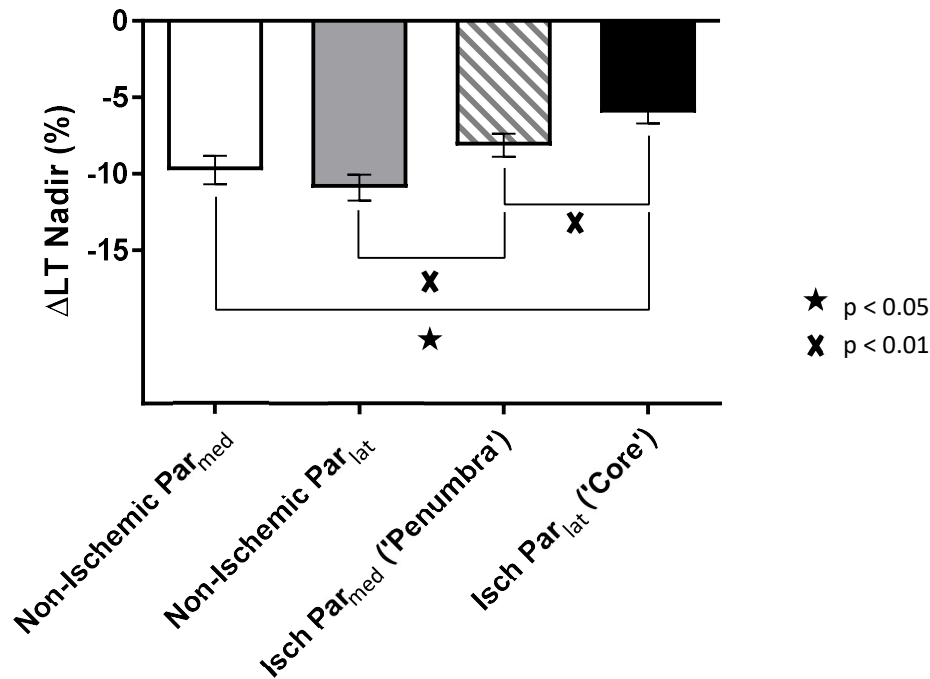


Figure 22. Less light scatter after OGD-SD in MCAo future ‘core’ in comparison to the non-ischemic hemisphere and future ‘penumbra’ regions in ischemic hemisphere. Δ LT nadir values after OGD-SD (n=31 slices) in the medial parietal (Par_{med}: $-8 \pm 0.8\%$; mean \pm S.E.M.) and lateral parietal (Par_{lat}: $-10 \pm 0.9\%$; mean \pm S.E.M.) regions of the non-ischemic hemisphere as well as medial parietal ‘penumbra’ of the ischemic hemisphere (Par_{med} ‘Penumbra’: $-8 \pm 0.8\%$; mean \pm S.E.M.) were significantly less than the lateral parietal ‘core’ of the ischemic hemisphere (Par_{lat} ‘Core’: $-6 \pm 0.7\%$; mean \pm S.E.M.). Significantly lower nadir Δ LT was also evident in ischemic hemisphere S1FL after OGD-SD in comparison to S1BF cortical regions in the non-ischemic hemisphere ($-8 \pm 0.8\%$ vs. $-10 \pm 0.9\%$; mean \pm S.E.M; $p < 0.05$).

Electrophysiology

Field EPSPs were recorded at increasing stimulation intensities at each recording site. There was no significant response differences between the ischemic and non-ischemic hemispheres at each of the individual intensities as shown in Figure 23. The amplitude of the fEPSPs in the ischemic vs. non-ischemic hemispheres (n = 12 vs. n = 6 recordings) were not significantly different at 50, 70, 100 and 130 mV stimulation intensities.

An ANOVA with 2 between-subject levels (hemisphere and intensity of stimulation) was performed on a pooled dataset containing EPSP amplitudes as a function of stimulus intensity. The analysis demonstrated a significant main effect for intensity ($F = 3.096$, $p < .05$, ω^2 estimate = 0.11). Post-hoc oneway analysis of variance employing Tukey correction (alpha level set to 0.05) for multiple comparisons indicated a general increase in evoked synaptic response as a function of increasing stimulation, as expected. However, there was not a significant main effect between the ischemic and non-ischemic hemisphere as a function of stimulation intensity.

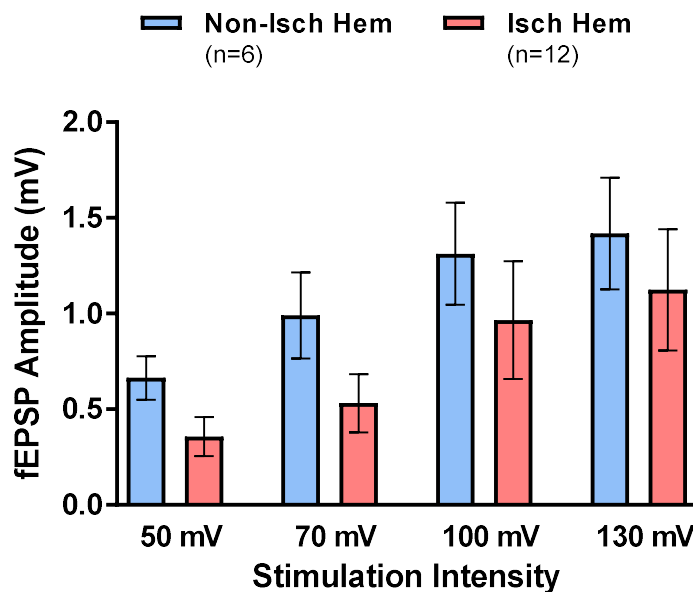


Figure 23. Amplitude of synaptic responses evoked by an increasingly strong stimulus was not significantly different in the ischemic vs. the non-ischemic hemisphere. The amplitude of the mean field EPSPs recorded in LII/III cortex of post-ischemic brain slices were not significantly different in the ischemic vs. non-ischemic hemispheres (mean \pm S.E.M.) at 50 mV (0.36 ± 0.10 vs. 0.66 ± 0.11 mV), 70 mV (0.53 ± 0.15 vs. 0.99 ± 0.22 mV), 100 mV (0.97 ± 0.31 vs. 1.31 ± 0.27 mV), 130 mV (1.12 ± 0.32 vs. 1.42 ± 0.29 mV).

We then patch clamped neocortical layer II/III pyramidal neurons in the ischemic or non-ischemic hemispheres. At 40X magnification there were abundant neurons in the future core

region of the ischemic hemisphere with normal morphology under contrast optics. Resting membrane potential, whole cell input resistance and the time constant were not significantly different between neurons within the lateral parietal neocortex (Par_{lat}) ‘core’ in comparison to neurons within medial parietal cortex (Par_{med}) ‘penumbra’ in the ischemic hemisphere, as shown in Table 3. Action potential width, amplitude and threshold as well as the fast afterhyperpolarization (fAHP) following a depolarizing pulse evoking a spike train were also compared in Par_{lat} ‘core’ vs. Par_{med} ‘penumbra’ neocortical pyramidal neurons in LII/III of the ischemic hemisphere. None of these properties were significantly different between the two regions (Table 3). Furthermore, the action potential width, amplitude and threshold as well as the resting membrane potential, whole cell input resistance, time constant and fAHP were not significantly different between the corresponding Par_{med} and Par_{lat} regions in the ischemic vs. non-ischemic hemispheres (Table 3).

Discrepancy of SD Onset Between Ischemic and Non-Ischemic Hemispheres Eliminated

A multiple comparisons ANOVA with one between-subject level (drug) and one within-subject level (hemisphere) was conducted to discern differences in latency to SD onset. The analysis revealed significant main effects for hemisphere ($F = 22.27$, $p < 0.001$, partial $\eta^2 = 0.37$) and drug pre-treatment ($F = 13.90$, $p < 0.001$, partial $\eta^2 = 0.42$), but no significant interaction. Separate *post-hoc* oneway analyses of variance (with Tukey correction for multiple comparisons) for latency to SD onset within the ischemic and non-ischemic hemispheres indicated that the ischemic ($F = 10.30$, $p < 0.001$) and non-ischemic ($F = 5.93$) hemispheres displayed differences in the latency to SD onset as a function of drug pre-treatment.

Further analyses using Student's t-test revealed a significantly delayed OGD-induced SD onset in the ischemic hemisphere was observed despite pre-treatment with the adenosine antagonist DPCPX (365 ± 26 vs. 260 ± 20 , $n=15$, $p < 0.01$). This was similar to control acsf pre-incubated brain slices (417 ± 20 vs. 297 ± 13 , $n=31$, $p < 0.001$) harvested after MCAo (Figure 24). The significantly slower wavefront velocity evident in the ischemic hemisphere of brain slices pre-incubated with control aCSF (1.7 ± 0.2 vs. 3.0 ± 0.2 , $n=5$, $p < 0.01$), was also unaffected by $1 \mu\text{M}$ DPCPX pre-treatment (1.3 ± 0.2 vs. 2.0 ± 1.2 , $n=5$, $p < 0.05$) as shown in Figure 25.

Ouabain at a high concentration (30-100 μM) inhibits the Na^+/K^+ pump activity thereby inducing SD. The latency to SD onset in the ischemic vs. non-ischemic hemisphere induced by 100 μM ouabain was not significantly different (301 ± 16 vs. 234 ± 5 , $p = 0.08$) (Fig. 24) and neither was the propagating SD wavefront speed (2.9 ± 0.3 vs. 3.5 ± 0.5 ; $p = 0.35$, $n=5$) as shown in Figure 25. The delayed latency to onset and slower propagating wavefront of SD in the ischemic hemisphere was not evident when SD was induced by chemically inhibiting the Na^+/K^+ pump with ouabain.

Ouabain at low doses has been reported to increase Na^+/K^+ pump activity (Gao et al. 2002; Oselkin et al. 2010). When post-ischemic brain slices were pre-incubated with $1 \mu\text{M}$ ouabain the latency to OGD-induced SD onset was not significantly different between the ischemic and non-ischemic hemispheres (418 ± 32 vs. 343 ± 29 ischemic vs. non-ischemic, $p = 0.09$, Figure 24) but the propagating SD wavefront was significantly slower in the ischemic vs. non-ischemic hemisphere (1.2 ± 0.2 vs. 1.7 ± 0.3 ; $p < 0.05$, $n=5$) as shown in Figure 25. The latency to OGD-induced SD onset in the non-ischemic hemisphere with low-dose ouabain was delayed to within the onset range displayed by the ischemic hemisphere (Fig. 24).

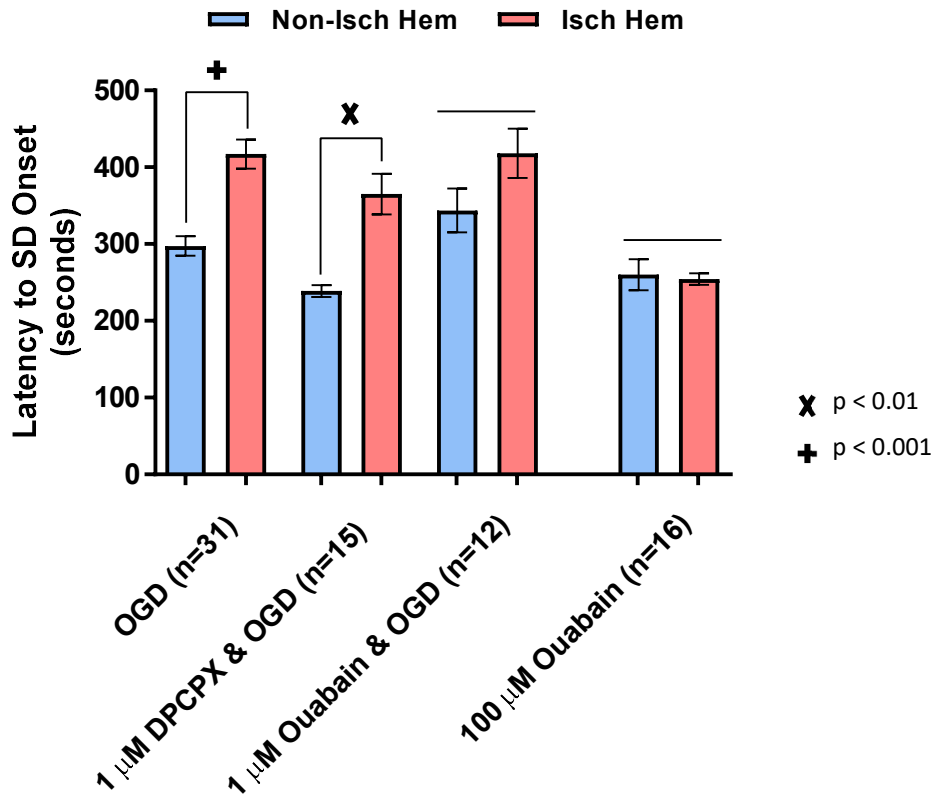


Figure 24. Na⁺/K⁺ pump modulation, but not adenosine A1 receptor inhibition, eliminates the delayed SD onset observed in the post-ischemic hemisphere. Average latency to SD onset was significantly delayed in the ischemic hemisphere vs. the non-ischemic hemisphere of post-ischemic brain slices pre-incubated with control acsf (417 ± 20 vs. 297 ± 13 , $p < 0.001$, \pm S.E.M.) and DPCPX (365 ± 26 vs. 260 ± 20 , $n=15$, $p < 0.01$, \pm S.E.M.). However, the significantly delayed latency to SD onset between the ischemic vs. the non-ischemic and hemispheres was absent with 20 min pre-incubation of post-ischemic brain slices with 1 μ M ouabain prior to OGD (418 ± 32 vs. 343 ± 29 ischemic vs. non-ischemic, $p = 0.09$, \pm S.E.M.), as well as when SD was induced by 100 μ M ouabain (301 ± 16 vs. 234 ± 5 , $p = 0.08$, \pm S.E.M.).

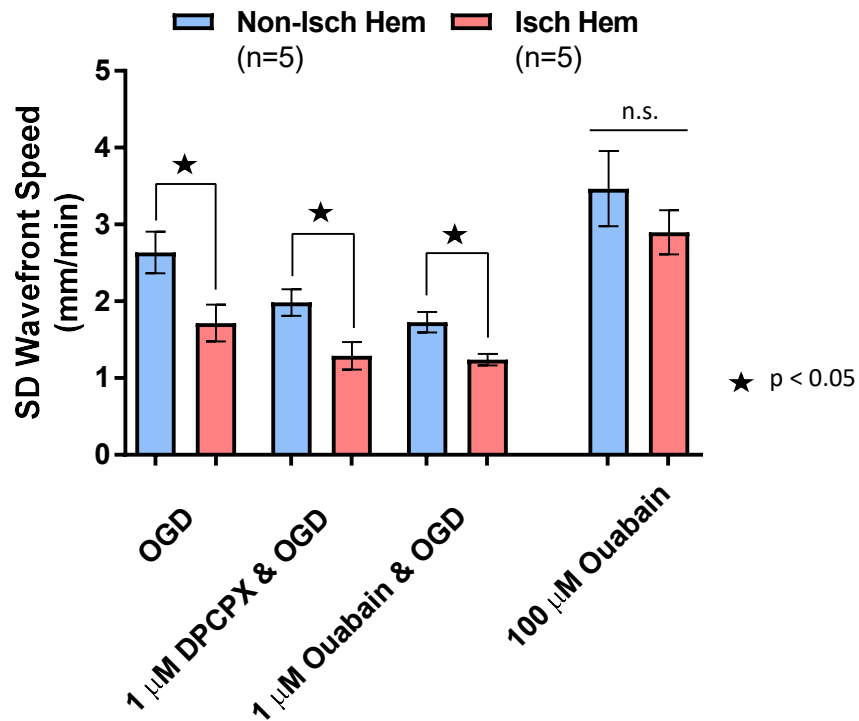


Figure 25. OGD-induced SD wavefront is slower in the ischemic hemisphere, but not significantly different during SD induced by saline containing 100 μM ouabain. The propagating SD wavefront in the ischemic hemisphere was significantly slower than in the non-ischemic hemisphere in post-ischemic slices pre-incubated with control aCSF (1.7 ± 0.2 vs. 3.0 ± 0.2 , $p < 0.01$, $n=5$), 1 μM DPCPX (1.3 ± 0.2 vs. 2.0 ± 1.2 ; $p < 0.05$, $n=5$) and 1 μM ouabain (1.2 ± 0.2 vs. 1.7 ± 0.3 ; $p < 0.05$, $n=5$) prior to OGD, but not during SD induced by 100 μM ouabain (2.9 ± 0.3 vs. 3.5 ± 0.5 ; $p = 0.35$, $n=5$).

4.5 Discussion

Post-Ischemic Resistance to SD

We used a novel approach to investigate the propensity of post-ischemic brain tissue to initiate and sustain SD. By harvesting coronal brain slices immediately after MCAo, we could investigate the post-ischemic higher brain without fluctuations in post-stroke CBF or brain temperature that can confound rodent stroke models. This allowed us to image SD initiation and

propagation throughout the gradient of post-ischemic neocortex from the future ‘core’ to ‘penumbra’ as well as in non-ischemic cortex. Our findings show that immediately following 30 minute MCAo and contrary to the expectation that post-ischemic gray matter is more susceptible to recurrent SD, there is instead a resistance to SD manifested both as a delayed latency to SD onset and a slower speed of SD propagation. Whether this reflects an absence of the vascular component is not known.

The ischemic ‘core’ is associated with loss of ionic homeostasis and neuronal activity when CBF levels drop below 10-20% of control values. The ischemic ‘penumbra’ corresponds to decline of synaptic transmission associated with CBF levels between 20-40% of control baseline (Astrup et al. 1981a; Strong et al. 1983; Hossmann 1994; Heiss 1992). Using digitally-constructed coronal images of *in vivo* MCAo in C57BL6 mice, < 20% CBF was observed in temporal and lateral parietal neocortex and CBF levels between 20-40% of control levels were observed in adjacent medial parietal neocortex (Belayev et al. 1997). In our experiments we recorded synaptic communication, single cell electrophysiology and SD in these neocortical areas of coronal brain slices harvested immediately after MCAo in the same mouse strain. By harvesting brain slices after MCAo we were able to observe post-ischemic electrophysiology and SD within a controlled temperature and aCSF medium in the absence of CBF fluctuations.

After harvesting brain slices and incubating them at 37°C in oxygenated aCSF we were able to observe SD after MCAo without the blood flow and temperature fluctuations that influence SD during ischemia. We found a slower propagating SD wavefront, delayed SD onset and less light scatter in the ischemic hemisphere. Delayed latency to OGD-induced SD onset after drug treatment or hypothermia is associated with better recovery of evoked synaptic communication in slices (Douglas et al. 2011; Anderson et al. 2005; Obeidat et al. 2000; Chen et al. 1993).

Attenuating the reduction of ΔLT after SD has also been associated with less dendritic injury (Risher et al. 2011). In vivo, delayed latency to SD onset could decrease the number or frequency of post-ischemic SD events, which has been demonstrated to decrease infarct volume following drug treatment (Mies et al. 1994; Busch et al. 1996). Our observations of less light scatter (i.e., less cell swelling) and intact electrophysiology in post-ischemic cortex along with a delayed latency to onset and slower propagation speed of SD implies an attenuation of post-ischemic SD. Thus, resistance to SD independent of blood flow appears to increase in brain slices harvested after MCAo.

Adenosine

Ilie et al. (2006) showed that DPCPX administration intraperitoneally could reverse suppression of electrocortical activity after in vivo transient global ischemia. In mouse brain slices, a greater duration and spatial extent of KCl-induced SD is associated with suppressed synaptic activity which is abolished by the adenosine A_1 receptor antagonist DPCPX (Lindquist and Shuttleworth 2012). Adenosine transiently increases after SD in peri-infarct regions (Lindquist and Shuttleworth 2014). Relative to pre-ischemic baseline, adenosine is elevated after MCAo to a much greater extent than glutamate and other metabolites (Sciotti et al. 1992). Furthermore, adenosine release is associated with decreased frequency of $[K^+]_{ext.}$ -induced SD (Kaku et al. 1994), delayed spontaneous onset of fluoroacetate-induced SD (Canals et al. 2008) and delayed hypoxia-induced SD (Lee and Lowenkopf 1993). Suppression of electrocortical activity is reversed by DPCPX after ischemia in the intact rat (Ilie et al. 2006). Thus we anticipated that the delayed latency to SD onset in the ischemic vs. non-ischemic hemisphere in our experiments could be reversed with adenosine A_1 receptor antagonism using DPCPX.

DPCPX at 1 μM blocked suppression of synaptic activity after SD in brain slices (Lindquist and Shuttleworth 2012). Our pre-treatment of post-ischemic brain slices with 1 μM DPCPX did not alter the delayed SD onset or slower propagating wavefront speed in the ischemic hemisphere. Therefore this post-ischemic inhibition we observe is not caused by adenosine-mediated suppression of synaptic activity. Similarly Lindquist and Shuttleworth (2012) found that KCl-induced SD duration and propagation speed was not affected by DPCPX in neocortical mouse brain slices. SD arising following ischemia occurs at much lower CBF levels than does adenosine elevation and synaptic failure (Hossmann 1994). So the SD inhibition we observe in the ischemic hemisphere immediately following MCAo is not adenosine-mediated.

The Na^+/K^+ pump

Approximately 40% of the brain's energy is utilized by Na^+/K^+ pump to maintain ionic homeostasis (Erecinska and Silver 1989; Astrup et al. 1981b). Modelling of SD indicates that a deficit of extrusion of $[\text{Na}^+]_{\text{int}}$ and sequestering of $[\text{K}^+]_{\text{ext}}$ is involved with SD initiation (Kager 2002; Dreier et al. 2013). In neocortical slices Na^+/K^+ pump blockade by high dose ouabain (30-100 μM) induces SD similar to OGD (Jarvis et al. 2001). Like with OGD-SD, there is a similar rapid, sustained depolarization (Balestrino et al. 1999; Tanaka et al. 1997; Dietz et al. 2008), a propagating SD wavefront of comparable speed (Anderson et al. 2005) and ensuing acute neuronal injury (Douglas et al. 2011; Anderson et al. 2005). However, 100 μM ouabain induces SD consistently earlier than does OGD (Tanaka et al. 1997; Anderson et al. 2005; Obeidat and Andrew 1998). In this study, ouabain-SD onset time and propagation speed were no different in the ischemic vs. non-ischemic hemispheres, unlike with OGD-SD where SD was delayed and more slowly propagating on the ischemic side. Decreased propagation of SD through brain tissue

stimulated by low frequency electrical stimulation was hypothesized to involve increased Na^+/K^+ pump activity (Reddy and Bures 1980). The delayed SD onset and slower SD propagation on the ischemic side of post-MCAo brain slices was over-ridden by frank chemical blockade of the pump by 100 μM ouabain.

In contrast to 100 μM ouabain which inhibits Na^+/K^+ pump activity, low-concentration ouabain increases Na^+/K^+ pump activity (Gao et al. 2002). Pre-exposure of cultured neurons to low-concentration ouabain increased Na^+/K^+ pump activity and decreased damage after exposure to anoxia and glucose deprivation (Oselkin et al. 2010). When we pre-incubated post-ischemic slices with a low (1 μM) dose of ouabain prior to OGD, the latency to SD onset between hemispheres was not significantly different. The delayed SD onset in the ischemic hemisphere was matched by SD onset in the non-ischemic side presumably by enhancement of Na^+/K^+ pump activity with low-concentration ouabain.

There is a greater proportion of α_3 -containing Na^+/K^+ pumps after simulated (Belliard et al. 2013) and in vivo ischemia (Schwinger et al. 1999). Considering that this isoform can extrude $[\text{Na}^+]_{\text{int}}$ at a much greater rate than α_1 -containing isoforms (Azarias et al. 2013), increased expression of the α_3 - Na^+/K^+ pump could be associated with a delayed latency to SD onset. In the brainstem, a delayed elevation of $[\text{K}^+]_{\text{ext}}$ is observed during ischemia (Bures and Buresová 1981) as well as a delayed onset of hypoxia-induced SD (Richter et al. 2010) and a greater resistance to terminal depolarization after OGD in comparison to higher gray matter (Brisson and Andrew 2012; Brisson et al. 2013; Brisson et al. 2014). Interestingly, the higher brain displays a greater ratio of Na^+/K^+ pumps with α_1 -subunits and less α_3 -subunits as found by data mining the Allen Brain Atlas which is confirmed by mRNA and protein expression (Andrew, unpublished). Thus,

specific experiments examining post-ischemic modulation of expression and function of the Na^+/K^+ pump and its influence upon SD would be worthwhile and are being addressed.

To summarize, we showed in Chapter 2 that brain slices harvested immediately after MCAo displayed normal neuronal morphology, synaptic communication and electrophysiology on the ischemic and non-ischemic side. A delayed latency to SD onset and slower wavefront propagation in the ischemic hemisphere during subsequent OGD of coronal slices was unaffected by adenosine A_1R inhibition by DPCPX. However, the post-ischemic resistance to SD associated with the delayed latency to SD onset and slower wavefront propagation during OGD was overridden when SD was induced by 100 μM ouabain exposure. Pre-incubation of post-ischemic brain slices with 1 μM ouabain also eliminated the discrepancy in post-ischemic SD onset between the non-ischemic and ischemic hemispheres.

Conclusions

- 1) Immediately following 30 minute MCAo and contrary to the expectation that post-ischemic gray matter is more susceptible to recurrent SD, there is instead a resistance to SD manifested in the ischemic hemisphere both as a delayed SD onset and a slower speed of SD propagation.
- 2) This mild resistance to SD is not explained as a detectable difference between hemispheres either in the evoked synaptic response or the intrinsic electrophysiological properties of single pyramidal neurons. Surprisingly, these characteristics appear unchanged in slices harvested immediately after a 30 minute MCAo.
- 3) The discrepancy in post-ischemic SD between the non-ischemic and ischemic hemispheres is a reversible phenomenon affected by ouabain. The possibility of a reversible suppression of SD that may involve the Na^+/K^+ pump is apparent, but requires further investigation.

Table 3. Baseline Electrophysiological Properties of Neurons Within ‘Core’ (Par_{lat}) and ‘Penumbra’ (Par_{med}) Post-Ischemic Neocortex and Corresponding Areas in the Non-Ischemic Hemisphere. Action potential width, amplitude and threshold as well as the resting membrane potential, whole cell input resistance, time constant and fAHP were not significantly different between Par_{med} and Par_{lat} regions in the ischemic hemisphere and corresponding Par_{med} and Par_{lat} regions in the non-ischemic hemisphere.

		Non-Isch Hem (Par _{lat} n =11, Par _{med} n=5)	Isch Hem (Par _{lat} n =10, Par _{med} n=11)
RMP	Par _{lat}	-71 ± 5.0	-71 ± 9.8
(mV)	Par _{med}	-74 ± 5.0	-71 ± 3.8
R_{in}	Par _{lat}	106 ± 35	110 ± 22
(MΩ)	Par _{med}	157 ± 19	115 ± 38
fAHP	Par _{lat}	9.2 ± 4.0	10.2 ± 4.9
(mV)	Par _{med}	9.7 ± 2.0	10.2 ± 5.8
Width of Action Potential	Par _{lat}	0.7 ± 0.1	0.74 ± 0.1
(msec)	Par _{med}	0.7 ± 0.1	0.72 ± 0.2
Action Potential Amplitude	Par _{lat}	83 ± 5.8	83 ± 11
(mV)	Par _{med}	83 ± 8.5	74 ± 15
Action Potential Threshold	Par _{lat}	-36 ± 2.5	-34 ± 7.3
(mV)	Par _{med}	-38 ± 3.1	-34 ± 4.9
Tau	Par _{lat}	15.3± 4.0	16.8 ± 7.5
(ms)	Par _{med}	18.1± 3.1	14.5 ± 4.8

Chapter 5

General Discussion

5.1 Leao's Prescient Observations of SD

Aristides Leao (1944) originally observed 'spreading depression of cortical activity' following noxious electrical stimulation of rabbit neocortex (Leão 1944). He related these observations to a similar negative slow voltage variation evident following prolonged interruption of circulation to the neocortex (Leao 1947). In his pioneering work, Leao presciently described a common phenomenon now referred to as 'spreading depolarization' (SD) that results in a slowly propagating wave (1-8 mm/min) of disrupted ionic homeostasis, membrane depolarization, neurotransmitter release as well as cellular swelling and dendritic beading (Somjen 2001; Dreier 2011; Hartings et al. 2017). These parameters are all similarly affected in a continuum from abrupt, non-damaging spreading depression events with rapid recovery in normal brain to prolonged or terminal depolarization in severely ischemic and metabolically compromised brain tissue (Hartings et al. 2017). Despite the fact that SD is observed within minutes of focal ischemia onset and is strongly correlated with infarct expansion in rodents and patients, no clinical investigation has attempted to attenuate SD in order to improve clinical outcome. Instead trials have targeted excitotoxicity, inflammation, antioxidants or thrombolysis. Thrombolysis is one of only two clinically-approved therapies (O'Collins et al. 2006), in addition to thrombectomy (Jovin et al. 2015; van den Berg et al. 2017). Difficulty in translating experimental investigations to clinical therapies is partly because we do not understand the fundamental cause of SD and how to prevent its recurrence after stroke or trauma.

By superfusing brain slices harvested after MCAo with either elevated $[\text{glu}]_{\text{ext}}$, elevated $[\text{K}^+]_{\text{ext}}$ or OGD saline solutions we were able to observe the response of the post-ischemic brain to further metabolic stress in the absence of temperature and CBF fluctuations. When $[\text{glu}]_{\text{ext}}$, $[\text{K}^+]_{\text{ext}}$, and OGD saline solutions were superfused onto post-ischemic brain slices, we observed an attenuated swelling, decreased incidence of SD and a delayed SD onset in the post-ischemic brain. Considering that intact synaptic communication, intrinsic electrophysiology and morphology were displayed by pyramidal neurons in brain slices harvested immediately after MCAo, the post-ischemic brain could be resistant to SD. However, most of these neurons are irretrievably swollen or necrotic when we image them 12 hours later. Furthermore, in response to OGD, these regions display attenuated swelling and a reduced ability to generate SD, reflecting this injury and electrical silence. This dramatic infarction proceeds during the first 12 hours despite reperfusion immediately following the 30-minute MCAo. These findings highlight the importance of examining SD and the infarct maturation *immediately* and within the ensuing *12 hours after* ischemia

Post-ischemic SD, synaptic communication and single neuron electrophysiology were studied and comprise this thesis. By observing SD in post-MCAo brain slices i) the precise site of ignition was localized, ii) the ensuing SD propagation was mapped with good spatial and temporal resolution and iii) tissue damage was identified following the wake of SD propagation, similar to experiments using non-ischemic neocortical slices (Obeidat and Andrew 1998) but with greater resolution than digitized coronal images captured during in vivo ischemia (Busch et al. 1996).

5.2 Post-Ischemic Electrophysiology

Few studies have examined changes in synaptic communication and single cell electrophysiology in the post-ischemic brain. In brain slices harvested *immediately* after MCAo, we found that synaptic communication in neocortical layers II-III was intact, supported by the normal neuronal morphology observed in our Golgi-Cox preparations. Passive single cell electrophysiological properties of post-ischemic layer II/III neocortical pyramidal neurons (resting membrane potential, input resistance, time constant) were similar to the non-ischemic hemisphere. The duration, amplitude and threshold of action potentials were also similar in cortical layer II/III pyramidal neurons within the ischemic and non-ischemic hemispheres. The fast afterhyperpolarization following action potentials and the time constant of the membrane potential as it decayed to the resting potential following action potential trains were also similar in ischemic and non-ischemic neocortical LII/III pyramidal neurons. These observations are comparable to the intact single cell electrophysiology observed in hippocampal CA1 pyramidal neurons 5 hours following global ischemia (Gao et al. 1998; Gao et al. 1999). The threshold, amplitude, and width of action potentials as well as the time (decay) constant following an action potential train in post-ischemic brain slices were also similar to regular-spiking neocortical pyramidal neurons in control animals from other studies (McCormick et al. 1985; Silva et al. 1991).

A striking finding of this thesis is that the brain areas known to be affected by MCAo appear surprisingly healthy immediately following 30 minutes of ischemia, yet the same region is devastated after 12 hours of reperfusion. Synaptic communication is absent in the ischemic territory of brain slices harvested *12 hours after* MCAo. There is extensive morphological damage throughout the ischemic infarct as well. Yet the few neurons that can be recorded within

the ischemic core in these brain slices show essentially normal electrophysiological properties. Our Golgi-Cox staining confirmed that these neurons indeed appeared uninjured despite being surrounded by severely necrotic neurons. We have not captured the timepoint where injury occurs and it undoubtedly varies across the stressed region. These observations raise two important questions. First what is special about these surviving neurons? Second, do they continue to survive and, if so, for how long? The loss of the majority of neurons in the infarct core certainly explains the inability of the core region to support SD when the 12 hour post-MCAo tissue is sliced. However, the decreased incidence and delayed onset of SD in brain slices harvested *immediately* after MCAo in our experiments is not easily explained. By superfusing post-ischemic brain slices with elevated extracellular glutamate, $[K^+]_{ext}$ or oxygen-and-glucose deprivation (OGD) aCSF, we were able to assess differences in swelling and SD between the non-ischemic and post-ischemic brain immediately and 12 hours after arterial occlusion and reperfusion.

5.3 Elevated $[K^+]_{ext}$, $[glu]_{ext}$ and Oxygen/Glucose Deprivation in the Post-Ischemic Brain

Elevated $[glu]_{ext}$, elevated $[K^+]_{ext}$ and CBF reduction occur following ischemia (Nedergaard and Hansen 1993; Shimada et al. 1990; Folbergrová et al. 1992; Obrenovitch et al. 1988; Satoh et al. 1999; Sciotti et al. 1992). Elevated $[glu]_{ext}$ arises along with SD (Zhou et al. 2013), but does not induce it (Jarvis et al. 2001). Elevated $[K^+]_{ext}$ triggers non-damaging SD (Nedergaard and Hansen 1988; Dietz et al. 2008; Jarvis et al. 2001; Anderson and Andrew 2002; Zhou et al. 2013). Initial conditions that arise within the ischemic core are simulated in the brain slice by depriving neocortical slices of oxygen and glucose. Within minutes of OGD superfusion of neocortical brain slices, a propagating wave of SD occurs with dendritic beading following in its

wake (Anderson et al. 2005; Andrew et al. 2007), similar to in vivo observations during photothrombotic ischemia (Murphy et al. 2008). The post-ischemic brain displays time-dependent variability in SD incidence and tissue damage in vivo (Hartings et al. 2003). By harvesting brain slices *immediately* and *12 hours* following MCAo the response of the post-ischemic brain to elevated $[\text{glu}]_{\text{ext}}$, elevated $[\text{K}^+]_{\text{ext}}$ or OGD were assessed in real-time with high spatial resolution in our experiments.

When 500 μM glutamate saline was superfused onto brain slices harvested immediately or 12 hours following MCAo, the ischemic hemisphere displayed a lower incidence of glutamate-induced swelling than the contralateral non-ischemic hemisphere. In other studies, 10 mM glutamate aCSF superfusion precipitated tissue swelling but not SD in hippocampal slices (Obeidat and Andrew 1998). In contrast in the current study, brain slices harvested immediately after MCAo display a decreased incidence of glutamate-induced swelling in the ischemic hemisphere during 500 μM glutamate saline superfusion. Considering that an increased expression of glutamate transporters has been previously observed in the post-ischemic brain (Zhang et al. 2010), an increased uptake of $[\text{glu}]_{\text{ext}}$ in post-ischemic neocortical brain slices is possible.

When 9.6mM $[\text{K}^+]_{\text{ext}}$ was superfused onto brain slices harvested immediately following MCAo, the ischemic hemisphere displayed a lower incidence of SD_{K^+} than the contralateral non-ischemic hemisphere. In studies by others, the latency to OGD-induced SD onset was accelerated by superfusing neocortical brain slices with 9.7mM $[\text{K}^+]_{\text{ext}}$ saline (Tanaka et al. 1997). A ceiling threshold of ~ 10 mM $[\text{K}^+]_{\text{ext}}$ is observed prior to SD eruption in non-ischemic and post-ischemic brain tissue (Heinemann and Lux 1977; Nedergaard and Hansen 1993; Hansen 1985). However, a delayed profile of $[\text{K}^+]_{\text{ext}}$ elevation is evident during ischemia (Nedergaard and Hansen 1993).

Thus, a decreased propensity of elevated $[K^+]_{ext}$ to ‘trigger’ SD is evident after ischemia in the intact animal and in post-MCAo brain slices.

The ischemic hemisphere of brain slices harvested 12 hours following MCAo also displayed less tissue swelling during $500 \mu M [glu]_{ext}$ and decreased incidence of SD during $9.6 mM [K^+]_{ext}$ saline superfusion, respectively. There was obvious damage in the ischemic hemisphere in Golgi-stained brain sections at 12 hours following ischemia and reperfusion. Synaptic communication was absent in the ischemic hemisphere of brain slices harvested 12 hours following MCAo. Thus, the failure of the ischemic hemisphere to elicit $[glu]_{ext}$ -induced swelling or SD_{K^+} at the later timepoint was likely a result of unresponsiveness of infarcted brain. During $9.6 mM [K^+]_{ext}$ saline superfusion, SD was evident in brain regions peripheral to the infarcted neocortex supplied by the unoccluded anterior cerebral artery. However, these SD events originated within the contralateral non-ischemic hemisphere and propagated across the longitudinal suture along the surface of the coronal brain slice and into the ischemic hemisphere, which does not occur in the intact brain during ischemia in vivo (Nedergaard and Hansen 1993). Therefore, an infarcted ischemic ‘core’ with a decreased propensity to tissue swelling and SD events was juxtaposed next to a medial ‘penumbra’ that could sustain SD_{K^+} in neocortical brain slices harvested 12 hours following 30 minute MCAo.

5.4 Delayed SD Onset and Decreased Incidence of Post-Ischemic SD

Superfusion of OGD saline onto neocortical brain slices is a more potent stimulus initiating and sustaining SD than elevated $[K^+]_{ext}$ saline. Following individual or successive waves of SD_{K^+} initiated by elevated $[K^+]_{ext}$ saline superfusion, neuronal morphology and synaptic communication remain intact (Anderson and Andrew 2002; Dietz et al. 2008; Andrew et al. 2007). In contrast, superfusion of neocortical brain slices with OGD results in terminal

depolarization of neurons, cessation of synaptic communication and evidence of neuronal damage (Anderson et al. 2005; Douglas et al. 2011; Brisson and Andrew 2012). OGD-induced SD results in terminal depolarization of neurons (Brisson and Andrew 2012) similar to SD events in the ischemic ‘core’ (Koroleva and Bures 1996; Nallet et al. 1999; Dijkhuizen et al. 1999). In contrast, SD_{K^+} can be induced without adverse effects upon synaptic communication or neuronal morphology (Anderson and Andrew 2002; Andrew et al. 2007) similar to SD propagating through non-ischemic neocortex in the intact animal (Nedergaard and Hansen 1988). When brain slices harvested immediately after MCAo were superfused with OGD saline, an SD event occurred in every brain slice. In contrast, OGD-SD was observed in the ischemic hemisphere of only 45% of brain slices harvested 12 hours following MCAo. This finding confirmed our previous observations of less responsive brain tissue at 12 hours following ischemia corresponds with infarction.

In contrast, OGD-induced SD occurred in the ischemic hemisphere of every brain slice harvested immediately following MCAo. OGD-induced SD also consistently occurred later in the ischemic hemisphere of brain slices harvested immediately following MCAo. Although SD spontaneously erupts with a high incidence in the initial 1-2 hours following ischemia, there is an abrupt decline of SD incidence in the 4-6 hours thereafter (Dijkhuizen et al. 1999; Koroleva and Bures 1996; Back et al. 1996; Hartings et al. 2003). This decline in SD has been hypothesized to involve an active suppression by post-ischemic brain tissue (Nallet et al. 1999). The delayed latency to SD onset we observed in the intact immediate post-ischemic brain could be supportive of an ‘adaptive mechanism of the post-ischemic tissue to limit or prevent further depolarizations’ suggested by Nallet and colleagues (1999).

SD erupting near the ischemic core results in terminal depolarization (Koroleva and Bures 1996; Nallet et al. 1999; Dijkhuizen et al. 1999). Terminal depolarization of neurons and failure of synaptic communication also occurs after OGD-SD in neocortical brain slices (Anderson et al. 2005; Douglas et al. 2011; Brisson and Andrew 2012). However, when drugs delay the latency to OGD-SD onset in rat neocortical brain slices, the likelihood of recovery of synaptic communication increases (Anderson et al. 2005; Douglas et al. 2011). The two drugs that most effectively delay SD onset and increase the likelihood of synaptic recovery are dibucaine and carbetapentane (Anderson et al. 2005; Douglas et al. 2011). SD onset was delayed in both ischemic and non-ischemic hemispheres in post-ischemic brain slices pre-incubated with carbetapentane or dibucaine. Thus, these two drugs also delay SD in the post-ischemic brain. In previous studies carbetapentane decreased episodic hypoperfusion that follows SD events following MCAo (Shin et al. 2006) and dibucaine decreased dendritic damage after photothrombosis-induced ischemia (Risher et al. 2011). We add to these findings by demonstrating that CP and DB delay SD onset in neocortical brain slices harvested immediately after MCAo.

The incidence of SD and infarct expansion vary over time following focal cerebral ischemia. A 25% incidence of spontaneous SD is observed after ischemia in vivo (Takano et al. 1996), comparable to the 25% incidence of spontaneous SD we observed in slices harvested immediately post-MCAo. High SD incidence immediately after ischemia is correlated with larger infarct volumes (Mies et al. 1994). Furthermore, a later secondary phase of increased SD correlates with infarct expansion approximately 12 hours following ischemia, regardless of reperfusion (Hartings et al. 2003). We observed mainly necrotic brain tissue in brain slices harvested 12 hours post-MCAo with disrupted synaptic communication. We did not observe an

increased incidence or propensity to SD initiation in response to further metabolic stress at this later time point in tissue near the core. One likely explanation for this discrepancy is that our ischemic gray matter, being in sliced form, is less synaptically connected to surrounding non-stroked tissue. Another explanation is that CBF fluctuations inherent in the reperfused post-ischemic brain (Shin et al. 2006; von Bornstädt et al. 2015) are lacking in post-MCAo brain slices. As CBF vacillates in vivo, the blood flow threshold associated with disruption of ion homeostasis and SD (Astrup et al. 1981a; Hossmann 1994) is likely triggered. Although SD normally erupts first in neurons (Zhou et al. 2010) followed by a glial response and vascular fluctuations thereafter (Chuquet et al. 2007), post-ischemic CBF fluctuations in the post-ischemic brain are likely a contributing factor to multiphasic episodes of SD and infarct expansion.

Given that SD results from a failure or overwhelming of the Na^+/K^+ pump, it is an obvious but neglected drug target candidate of SD suppression through altered expression or function. This transporter restores the membrane gradient following action potentials and is the key determinant in membrane potential maintenance during seizure and ischemia (Dreier et al. 2013). Inhibition of the Na^+/K^+ pump with 30-100 μM ouabain in neocortical slices produces a propagating SD-like wavefront similar to OGD (Brisson et al. 2012; Dietz et al. 2008; Anderson et al. 2005; Tanaka et al. 1997). However SD onset occurs earlier with ouabain than OGD (Tanaka et al. 1997; Anderson et al. 2005). Furthermore, ouabain inhibits the Na^+/K^+ pump at a high-concentration but increases pump activity at lower concentrations (Gao et al. 2002). We found that the normally delayed OGD-SD onset and the slower speed of the SD wavefront were nullified when SD was initiated by 100 μM ouabain in the ischemic hemisphere. Furthermore, the discrepancy of the latency to OGD-SD onset between the ischemic and non-ischemic

hemisphere was nullified when post-ischemic neocortical brain slices were pre-incubated with low-dose (1 μ M) ouabain. A large depolarizing inward current (i.e., SD) is induced by high-concentration ouabain and a small net hyperpolarizing outward current is evoked by low-concentration ouabain (Gao et al. 2002). Modulation of the Na^+/K^+ pump with high and low dose ouabain eliminated the discrepancy of SD onset between the ischemic and non-ischemic hemispheres. However, we did not establish clear evidence of altered post-ischemic Na^+/K^+ pump expression or function causing the delayed latency to SD onset in the ischemic hemisphere. A more accurate description of our observations is that the discrepancy in post-ischemic SD between the non-ischemic and ischemic hemispheres is a reversible phenomenon affected by ouabain. Whether differences in pump isoform expression underlies these regional differences is under study in the Andrew lab.

5.5 Conclusions

Overall, this thesis emphasizes the importance of further investigation into the mechanism of SD initiation and infarct maturation over the initial 12 hours following ischemia. We found that infarction proceeds in the initial 12 hours following ischemia despite reperfusion after 30 minutes of middle cerebral artery occlusion. This infarction occurs despite initial observation of intact single cell electrophysiology, synaptic communication and single cell electrophysiology in brain regions known to be affected by the occluded middle cerebral artery. In this thesis we also showed that carbetapentane and dibucaine delay SD onset in post-ischemic neocortical brain slices similar to their effects upon non-ischemic neocortical brain slices in other studies (Anderson et al. 2005). The Andrew lab is examining if these two drugs work directly on stimulating or preserving the function of the Na^+/K^+ pump. A decreased propensity to SD and

swelling in the ischemic hemisphere occurred when post-MCAo brain slices were superfused with elevated $[K^+]_{ext}$, elevated $[glu]_{ext}$ or oxygen and glucose deprivation. This novel finding is somewhat counterintuitive to the increased incidence of SD observed along with elevated $[K^+]_{ext}$ and $[glu]_{ext}$ 1-2 hours following ischemia (Nedergaard and Hansen 1993; Shimada et al. 1990; Sciotti et al. 1992). However, the incidence of SD in the post-ischemic brain abruptly declines after an initial 1-2 hours in peak SD incidence (Dijkhuizen et al. 1999; Koroleva and Bures 1996; Back et al. 1996; Hartings et al. 2003). This decline in post-ischemic SD for 4-6 hours was hypothesized by others to involve a post-ischemic suppression of SD (Nallet et al. 1999). Our findings of a decreased propensity to SD and swelling in response to further metabolic stress in the intact brain 1-5 hours following ischemia support this hypothesis. In conclusion, the investigation and cessation of post-ischemic SD over extended time periods are worthy of future investigation.

5.6 Strengths and Limitations of this Study

We have already discussed the variability of CBF and its effects upon SD in the intact post-ischemic brain which are reduced by harvesting brain slices after MCAo. Temperature variability also arises after focal cerebral ischemia. Following MCAo, core body temperature declines and renders the brain hypothermic (Barber et al. 2004). When core temperature is maintained in the normothermic range, the variability of the infarct volume declines (Barber et al. 2004). Hypothermia induced during ischemia also results in a delayed latency to SD onset and a slower propagating wavefront speed (Chen et al. 1993; Sasaki et al. 2009). As well, hypothermia decreases OGD-induced SD incidence and damage in neocortical brain slices (Obeidat and Andrew 1998; Obeidat et al. 2000). Controlling temperature during focal cerebral ischemia and

superfusion of brain slices with experimental aCSF imparts less experimental variability when monitoring SD in the post-ischemic brain.

There are some limitations to the brain slice technique. Neocortical brain slices harvested following MCAo and incubated in oxygenated aCSF results in partial restoration of glucose and oxygen to ischemic gray matter and does not reproduce in vivo reperfusion. However, infarct maturation proceeds during the 12 hours following MCAo despite reperfusion (Hartings et al. 2003), as evident in brain slices harvested 12 hours after MCAo. Although post-ischemic brain slices cannot replicate in vivo ischemia/reperfusion, insight into infarct maturation during isolated time windows is possible by harvesting brain slices at specific timepoints following MCAo. With the brain slice technique, gross perturbations of ions and metabolites observed after ischemia (Hansen and Zeuthen 1981; Obrenovitch et al. 1988) are not replicated. However, the response of the post-ischemic brain to isolated metabolic stressors and initiators of SD are facilitated by superfusing neocortical brain slices with specific experimental saline solutions.

Another limitation of cerebral brain slices is the inability to observe SD initiation and propagation across the surface topography of neocortex as commonly imaged in vivo. However, by observing the initiation and propagation of SD in post-MCAo brain slices we are able to quantify the speed of the propagating SD wavefront and latency to SD onset as well as the specific stereotaxic co-ordinates of the SD initiation site. Previous in vivo studies that observed post-ischemic SD in the coronal plane used digitally-reconstructed images with low resolution (Busch et al. 1996). Experimenting upon post-MCAo brain slices enables observation of time-dependent infarct maturation as well as any post-ischemic suppression of activity or resistance to be interrogated in experiments with controlled variables.

Although spreading depolarization is only one of many post-stroke pathogenic mechanisms, it is an ideal therapeutic target because it occurs within minutes after ischemia onset and declines over the following 24 hrs. During the initial acute phase of ischemia many molecular targets for therapy mediate injury, but these same mechanisms contribute to neurovascular remodelling and neuroplasticity soon thereafter (Lo 2008; Tymianski 2011). SD occurs in the initial minutes following ischemia, abruptly declines after 2 hours and then occurs sporadically thereafter. These properties of post-ischemic SD are ideal for therapeutic intervention that minimizes interference with the ‘injury-to-repair’ transition that has not been considered in stroke therapy in previous decades (Lo 2008). Other deleterious post-stroke cascades involve feedback loops that increase intracellular calcium and reactive oxygen species which lead to mitochondrial membrane disruption and neuronal death (Tymianski 2011). We have not monitored these other important aspects of ischemic core deterioration, as well as astrocyte reactivity, alteration of the blood-brain barrier, infiltration of blood cells and the response of microglia. Each of these aspects could be studied in future experiments using the MCAo cerebral slice technique.

5.7 Future Directions

This thesis has provided impetus to further examine the fate of the ischemic core as it evolves during 24 and 72 hours post-ischemia. Despite the devastating damage to most neurons in the 12 hour infarct there are single pyramidal neurons embedded throughout the infarct that appear morphologically and electrophysiologically intact. This is an important finding that will be followed up in the Andrew and Jin laboratories. As noted earlier, what properties do these neurons possess that allows them to resist injury while their neighbours die? One explanation that our laboratories will pursue is that these neurons express more of the protective $\alpha 3$ pump

isoform than their $\alpha 1$ -expressing neighbours. This question is being examined by using pump isoform antibodies to immunohistochemically stain the surviving neurons. More accurately, laser capture microscopy can be employed to literally cut out single neurons in section and analyse their isoform expression. Does this selective survival continue past 12 hours post-ischemia? This will be answered in the future by extending the survival times of post-MCAo mice to 24 and 72 hours.

Investigations are currently underway in the Andrew and Jin labs examining both mRNA expression and protein expression of the Na^+/K^+ pump isoforms $1\alpha 1$ and $1\alpha 3$. As follow-up to the findings in this thesis, these studies will be documenting regional changes in mRNA and protein expression of these isoforms in both ischemic and non-ischemic hemispheres at 12, 24 and 72 hours to observe if and where there are increases in the more 'stroke-resistant' isoform $1\alpha 3$. Moreover simultaneous measures of isoform protein translation are being carried out.

This thesis further demonstrates the early recovery of synaptic communication and intrinsic electrophysiology by post-ischemic neocortical pyramidal neurons, supported by our finding that morphological damage to neurons appear minimal after 30 minutes of focal stroke. Yet brain slices harvested after 12 hours of reperfusion following focal cerebral ischemia display a large infarct of necrotic neurons and swollen/beaded neurons devoid of synaptic communication. Not surprisingly, there were few intact neurons with normal electrophysiology and intact morphology within this infarcted region. Our discovery of even a few surviving pyramidal neurons scattered through the MCAo infarct 12 hours post-stroke has sparked interest in a more detailed study of these neurons to determine if they continue to maintain their viability at later survival times of 24 and 72 hours. If the neurons continue to survive, we will use laser capture microscopy to start to

characterize, for example, the single-cell expression of the pump isoforms by these resilient neurons.

References

- Aitken, P G, D Fayuk, G G Somjen, and Turner, D.A. (1999). Use of intrinsic optical signals to monitor physiological changes in brain tissue slices. *Methods: A Companion to Methods in Enzymology*. 18 (2): 91–103.
- Anderson, T R, and Andrew, R.D. (2002). Spreading depression: imaging and blockade in the rat neocortical brain slice. *Journal of Neurophysiology*. 88 (5): 2713–25.
- Anderson, T.R., Jarvis, C.R., Biedermann, A.J., Molnar, C., and Andrew, R.D. (2005). Blocking the anoxic depolarization protects without functional compromise following simulated stroke in cortical brain slices. *Journal of Neurophysiology*. 93 (2): 963–79.
- Andrew, R.D., Adams J.R., and Polischuk, T.M. (1996). Imaging NMDA- and kainate-induced intrinsic optical signals from the hippocampal slice. *Journal of Neurophysiology*. 76 (4): 2707–17.
- Andrew, R.D, Jarvis, C.R. and Obeidat, A.S. (1999). Potential sources of intrinsic optical signals imaged in live brain slices. *Methods: A Companion to Methods in Enzymology*. 18 (2):185–196.
- Andrew, R.D., Labron, M.W., Boehnke, S.E., Carnduff, L., and Kirov, S.A. (2007). Physiological evidence that pyramidal neurons lack functional water channels. *Cerebral Cortex*. 17 (4): 787–802.
- Andrew, R.D., Lobinowich, M.E. and Osehobo, E.P. (1997). Evidence against volume regulation by cortical brain cells during acute osmotic stress. *Experimental Neurology* 143 (2): 300–312.
- Andrew, R.D., and MacVicar, B.A. (1994). Imaging cell volume changes and neuronal excitation in the hippocampal slice. *Neuroscience* 62 (2): 371–83.

- Astrup, J., Siesjö, B.K., and Symon, L. (1981a). Thresholds in cerebral ischemia - the ischemic penumbra. *Stroke*. 12 (6): 723–25.
- Astrup, J., Sørensen, P.M. and Sørensen, H.R. (1981b). Oxygen and glucose consumption related to Na⁺-K⁺ transport in canine brain. *Stroke*. 12 (6): 726–30.
- Astrup, J., Symon, L., Branston, N.M., and Lassen, N.A. (1977). Cortical evoked potential and extracellular K⁺ and H⁺ at critical levels of brain ischemia. *Stroke*. 8 (1): 51–57.
- Attwell, D, and Laughlin, S.B. (2001). An energy budget for signaling in the grey matter of the brain. *Journal of Cerebral Blood Flow and Metabolism*. 21 (10): 1133–45.
- Ayata, C., Shin, H.K., Salomone, S., Ozdemir-Gursoy, Y., Boas, D.A., Dunn, A.K., and Moskowitz, M.A. (2004). Pronounced hypoperfusion during spreading depression in mouse cortex. *Journal of Cerebral Blood Flow & Metabolism*. 24: 1172-1182.
- Azarias, G., Kruusmagi, M., Connor, S., Akkuratov, E.E., Liu, X.-L., Lyons, D., Brismar, H., Broberger, C., and Aperia, A. (2013). A specific and essential role for Na,K-ATPase $\alpha 3$ in neurons co-expressing $\alpha 1$ and $\alpha 3$. *Journal of Biological Chemistry*. 288 (4): 2734–43.
- Back, T., Ginsberg, M.D., Dietrich, W.D., and Watson, B.D. (1996). Induction of spreading depression in the ischemic hemisphere following experimental middle cerebral artery occlusion: effect on infarct morphology. *Journal of Cerebral Blood Flow and Metabolism* 16 (2): 202–13.
- Back, T., Kohno, K., and Hossmann, K.-A. (1994). Cortical negative DC deflections following middle cerebral artery occlusion and KCl-induced spreading depression: effect on blood flow, tissue oxygenation, and electroencephalogram. *Journal of Cerebral Blood Flow and Metabolism*. 14 (1): 12–19.
- Baker, C.J., Onesti, S.T., and Solomon, R.A. (1992). Reduction by delayed hypothermia of

- cerebral infarction following middle cerebral artery occlusion in the rat: a time-course study. *J Neurosurg.* 77: 438–44.
- Balestrino, M. (1995). Pathophysiology of anoxic depolarization: new findings and a working hypothesis. *Journal of Neuroscience Methods.* 59: 99-103.
- Balestrino, M., Young, J., and Aitken, P. (1999). Block of (Na⁺,K⁺)ATPase with ouabain induces spreading depression-like depolarization in hippocampal slices. *Brain Research* 838 (1-2): 37–44.
- Barber, P.A., Hoyte, L., Colbourne, F., and Buchan, A.M. (2004). Temperature-regulated model of focal ischemia in the mouse: a study with histopathological and behavioral outcomes. *Stroke* 35 (7): 1720–25.
- Barber, P.A., Hoyte, L., Kirk, D., Foniok, T., Buchan, A., Tuor, U. (2005). Early T1- and T2-weighted MRI signatures of transient and permanent middle cerebral artery occlusion in a murine stroke model studied at 9.4 T. *Neuroscience Letters.* 388: 54-59.
- Belayev, L., Zhao, W., Busto, R., and Ginsberg, M.D. (1997). Transient middle cerebral artery occlusion by intraluminal suture: I. Three-dimensional autoradiographic image-analysis of local cerebral glucose metabolism-blood flow interrelationships during ischemia and early recirculation. *Journal of Cerebral Blood Flow and Metabolism.* 17 (12): 1266–80.
- Belliard, A., Sottejeau, Y., Duan, Q., Karabin, J.L., and S V Pierre, S.V. (2013). Modulation of cardiac Na⁺,K⁺-ATPase cell surface abundance by simulated ischemia/reperfusion and ouabain preconditioning. *AJP: Heart and Circulatory Physiology.* 304: H94-H103.
- Benveniste, H., Drejer, J., Schousboe, A. and Diemer, N.H. (1984). Elevation of the extracellular concentrations of glutamate and aspartate in rat hippocampus during transient cerebral ischemia monitored by intracerebral microdialysis. *Journal of Neurochemistry.* 43 (5):

1369–74.

- Bere, Z., Obrenovitch, T.P., Bari, F., and E. Farkas, E. (2014). Ischemia-induced depolarizations and associated hemodynamic responses in incomplete global forebrain ischemia in rats. *Neuroscience*. 260: 217–26.
- Branston, N.M., Strong, A.J. and Symon, L. (1977). Extracellular potassium activity, evoked potential and tissue blood flow relationships during progressive ischaemia in baboon cerebral cortex. *Journal of the Neurological Sciences*. 32 (3): 305–21.
- Brisson, C.D., and Andrew, R.D. (2012). A neuronal population in hypothalamus that dramatically resists acute ischemic injury compared to neocortex. *Journal of Neurophysiology*. 108: 419-430.
- Brisson, C.D., Hsieh, Y.-T., Kim, D., Jin, A.Y., and Andrew, R.D. (2014). Brainstem neurons survive the identical ischemic stress that kills higher neurons: insight to the persistent vegetative state. *PloS One* 9 (5): e96585.
- Brisson, C.D., Lukewich, M.K, and Andrew, R.D. (2013). A distinct boundary between the Higher Brain's Susceptibility to Ischemia and the Lower Brain's Resistance. *PLoS ONE* 8 (11): e79589.
- Brown, C.E., Wong, C. and Murphy, T.H. (2008). Rapid morphologic plasticity of peri-infarct dendritic spines after focal ischemic stroke. *Stroke* 39 (4): 1286–91.
- Buchan, A., and Pulsinelli, W.A. (1990). Hypothermia but not the N-Methyl-D-Aspartate antagonist, MK-801, attenuates neuronal damage in gerbils subjected to transient global ischemia. *The Journal of Neuroscience*. 10 (1): 311–16.
- Bures, J, and Buresová, O. (1981). Cerebral $[K^+]_e$ increase as an index of the differential susceptibility of brain structures to terminal anoxia and electroconvulsive shock. *Journal of*

Neurobiology 12 (3): 211–20.

Busch, E., Gyngell, M.L., Eis, M., Hoehn-Berlage, M., and Hossmann, K.-A. (1996). Potassium-induced cortical spreading depressions during focal cerebral ischemia in rats: contribution to lesion growth assessed by diffusion-weighted NMR and biochemical imaging. *Journal of Cerebral Blood Flow and Metabolism*. 16 (6): 1090–99.

Busto, R., Dietrich, W.D., Globus, M.Y., Valdés, I., Scheinberg, P., and Ginsberg, M.D. (1987). Small differences in intraischemic brain temperature critically determine the extent of ischemic neuronal injury. *Journal of Cerebral Blood Flow and Metabolism*. 7: 729–38.

Canals, S., Larrosa, B., Pintor, J., Mena, M., and Herreras, O. (2008). Metabolic challenge to glia activates an adenosine-mediated safety mechanism that promotes neuronal survival by delaying the onset of spreading depression waves. *Journal of Cerebral Blood Flow and Metabolism*. 28: 1835–44.

Carmichael, ST. (2005). Rodent models of focal stroke: size mechanism, and purpose. *NeuroRx: The Journal of the American Society for Experimental Neurotherapeutics*. 2: 396-409.

Chen, Q., Chopp, M., Bodzin, G., and Chen, H. (1993). Temperature modulation of cerebral depolarization during focal cerebral ischemia in rats: correlation with ischemic injury. *Journal of Cerebral Blood Flow and Metabolism*. 13 (3): 389–94.

Chuquet, J., Hollender, L., and Nimchinsky, E.A. (2007). High-resolution in vivo imaging of the neurovascular unit during spreading depression. *The Journal of Neuroscience*. 27 (15): 4036–44.

Connolly, E.S., Winfree C.J., Stern, D.M., Solomon, R.A., Pinsky, D.J. (1996). Procedural and strain-related variable significantly affect outcome in a murine model of focal cerebral ischemia. *Neurosurgery*. 38 (3): 523-532.

- Connors, W. (1991). Laminar distribution of neuronal membrane properties in neocortex of normal and reeler mouse. *Journal of Neurophysiology*. 66 (6): 2034-2040.
- Corbett, D., Evans, S., Thomas, C., Wang, D., and Jonas, R.A. (1990). MK-801 reduced cerebral ischemic injury by inducing hypothermia. *Brain Research*. 514 (2): 300–304.
- Dietz, R.M, Weiss, J.H., and Shuttleworth, C.W. (2008). Zn²⁺ influx is critical for some forms of spreading depression in brain slices. *The Journal of Neuroscience*. 28 (32): 8014–24.
- Dijkhuizen, R.M, Beekwilder, J.P., van der Worp, H.B., Berkelbach van der Sprenkel, J.W., Tulleken, K.A., and Nicolay, K. (1999). Correlation between tissue depolarizations and damage in focal ischemic rat brain. *Brain Research*. 840 (1-2): 194–205.
- Dohmen, C., Sakowitz, O.W., Fabricius, M., Bosche, B., Reithmeier, T., Ernestus, R.I., Brinker, G., et al. (2008). Spreading depolarizations occur in human ischemic stroke with high incidence. *Annals of Neurology*. 63 (6): 720–28.
- Douglas, H.A., Callaway, J.K., Sword, J., Kirov, S.A., and Andrew, R.D. (2011). Potent inhibition of anoxic depolarization by the sodium channel blocker dibucaine. *Journal of Neurophysiology*. 105 (4): 1482–94.
- Dreier, J.P. (2011). The role of spreading depression, spreading depolarization and spreading ischemia in neurological disease. *Nature Medicine*. 17 (4): 439–47.
- Dreier, J.P., Körner, K., Ebert, N., Görner, A., Rubin, I., Back, T., Lindauer, U., et al. (1998). Nitric oxide scavenging by hemoglobin or nitric oxide synthase inhibition by N-nitro-L-arginine induces cortical spreading ischemia when K⁺ is increased in the subarachnoid space. *Journal of Cerebral Blood Flow and Metabolism*. 18 (9): 978–90.
- Dreier, J.P., Fabricius, M., Ayata, C., Sakowitz, O.W., Shuttleworth, C.W., Dohmen, C., Graf, R., et al. (2017). Recording, analysis, and interpretation of spreading depolarizations in

- neuro-intensive care: review and recommendations of the COSBID research group. *Journal of Cerebral Blood Flow and Metabolism*. 35 (5): 1595-1625.
- Dreier, J.P., Isele, T., Reiffurth, C., Offenhauser, N., Kirov, S.A., and Dahlem, M.A. (2013). An abrupt, massive release of gibbs free energy from the human brain. *Neuroscientist*. 19 (1): 24–42.
- Dreier, J.P., Major, S., Manning, A., Woitzik, J., Drenckhahn, C., Steinbrink, J., Tolias, C., et al. (2009). Cortical spreading ischaemia is a novel process involved in ischaemic damage in patients with aneurysmal subarachnoid haemorrhage. *Brain*. 132 (7): 1866–81.
- Erecinska, M., and Silver, I.A. (1989). ATP and brain function. *Journal of Cerebral Blood Flow and Metabolism*. 9: 2–19.
- Fabricius, M., Fuhr, S., Bhatia, R., Boutelle, M., Hashemi, P., Strong, A.J., and Lauritzen, M. (2006). Cortical spreading depression and peri-infarct depolarization in acutely injured human cerebral cortex. *Brain*. 129 (3): 778–90.
- Farkas, E., Pratt, R., Sengpiel, F., and Obrenovitch, T.P. (2008). Direct, live imaging of cortical spreading depression and anoxic depolarisation using a fluorescent, voltage-sensitive dye. *Journal of Cerebral Blood Flow & Metabolism* 28 (2): 251–62.
- Fayuk, D., Aitken, P.G., Somjen, G.G., and Turner, D.A. (2002). Two different mechanisms underlie reversible, intrinsic optical signals in rat hippocampal slices. *Journal of Neurophysiology*. 87 (4): 1924–37.
- F.D. NeuroTechnologies, Inc. (2012). FD Rapid GolgiStain™ Kit User Manual Version 2012-03.
- Feigin, V.L. (2005). Stroke epidemiology in the developing world. *The Lancet*. 365: 2160–61.
- Feng, G., Mellor, R.H., Bernstein, M., Keller-Peck, C., Nguyen, Q.T., Wallace, M., Nerbonne,

- J.M., Lichtman, J.W., and Sanes, J.R. (2000). Imaging neuronal subsets in transgenic mice expressing multiple spectral variants of GFP. *Neuron* 28 (1): 41–51.
- Fujii, M., Hideaki, H., Meng, W., Vonsattel, J.P., Huang, Z., Moskowitz, M.A. (1997). Strain-related differences in susceptibility to transient forebrain ischemia in SV-129 and C57BL6 mice. *Stroke*. 28: 1805-1811.
- Folbergrová, J., Memezawa, H., Smith, M.L. and Siesjö, B.K. (1992). Focal and perifocal changes in tissue energy state during middle cerebral artery occlusion in normo- and hyperglycemic rats. *Journal of Cerebral Blood Flow and Metabolism*. 12 (1): 25–33.
- Gao, J., Wymore, R.S., Wang, Y., Gaudette, G.R., Krukenkamp, I.B., Cohen, I.S., and Mathias, R.T. (2002). Isoform-specific stimulation of cardiac Na/K pumps by nanomolar concentrations of glycosides. *The Journal of General Physiology*. 119 (4): 297–312.
- Gao, T. M., Pulsinelli, W.A., and Xu, Z.C. (1998). Prolonged enhancement and depression of synaptic transmission in CA1 pyramidal neurons induced by transient forebrain ischemia in vivo. *Neuroscience*. 87 (2): 371–83
- Gao, T. M., Pulsinelli, W.A., and Xu, Z.C.. (1999). Changes in membrane properties of CA1 pyramidal neurons after transient forebrain ischemia in vivo. *Neuroscience*. 90 (3): 771–80.
- Ginsberg, M.D. (2008). Neuroprotection for ischemic stroke: past, present and future. *Neuropharmacology*. 55 (3): 363–89.
- Globus, M.Y., Busto, R., Dietrich, W.D., Martinez, E., Valdes, I., and Ginsberg, M.D. (1988). Effect of ischemia on the in vivo release of striatal dopamine, glutamate, and gamma-aminobutyric acid studied by intracerebral microdialysis. *Journal of Neurochemistry*. 51 (5): 1455–64.
- Grinvald, A., and Hildesheim, R. (2004). VSDI: a new era in functional imaging of cortical

- dynamics. *Nature Reviews Neuroscience*. 5 (11): 874–85.
- Grinvald, A., Mankner, A., and Segal, M. (1982). Visualization of the spread of electrical activity in rat hippocampal slices by voltage-sensitive optical probes. *J Physiol*. 333: 269–91.
- Guo, H-C., Guo, F., Zhang, L.-N., Zhang, R., Chen, Q., Li, J.-X., Yin, J., and Wang. Y.-L. (2011). Enhancement of Na/K Pump activity by chronic intermittent hypobaric hypoxia protected against reperfusion injury. *American Journal of Physiology. Heart and Circulatory Physiology*. 300 (6): H2280–87.
- Hagberg, H., Lehmann, A., Sandberg, M., Nyström, B., Jacobson, I., and Hamberger, A. (1985). Ischemia-induced shift of inhibitory and excitatory amino acids from intra- to extracellular compartments. *Journal of Cerebral Blood Flow and Metabolism*. 5 (3): 413–19.
- Hansen, A.J., and Zeuthen, T. (1981). Extracellular ion concentrations during spreading depression and ischemia in the rat brain cortex. *Acta Physiologica Scandinavica*. 113 (4): 437–45.
- Hansen, A.J. (1985). Effect of anoxia on ion distribution in the brain. *Physiological Reviews*. 65 (1). 101-148.
- Hartings, J.A., Bullock, M.R., Okonkwo, D.O., Murray, L.S., Murray, G.D., Fabricius, M., Maas, A.I., et al. (2011). Spreading depolarisations and outcome after traumatic brain injury: a prospective observational study. *Lancet Neurology*. 10 (12): 1058–64.
- Hartings, J.A, Rolli, M.L. May Lu, X.-C., Tortella, F.C. (2003). Delayed secondary phase of peri-infarct depolarizations after focal cerebral ischemia: relation to infarct growth and neuroprotection. *The Journal of Neuroscience*. 23 (37): 11602–10.
- Hartings, J.A, Shuttleworth, C.W., Kirov, S.A., Ayata, C., Hinzman, J.M., Foreman, B., Andrew, R.D., et al. (2017). The continuum of spreading depolarizations in acute cortical lesion

- development: examining Leao's legacy. *Journal of Cerebral Blood Flow and Metabolism*. 37 (5): 1571-1594.
- Hatfield, R.H., Gill, R. and Brazell, C. (1992). The dose-response relationship and therapeutic window for dizocilpine (MK-801) in a rat focal ischemia model. *European Journal of Pharmacology*. 216 (1): 1-7.
- Heinemann, U., and Lux, H.D. (1977). Ceiling of stimulus induced rises in extracellular potassium concentration in the cerebral cortex of cat. *Brain Research*. 120 (2): 231-49.
- Heiss, W D. (1992). Experimental evidence of ischemic thresholds and functional recovery. *Stroke*. 23 (11): 1668-72.
- Hille, B. (2001). *Ion Channels of Excitable Membranes* (Third Edition). Sinauer Associates, Inc. Sunderland, Massachusetts: pp. 38-51.
- Hillered, L., Hallström, A., Segersvärd, S., Persson, L. and Ungerstedt, U. (1989). Dynamics of extracellular metabolites in the striatum after middle cerebral artery occlusion in the rat monitored by intracerebral microdialysis. *Journal of Cerebral Blood Flow and Metabolism*. 9 (5): 607-16.
- Hossmann, K.-A. (1994). Viability thresholds and the penumbra of focal ischemia. *Annals of Neurology* 36 (4): 557-65.
- Hossmann, K.-A. Nagashima G., Klatzo, I. (1990). Repetitive ischemia of cat brain: pathophysiological observations. *Neurological Research*. 12 (3): 158-164.
- Iijima, T, Mies, G. and Hossmann, K.A. (1992). Repeated negative dc deflections in rat cortex following middle cerebral artery occlusion are abolished by MK-801: effect on volume of ischemic injury. *Journal of Cerebral Blood Flow and Metabolism*. 12 (5): 727-33.
- Iijima, T., Shimase, C., Iwao, Y. and Sankawa, H. (1998). Relationships between glutamate

- release, blood flow and spreading depression: real-time monitoring using an electroenzymatic dialysis electrode. *Neuroscience Research*. 32 (3): 201–7.
- Ilie, A., Ciocan, D., Zagrean, A., Nita, D.A., Zagrean, L. and Moldovan, M. (2006). Endogenous activation of adenosine A(1) receptors accelerates ischemic suppression of spontaneous electrocortical activity. *Journal of Neurophysiology*. 96 (5): 2809–14.
- Jarvis, C.R., Anderson, T.R. and Andrew, R.D. (2001). Anoxic depolarization mediates acute damage independent of glutamate in neocortical brain slices. *Cerebral Cortex*. 11 (3): 249–59.
- Jarvis, C.R., Lilje, L., Vipond, G.J., and Andrew, R.D. (1999). Interpretation of intrinsic optical signals and calcein fluorescence during acute excitotoxic insult in the hippocampal slice. *NeuroImage*. 10 (4): 357–72.
- Joshi, I., and Andrew, R.D. (2001). Imaging anoxic depolarization during ischemia-like conditions in the mouse hemi-brain slice. *Journal of Neurophysiology*. 85 (1): 414–24.
- Jovin TG, Chamorro EC, de Miguel CA, Rovira, MA, San Roman, L et al. (2015). *New England Journal of Medicine*. 372 (24): 2296-2307.
- Kager, H. (2002). Conditions for the triggering of spreading depression studied with computer simulations. *Journal of Neurophysiology*. 88 (5): 2700–2712.
- Kaku, T., Hada, J., and Hayashi, Y. (1994). Endogenous adenosine exerts inhibitory effects upon the development of spreading depression and glutamate release induced by microdialysis with high K⁺ in rat hippocampus. *Brain Research*. 658 (1-2): 39–48.
- Katsman, D., Zheng, J., Spinelli, K. and Carmichael, S.T. (2003). Tissue microenvironments within functional cortical subdivisions adjacent to focal stroke. *Journal of Cerebral Blood Flow & Metabolism*. 997–1009.

- Koroleva, V.I., and Bures, J. (1996). The use of spreading depression waves for acute and long-term monitoring of the penumbra zone of focal ischemic damage in rats. *Proceedings of the National Academy of Sciences of the United States of America*. 93 (8): 3710–14.
- Koziumi, J., Yoshida, Y., Nakazava, T., Ooneda, J. (1986). Experimental studies of ischemic brain slices of ischemic brain edema. 1. A new experimental model of cerebral embolism in rats in which recirculation can be introduced in the ischemic area. *Jpn. J. Stroke*. 8: 1-8.
- Lauritzen, M, Hansen, A.J., Kronborg, D. and Wieloch, T. (1990). Cortical spreading depression is associated with arachidonic acid accumulation and preservation of energy charge. *Journal of Cerebral Blood Flow and Metabolism*. 10 (1): 115–22.
- Leão, A.A.P. (1947). Further observations on the spreading depression of activity in the cerebral cortex. *Journal of Neurophysiology*. 10 (6): 409–14.
- Leão, A.A.P. (1944). Spreading depression of activity in the cerebral cortex. *Journal of Neurophysiology*. 7 (6): 359–90.
- Lee, K.S., and Lowenkopf, T. (1993). Endogenous adenosine delays the onset of hypoxic depolarization in the rat hippocampus in vitro via an action at A1 receptors. *Brain Research*. 609: 313–15.
- Lindquist, B.E., and Shuttleworth, C.W. (2012). Adenosine receptor activation is responsible for prolonged depression of synaptic transmission after spreading depolarization in brain slices. *Neuroscience*. 223: 365–76.
- Lindquist, B.E., and Shuttleworth, C.W. (2014). Spreading depolarization-induced adenosine accumulation reflects metabolic status in vitro and in vivo. *Journal of Cerebral Blood Flow and Metabolism*. 34 (11). Nature Publishing Group: 1779–90.
- Lipton, P. (1999). Ischemic cell death in brain neurons. *Physiological Reviews*. 79 (4): 1431–

1568.

- Lo, E. (2008). A new penumbra: transitioning from injury to repair after stroke. *Nature Medicine*. 14 (5): 497-500.
- Longa, E.Z., Weinstein, P.R., Carlson, S. and Cummins, R. (1989). Reversible middle cerebral artery occlusion without craniectomy in rats. *Stroke*. 20 (February 1989): 84–91.
- Maeda, K., Hata, R. and Hossmann, K.A. 1999. Regional metabolic disturbances and cerebrovascular anatomy after permanent middle cerebral artery occlusion in C57black/6 and SV129 Mice. *Neurobiology of Disease*. 6 (2): 101–8.
- McColl, B.W., Carswell, H.V., McCulloch, J. and Horsburgh, K. (2004). Extension of cerebral hypoperfusion and ischaemic pathology beyond MCA territory after intraluminal filament occlusion in C57Bl/6J Mice. *Brain Research*. 997 (1): 14–22.
- McCormick, D.A, Connors, B.W., Lighthall, J.W. and Prince, D.A. (1985). Comparative electrophysiology of pyramidal and sparsely spiny stellate neurons of the neocortex. *Journal of Neurophysiology*. 54 (4): 782–806.
- Mies, G., Iijima, T., and Hossmann, K.-A. (1993). Correlation between peri-infarct DC shifts and ischaemic neuronal damage in rat. *Neuroreport*. 4: 709-711.
- Mies, G., Kohno, K. and Hossmann, K.-A. (1994). Prevention of periinfarct direct current shifts with glutamate antagonist NBQX following occlusion of the middle cerebral artery in the rat. *Journal of Cerebral Blood Flow and Metabolism*. 14 (5): 802–7.
- Mies, G. (1997). Blood flow dependent duration of cortical depolarizations in the periphery of focal ischemia of rat brain. *Neuroscience Letters*. 221 (2-3): 165–68.
- Morimoto, T., Globus, M.Y., Busto, R., Martinez, E. and Ginsberg, M.D. (1996). Simultaneous measurement of salicylate hydroxylation and glutamate release in the penumbral cortex

- following transient middle cerebral artery occlusion in rats. *Journal of Cerebral Blood Flow and Metabolism*. 16 (1): 92–99.
- Murphy, T.H., Li, P., Betts, K. and Liu, R. (2008). Two-photon imaging of stroke onset in vivo reveals that NMDA-receptor independent ischemic depolarization is the major cause of rapid reversible damage to dendrites and spines. *The Journal of Neuroscience*. 28 (7): 1756–72.
- Nagashima, G. (1994). Cumulative effect of repetitive ischemia: pathophysiological findings. *Bull. Tokyo Med. Dent. Univ.* 41: 23-36.
- Nakamura, H., Strong, A.J., Dohmen, C., Sakowitz, O.W., Vollmar, S., Sué, M., Kracht, L. et al. (2010). Spreading depolarizations cycle around and enlarge focal ischaemic brain lesions. *Brain*. 133 (7): 1994–2006.
- Nallet, H., MacKenzie, E.T., and Roussel, S. (1999). The nature of penumbral depolarizations following focal cerebral ischemia in the rat. *Brain Research*. 842 (1): 148–58.
- Nedergaard, M., and Hansen, A.J. (1988). Spreading depression is not associated with neuronal injury in the normal brain. *Brain Research*. 449 (1-2): 395–98.
- Nedergaard, M., and Hansen, A.J. (1993). Characterization of cortical depolarizations evoked in focal cerebral ischemia. *Journal of Cerebral Blood Flow and Metabolism*. 13: 568–74.
- O’Collins, V.E., Macleod, M.R., Donnan, G.A., Horky, L.L., Van Der Worp, B.H., and Howells, D.A. (2006). 1,026 experimental treatments in acute stroke. *Annals of Neurology*. 59 (3): 467–77.
- Obeidat, A.S., and Andrew, R.D. (1998). Spreading depression determines acute cellular damage in the hippocampal slice during oxygen/glucose deprivation. *The European Journal of Neuroscience*. 10 (11): 3451–61.

- Obeidat, A.S., Jarvis, C.R., and Andrew, R.D. (2000). Glutamate does not mediate acute neuronal damage after spreading depression induced by O₂/glucose deprivation in the hippocampal slice. *Journal of Cerebral Blood Flow and Metabolism*. 20 (2): 412–22.
- Obrenovitch, T.P., Garofalo, O., Harris, R.J., Bordi, L., Ono, M., Momma, F., Bachelard, H.S. and Symon, L. (1988). Brain tissue concentrations of ATP, phosphocreatine, lactate, and tissue pH in relation to reduced cerebral blood flow following experimental acute middle cerebral artery occlusion. *Journal of Cerebral Blood Flow and Metabolism*. 8 (6): 866–74.
- Oselkin, M., Tian, D., and Bergold, P.J. (2010). Low-dose cardiotonic steroids increase sodium-potassium ATPase activity that protects hippocampal slice cultures from experimental ischemia. *Neuroscience Letters*. 473 (2): 67–71.
- Park, C.K., Nehls, D.G., Graham, D.I., Teasdale, G.M., and McCulloch, J. (1988). The glutamate antagonist MK-801 reduces focal ischemic brain damage in the rat. *Annals of Neurology*. 24 (4): 543–51.
- Petersen, C.C.H., Grinvald, A., Sakmann, B. (2003). Spatiotemporal dynamics of sensory responses in layer 2/3 of rat barrel cortex measured in vivo by voltage-sensitive dye imaging combined with whole-cell voltage recordings and neuron reconstructions. *Journal of Neuroscience*. 23 (4): 1298-1309.
- Phillis, J.W., Walter, G.A., and Simpson, R.E. (1991). Brain adenosine and transmitter amino acid release from the ischemic rat cerebral cortex: effects of the adenosine deaminase inhibitor deoxycoformycin. *Journal of Neurochemistry*. 56 (2): 644–50.
- Pietrobon, D., and Moskowitz, M.A. (2014). Chaos and commotion in the wake of cortical spreading depression and spreading depolarizations. *Nature Reviews. Neuroscience*. 15 (6): 379–93.

- Piper, R.D., Lambert, G.A., and Duckworth, J. W. (1991). Cortical blood flow changes during spreading depression in cats. *The American Journal of Physiology*. 261: H96–102.
- Polischuk, T M, and Andrew, R.D. (1996). Real-time imaging of intrinsic optical signals during early excitotoxicity evoked by domoic acid in the rat hippocampal slice. *Canadian Journal of Physiology and Pharmacology*. 74 (6): 712–22.
- Pulsinelli, W.A., and Buchan, A.M. (1988). The four-vessel occlusion rat model: method for complete occlusion of vertebral arteries and control of collateral circulation. *Stroke*. 19 (7): 913–14.
- Reddy, M.M., Bures, J. (1980). Cortical (K^+)_e and the stimulation induced blockade of spreading depression in the rat cerebral cortex. *Neuroscience Letters*. 17: 243-247.
- Richter, F., Bauer, R., Lehmenkühler, A, and Schaible, H. A. (2010). The relationship between sudden severe hypoxia and ischemia-associated spreading depolarization in adult rat brainstem in vivo. *Experimental Neurology*. 224 (1): 146–54.
- Risher, W.C., Andrew, R.D., and Kirov, S.A. (2009). Real-time passive volume responses of astrocytes to acute osmotic and ischemic stress in cortical slices and in vivo revealed by two-photon microscopy. *Glia*. 57 (2): 207–21.
- Risher, C.W., Lee, M.R., Fomitcheva, I.V., Hess, D.C., and Kirov, S.A. (2011). Dibucaine mitigates spreading depolarization in human neocortical slices and prevents acute dendritic injury in the ischemic rodent neocortex. *PLoS ONE*. 6 (7): e22351.
- Sasaki, T., Takeda, Y., Taninishi, H., Arai, M., Shiraishi, K., and Morita, K. (2009). Dynamic changes in cortical NADH fluorescence in rat focal ischemia: evaluation of the effects of hypothermia on propagation of peri-infarct depolarization by temporal and spatial analysis. *Neuroscience Letters*. 449 (1): 61–65.

- Satoh, M, Asai, S., Katayama, Y., Kohno, T., and Ishikawa, K. (1999). Real-time monitoring of glutamate transmitter release with anoxic depolarization during anoxic insult in rat striatum. *Brain Research*. 822 (1-2): 142–48.
- Saver, J.L., Albers, G.W., Dunn, B., Johnston, K.C., and Fisher, M. (2009). Stroke Therapy Academic Industry Roundtable (STAIR) recommendations for extended window acute stroke therapy trials. *Stroke*. 40 (7): 2594–2600.
- Schwinger, R. H. G., Wang, J., Frank, K., Muller-Ehmsen, J., Brixius, K., McDonough, A.A., and Erdmann, E. (1999). Reduced sodium pump $\alpha 1$, $\alpha 3$, and $\beta 1$ -isoform protein levels and Na^+ , K^+ -ATPase Activity but unchanged Na^+ - Ca^{2+} exchanger protein levels in human heart failure. *Circulation*. 99 (16): 2105–12.
- Sciotti, V.M., Roche, F.M., Grabb, M.C., and Van Wylen, D.G.L. (1992). Adenosine receptor blockade augments interstitial fluid levels of excitatory amino acids during cerebral ischemia. *J Cereb Blood Flow Metab*. 12: 646–55.
- Shibata, M., Leffler, C.W., and Busija, D.W. (1990). Cerebral hemodynamics during cortical spreading depression in rabbits. *Brain Research*. 530: 267–74.
- Shimada, N, Graf, R., Rosner, G., and Heiss, W.D. (1990). Differences in ischemia-induced accumulation of amino acids in the cat cortex. *Stroke; a Journal of Cerebral Circulation*. 21 (10): 1445–51.
- Shin, H. K., Dunn, A.K., Jones, P.B., Boas, D.A., Moskowitz, M.A., and Ayata, C. (2006). Vasoconstrictive neurovascular coupling during focal ischemic depolarizations. *Journal of Cerebral Blood Flow and Metabolism*. 26 (8): 1018–30.
- Silva, L.R., Gutnick, M.J., and Connors, B.W. (1991). Laminar distribution of neuronal membrane properties in neocortex of normal reeler mouse. *Journal of Neurophysiology*. 66

(6): 2034-2040.

Somjen, G.G. (2001). Mechanisms of spreading depression and hypoxic spreading depression-like depolarization. *Physiological Reviews*. 81 (3): 1065–96.

Steffensen, A.B., Sword, J., Croom, D., Kirov, S.A., and MacAulay, N. (2015). Chloride cotransporters as a molecular mechanism underlying spreading depolarization-induced dendritic beading. *Journal of Neuroscience*. 35 (35): 12172–87.

Strong, A.J., Venables, G.S., and Gibson, G. (1983). The cortical ischaemic penumbra associated with occlusion of the middle cerebral artery in the cat: 1. topography of changes in blood flow, potassium ion activity, and EEG. *Journal of Cerebral Blood Flow and Metabolism*. 3 (1): 86–96.

Sukhotinsky, I., Dilekoz, E., Moskowitz, M.A., and Ayata, C. (2008). Hypoxia and hypotension transform the blood flow response to cortical spreading depression from hyperemia into hypoperfusion in the rat. *Journal of Cerebral Blood Flow & Metabolism*. 28 (7): 1369–76.

Sukhotinsky, I., Yaseen, M.A., Sakadžić, S., Ruvinskaya, S., Sims, J.R., Boas, D.A., Moskowitz, M.A., and Ayata, C. (2010). Perfusion pressure-dependent recovery of cortical spreading depression is independent of tissue oxygenation over a wide physiologic range. *Journal of Cerebral Blood Flow & Metabolism*. 30 (6): 1168–77.

Takano, K., Latour, L. L., Formato, J.E., Carano, R.A., Helmer, K.G., Hasegawa, Y., Sotak, C.H., and Fisher, M. (1996). The role of spreading depression in focal ischemia evaluated by diffusion mapping. *Annals of Neurology*. 39 (3): 308–18.

Takaoka, S., Pearlstein, R.D., and Warner D.S. (1996). Hypothermia reduces the propensity of cortical tissue to propagate direct current depolarizations in the rat. *Neuroscience Letters* 218: 25-28.

- Tanaka, E, Yamamoto, S., Kudo, Y., Mihara, S., and Higashi, H. (1997). Mechanisms underlying the rapid depolarization produced by deprivation of oxygen and glucose in rat hippocampal CA1 neurons in vitro. *Journal of Neurophysiology*. 78 (2): 891–902.
- Tidow, H., Aperia, A., and Nissen, P. (2010). How are ion pumps and agrin signaling integrated? *Trends in Biochemical Sciences*. 35 (12). Elsevier Ltd: 653–59.
- Tóth, M., Little, P., Arnberg, F., Häggkvist, J., Mulder, J., Halldin, C., Gulyás, B., and Holmin, S. (2016). Acute neuroinflammation in a clinically relevant focal cortical ischemic stroke model in rat: longitudinal positron emission tomography and immunofluorescent tracking. *Brain Structure and Function*. 221 (3): 1279–90.
- Tymianski, M. 2011. Emerging mechanisms of disrupted cellular signaling in brain ischemia. *Nature Neuroscience*. 14 (11): 1369–73.
- van den Berg LA, Dijkgraaf, MGW, Berkhemer OA, Fransen, PSS et al. (2017). Two-year outcome after endovascular treatment for acute ischemic stroke. *New England Journal of Medicine*. 376 (14): 1341–50.
- von Bornstädt, D., Houben, T., Seidel, J.L., Zheng, Y., Dilekoz, E., Qin, T., Sandow, N. et al. (2015). Supply-demand mismatch transients in susceptible peri-infarct hot zones explain the origins of spreading injury depolarizations. *Neuron*. 85 (5): 1117–31.
- White, S.H., Brisson, C.D., and Andrew, R.D. (2012). Examining protection from anoxic depolarization by the drugs dibucaine and carbetapentane using whole cell recording from CA1 Neurons. *Journal of Neurophysiology*. 107: 2083-2095.
- Wilkins, J. T., Ning, H., Berry, J., Zhao, L., Dyer, A.R., and Lloyd-Jones, D.M. (2012). Lifetime risk and years lived free of total cardiovascular disease. *Jama*. 308 (17): 1795–1801.

- Windmuller, O., Lindauer, U., Foddis, M., Einhaupl, K.M., Dirnagl, U., Heinemann, U., and Dreier, J.P. (2005). Ion changes in spreading ischaemia induce rat middle cerebral artery constriction in the absence of NO. *Brain*. 128 (9): 2042–51.
- Woitzik, J., Hecht, N., Pinczolits, A., Sandow, N., Major, S., Winkler, M.K.L., Weber-Carstens, S., et al. (2013). Propagation of cortical spreading depolarization in the human cortex after malignant stroke. *Neurology*. 80 (12): 1095–1102.
- Yamada, A, Tanaka, E., Niiyama, S., Yamamoto, S., Hamada, M. and Higashi, H. (2004). Protective actions of various local anesthetics against the membrane dysfunction produced by in vitro ischemia in rat hippocampal CA1 neurons. *Neurosci Res*. 50 (3): 291–98.
- Zhang, S., Boyd, J., Delaney, K., Murphy, T.H. (2005). Rapid reversible changes in dendritic spine structure in vivo gated by the degree of ischemia. *Journal of Neuroscience*. 25 (22): 5333–38.
- Zhang, W, Miao, Y., Zhou, S., Wang, B. Luo, Q. and Qiu, Y. (2010). Involvement of glutamate transporter-1 in neuroprotection against global brain ischemia-reperfusion injury induced by postconditioning in rats. *International Journal of Molecular Sciences*. 11 (11): 4407–16.
- Zhang, Z.G., Chopp, M. and Chen, H. (1993). Duration dependent post-ischemic hypothermia alleviates cortical damage after transient middle cerebral artery occlusion in the rat. *Journal of the Neurological Sciences*. 117 (1-2): 240–44.
- Zhou, N., Gordon, G.R.J., Feighan, D., and MacVicar, B.A. (2010). Transient swelling, acidification, and mitochondrial depolarization occurs in neurons but not astrocytes during spreading depression. *Cerebral Cortex*. 20 (11): 2614–24.
- Zhou, N., Rungta, R.L, Malik, A., Han, H., Wu, D.C., and MacVicar, B.A. (2013). Regenerative

glutamate release by presynaptic NMDA receptors contributes to spreading depression.

Journal of Cerebral Blood Flow and Metabolism. 33 (10): 1582–94.